ATMOSPHERIC TEMPERATURE STRUCTURE IN THE roAp STARS

by

Rodney Medupe

Thesis presented to the Faculty of
Science at the University of Cape Town
for the Degree of MASTER OF SCIENCE

Supervisor: Assoc Professor D.W Kurtz

Department of Astronomy
UNIVERSITY OF CAPE TOWN
October 1996

AST 520 MEDIA

98/3039

Abstract

The rapidly oscillating Ap (roAp) stars are a sub–group of the chemically peculiar stars of class 2 (CP2), which are characterised by peculiar spectra and anomalously strong lines of Sr, Cr, Eu and other rare earth elements. They have strong global dipole magnetic fields with effective strengths of up to a few thousand gausses. Stars showing these phenomena cover the spectral range B8p to F0 V-IV.

About 20 years ago rapid non–radial pulsations were discovered in the coolest members of the CP2 group, namely the roAp stars. These pulsations are due to high over–tone, low degree p modes with periods between 5.6 and 15 minutes. Since then, studies of these rapid oscillations have revealed a lot of information about these stars. The eigenfrequency spectra of roAp stars can potentially reveal information such as their rotation periods, rotational inclinations, magnetic geometries, internal magnetic field strengths, radii, masses, luminosities and ages.

Matthews *et al.* (1990, 1996) suggested a technique to empirically determine the T(τ) relation for roAp stars. This technique involves comparing the pulsation amplitudes obtained from multi–colour photometry to the ones calculated from black–body pulsator models (assuming dipole mode pulsations). This comparison yielded limb–darkening coefficients which were used to determine T(τ) in a way similar to what was done for the sun. Matthews *et al.* based their idea on the observed fact that pulsation amplitudes of roAp stars drop sharply with increasing wavelength. They thus explained this sharp decline of amplitude with wavelength in terms of the strongly wavelength dependent limb–darkening.

The initial aim of this thesis was to investigate the technique proposed by Matthews *et al.*, and to apply it to a number of roAp stars. However, when a linearised expression for the variation of the pulsation amplitude with wavelength, limb–darkening, inclination of the pulsation axis α, and $\frac{\Delta T}{T_o}$ (where ΔT is the polar pulsational temperature semi–amplitude and T_o is the atmospheric temperature) was derived, it was discovered that limb–darkening is too small an effect to account for the observed amplitudes. The result is based on the Wien approximation and uses the Planck function to represent intensity. Therefore, limb–darkening cannot be measured from the amplitude *vs* wavelength data. This analysis and the results thereof are reported in this thesis. Numerical models based on realistic treatment of the intensity spectra (obtained from model atmospheres) are used to confirm and refine the analytical results.

The linearised expression mentioned above suggests that an important factor that explains the sharp decline of amplitude with wavelength is the variation of the ratio $\frac{\Delta T}{T_o}$ with wavelength. Therefore, if the T(τ) structure of a star is known *a priori* (from model atmospheres), the variation of ΔT with wavelength can be determined. This new technique, together with the variation of opacity with wavelength in the atmospheres of roAp stars, is applied to HD 134214, HD 137949, HD 128898, HD 101065 and HR 3831 to determine $\Delta T \cos\alpha$ as a function of atmospheric depth. HR 3831 was observed at various rotation phases to investigate the effect of rotation on the derived $\Delta T \cos\alpha$ *vs* atmospheric depth relation. Preliminary results on this are included in this thesis.

Acknowledgements

Montsamaisa bosigo ke mo leboga bosele

He or she who helps me to walk through the night I shall thank during the day

With that **Setswana** proverb, I will like to thank the following people:

- **Professor Don W. Kurtz**, my supervisor. It is through you that I have come to realize what a joy astronomy is. I particularly want to thank you for having made astronomy an easy choice for my postgraduate studies, I shall always remember you for that. It has always been a joy to chat to you. You shone the brightest torch for me through the darkest of the nights.
- **Professor Hiromoto Shibahashi**, for the fruitful and interesting discussions we had at the initiation of this project and for the nice climb up Table mountain.
- **Dr. Jaymie Matthews**, also for the fruitful and interesting discussions we had at the initiation of this project, and for the interesting discussions we had at Sutherland when we were observing together.
- **Dr. Frederich Kupka**, for the useful discussions we had though email, and for kindly making your model atmosphere of α Cir available to me.
- **Dr. Peter Martinez**, for helping me learn Fortran, and for your always useful suggestions.
- **Dr. Michael Albrow**, for helping set up ATLAS9 model atmosphere program running, and for always making time to answer my questions.
- **Dr. Robert L. Kurucz** , for providing me with ATLAS9 cdroms.
- **Dr. Tony Lynas–Gray**, for the discussions we had about opacities.
- **Dr. David Buckley**, for always making my visits to Sutherland observatory, and the SAAO offices comfortable, and for being one of the people (together with Don Kurtz) responsible for building my interest in astronomy.
- **Dr. David Kilkenny**, for providing me with the STAP response functions.

- **Dr. Darragh O' Donoghue**, for providing me with the FORTRAN routine for calculating the heliocentric correction, and for the useful discussions we had.
- **Dr. John Menzies**, for providing me with the MP response functions.
- **Francois van Wyk**, for making my observing in Sutherland fun, and for always being there for me when I needed help, and for teaching me the tricks of star identifications.
- **Fred Marang**, also for making my observing in Sutherland fun, and teaching me to identify stars.
- **Kgabo Sepuru**, the computer wizard, for creating Figures 3.1 and 3.4 for me.
- **Professor Brian Warner**, for the useful discussions we had, and for creating a nice working environment in our department for me.
- **Dr. Bob Stobie**, for creating a good working environment at SAAO, and for giving me motivation to study astronomy.
- **Dr. Luis Balona**, for kindly making the computing facilities at SAAO available to me.
- **Avrohom Weissman**, the Vax system manager, for kindly giving me big disk space for me to run ATLAS9 on.
- **Dr. George Coyne**, the director of the Vatican summer school (VSS95), for selecting me to attend the VSS95, from which I learnt many things and the motivation to continue with astronomy.
- **Professor Chris Impey**, a lecturer at the VSS95, for the great discussions we had, which have made great impact on the way I view life.
- **Professor William Stoeger**, a lecturer at the VSS95, for the great discussions we had.
- This thesis was printed and put in a bound form at the **Institute of Physics and Astronomy, Aarhus University**, I thus wish to thank the institute for making all their facilities available to me, and in particular to thank Professor Jørgen Christensen–Dalsgaard (I am at the institute because of him), and Anette Skovgaard.

I acknowledge the generous financial support from the AW/UCT Mellon Foundation and the Foundation for Research and Development (FRD).

A Dedication

Motho ke motho ka ba bangwe
I belong, therefore, I am

A great African philosophy of Botho, Ubuntu.

This work would not have been possible without the support of the following:

- **Mama, mme Dimakatso Angelina Medupe**, my mother, for your constant love and words of encouragement. Motsadi wa me, dilo tsotlhe tse di ntle tse ke di dirang, ke tsa gago, ke go lebogela lorato, le kgodiso e ntle e o e mphileng, tse ke ditiro tsa gago.
- **Papa, rre Mothibi, Justice Medupe**, my father, for your everlasting support and guidance. Motsadi wa me ke lebogela ditiro tsotlhe tse o di ntiretseng mo botshelong jwa me, lerato le tlhokomelo tse o di nneetseng, di tla nna le nna, mo pelong ya me go ya go ile.
- **Nnake, Thapelo Medupe**, my younger brother, for being such a great brother, ke go rotloetsa thata ka tironyana e.
- **Nkgonne, Basi Batyi**, my elder brother, for being a great brother, thank you for your support. Le wena ke a go rotloetsa.
- **Oumama, mme Mmasaria, Elisabeth Madras**, my grandmother, ke go lebogelela kgodiso le tlhokomelo e o e mphileng, ga nkitla ke go lebala.
- **Oumama, mme Mmasheleng Medupe**, my grandmother, ke go lebogela lorato lwa gago, o mo pelong ya me ka dinako tsotlhe.

And to ...

- **Gaone Eli Mmatli**, for many things, ke lebogela lorato lwa gago.
- **Buti Ronald Teemane**, for being such a great friend throughout my life. Tsala ke solohela ha botsala jwa rona bo tla kgaogangwa ke loso. Tiro e, jaaka tse dingwe di ne di seke tsa kgonagala ntleng le tlhokomelo, bopelontle le lorato lwa gago.

And the following people: **Tsepile Sopeng**, for all the support you gave me and our friendship, **Fortunate Mashinini**, a great friend, **Johan Fynbo**, a great friend, Tak fordi du overbeviste mig, at Danmark er et godt sted, **Nelson Toteng** and **Bosha Toteng and family**, the hospitality you have always shown me is appreciated, **Gabo Maphakwane**, thanks for your friendship, **Winnie Lepedi**, for the great times, **Yuri Andersson**, thanks for being such a special friend, **Francois Vuille**, for all the great times we had, **Lerothodi Leeuw**, malebo wetsho, **Patrick Woudt**, **Mthobeli Zimba** and **Andreas Ngomane**, ierie man, **Anne Christine Møller**, mange Tak. The list is endless.

A special dedication to the following aspirant astronomers:

- Dimakatso Makobe
- Molebatsi Molebatsi
- Sabelo Lwana

This work is for all of you, hopefully to encourage you to go further, and reach for your dreams. I know you will make it. Masego!

Contents

Chapter 1

Introduction

1.1 Introduction

The sun is the only single star for which the $T(\tau)$ relation has been determined empirically. This is because only the sun can provide disk resolved information due to its proximity to us. So one can measure limb–darkening directly and hence $T(\tau)$.

Limb–darkening has been measured empirically from the observation of the primary minima of some eclipsing binaries. The primary minima resulting from annular eclipses for some binaries show continuous light variations. These variations indicate limb–darkening on the eclipsed stars. Wood (1963) tabulates systems for which limb–darkening has been measured and the measured coefficients. However, the accuracy of the limb–darkening thus measured is so poor that the limb–darkening coefficients have not been used to determine the $T(\tau)$ structure for these stars.

For other stars astronomers have had to be content with obtaining $T(\tau)$ from model atmospheres calculated under several simplifying assumptions (this is discussed in section 3.3.2). It was therefore welcome when a suggestion was made by Matthews *et al.* (1990) (which I shall as of now refer to as the Matthews' technique) that it is possible to determine $T(\tau)$ empirically for the rapidly oscillating Ap stars (henceforth roAp stars). Before we go on to describe the Matthews' technique in detail it is informative to introduce the subject of this thesis, namely the roAp stars. We shall do this in two parts, in the first part we shall give general properties of the roAp stars as a sub–group, then we shall describe the properties of

those individual stars which we studied. This all forms the first chapter. The second chapter deals with data collection, reduction and analysis. Chapter 3 deals with the interpretation of the data in terms of the models made. The fourth and last chapter deals with the conclusion and discussion of the results obtained in chapter 3.

1.2 The chemically peculiar A–type stars

Lower main sequence stars of $T_{eff} \leq 7000\,K$ are remarkably homogeneous with respect to their rotation (which is uniformly slow) and their approximately solar chemical composition (Preston 1974). However in the temperature range $7000\,K \leq T_{eff} \leq 30000\,K$ lie several families of chemically peculiar (CP) stars. Preston (1974) distinguished four different groups based primarily on abundance anomalies amongst other criteria. The CP1 class contains non–magnetic and slowly rotating metallic line (Am) stars that occupy the temperature range $7400\,K \leq T_{eff} \leq 10200\,K$. The subject of this thesis, the rapidly oscillating Ap stars are a sub–group of the CP2 class which occupy the temperature range $7400\,K \leq T_{eff} \leq 23000\,K$. The rest of this section is devoted to the discussion of this class. The main sequence stars that show enhanced lines of Hg II and Mn II and no detectable magnetic fields are put in the CP3 class. They occupy the temperature domain $10000\,K \leq T_{eff} \leq 15000\,K$ and are slow rotators as well. Preston's CP4 class contains He–weak stars in the temperature domain $13000\,K \leq T_{eff} \leq 20000\,K$. Maitzen (1984) extended Preston's CP4 class to distinguish the magnetic He–weak stars (which he named CP4) and the non–magnetic He–weak stars (the CP5 class). He added two further classes: CP6, which contains the magnetic He–strong stars, and the CP7 class in which the non–magnetic He–strong stars belong.

The CP2 stars are for traditional reasons called Ap stars, even though they cover the spectral type B8p to F0p V–IV. Throughout this thesis I shall use the CP2 and Ap appellations interchangeably when referring to these stars. The rapidly oscillating stars are members of the cool SrCrEu subclass of the CP2 group. The CP2 group stars are characterised by strong global dipole magnetic fields with effective strengths of a few hundred to a few thousand gausses. Their spectra show enhanced lines of the Fe–peak elements and greatly enhanced lines of rare earth elements compared with spectra of normal stars.

The line strength anomalies are generally accepted to be mostly due to atmospheric abundance anomalies (as a result of radiative diffusion) rather than abnormal atmospheric structure. Diffusion (developed by Michaud 1970) occurs in stars whose atmospheres are stable enough against turbulent mixing that radiation pressure pushes those elements that have

many absorption lines near flux maximum to the surface of the star. This is because photons have momentum, and as they get absorbed by an element (an atom or ion) they add to the net momentum of such an element. Thus the more absorption lines an element has the more momentum it will have (as it absorbs each photon) to move in the direction of radiation. Elements that have few absorption lines near flux maximum or that are cosmically abundant, so that their lines are saturated (and cannot absorb any more photons) sink under their own weight in a sea of hydrogen. Michaud (1970) points out that in the Ap stars the magnetic fields can help provide the stability needed in the atmosphere for diffusion processes to become important.

Other attempts to explain the line strength anomalies involve the accretion of planetesimals, interior nuclear processes with mixing, surface nuclear processes and magnetic accretion from the interstellar medium. The diffusion hypothesis is most acceptable because of the following reasons:

- It can account qualitatively for the observed abundance anomalies.
- It is consistent with the requirement that the abundance anomalies be confined to thin layers of the atmosphere.
- It allows patchy abundance distribution by invoking various magnetic field geometries.
- It explains why Ap stars rotate slowly. Rotation distorts the shape of the star and sets meridional currents in motion whose speed increases with increasing rotational speed. There is a critical rotational velocity above which the meridional currents become turbulent. Thus stars rotating faster than their critical frequency cannot support diffusion because they have turbulent atmospheres.

The diffusion hypothesis, however, has too many free parameters to explain the observations quantitatively. The presence of strong magnetic field such as in Ap stars increases the number of free parameters in diffusion models (Alecian 1986). Another problem is that the diffusion velocities predicted are so small (10^{-4} to 1 $\mathrm{cm\,s^{-1}}$) that they require the star to be exceedingly stable against turbulence in the diffusion zones. Irrespective of these problems diffusion is the best hypothesis invoked to explain the Ap phenomenon so far.

These abundance anomalies are believed to be confined to a thin layer in the atmosphere for two reasons:

- Ap stars are observed to have only main sequence and subgiant luminosities, by the time Ap stars become giants, their line strength anomalies disappear.

- The abundances of certain rare earth elements (Eu for example, which is overabundant by a factor of 10^4 in some cases) are so great that a significant supply of such elements in the universe would be found in the Ap stars, if the observed abundances extended throughout the star.

Before I discuss the light variabilities in these stars I need to distinguish the mean light variations and the pulsational light variabilities. Throughout this thesis I will use the term 'mean light' to refer to light variability occurring on a time–scale of the rotation period in order to distinguish it from the light variations due to pulsation, which occur on a time scale of minutes (for roAp stars).

Early this century some Ap stars were found to be spectrum variables. The nature of these variations are such that not all elements vary in phase, although the lines of a given ion always appear to vary together (Deutsch 1947). The variable lines usually include those strong features that are characteristic of peculiar stars, including Sr, Cr and Eu. The phase relationships of various elements are not the same from star to star. In those Ap stars for which spectrum variations have been studied for a long time no changes in the period and phase are detected. This implies that Ap stars are rigid rotators, unlike the sun which shows differential rotation. This rigid rotation has been used together with spectrum variations to model the distribution of spots or areas on the surface where the anomalously strong lines originate.

In the second decade of this century light variations which are in phase (or antiphase) with spectrum variations were discovered in some Ap stars. It is now a well established fact that the majority of the Ap stars show these long–term light variations. The amplitudes range typically from 0.01 to 0.10 mag (Wolff 1983). Stepien (1968) compared his UBV measurements (of 16 Ap stars) with earlier measurements and found no evidence for long term changes in the periods, amplitudes or shapes of the light curves. Although the light variations are in phase with magnetic variations, the light variation amplitudes are not correlated with magnetic field strengths, periods of variation, spectral peculiarity, mean colours or line widths. The amplitude and character of the oscillations are wavelength dependent.

In the late 1940's H.W. Babcock discovered variable magnetic fields in some Ap stars. The measured fields varied in phase with the spectrum and light variations.

1.2.1 The oblique rotator model

The oblique rotator model was developed by Stibbs (1950) in order to account for the form of the magnetic, spectrum and light variations in the magnetic Ap stars. This model assumes the geometry shown in Figure 1.1. The magnetic field is frozen–in to the stellar atmosphere and has an axis inclined by an angle β to the rotation axis. The rotation axis is inclined by an angle i to the line–of–sight.

Let us consider the magnetic variations. Virtually all magnetic field observations in literature are of the mean longitudinal or effective magnetic field B_{eff} (Borra *et al.* 1982). The transverse component of the field is difficult to measure, it requires the measurement of the linear polarisation in the absorption lines, and linear polarisation is small for typical stellar magnetic fields and line profiles. Only a few measurements of the transverse component of the magnetic have been published. The mean surface magnetic field is only measurable for stars which show Zeeman splitting in their spectral lines. The B_{eff} is related to the polar field strength H_p by:

$$B_{eff} \propto H_p \, P_\ell \, (\cos \alpha) \tag{1.1}$$

where $P_\ell(\cos \alpha)$ is the Legendre polynomial appropriate to the magnetic field configuration, and α is the inclination of the magnetic field axis with respect to the line–of–sight (figure 1.1).

The cosine formula for spherical geometry, (see Smart 1977 for proof) when applied to the geometry in figure 1.1 gives

$$\cos \alpha = \cos \, i \cos \beta + \sin \, i \sin \beta \cos \Omega \, t \tag{1.2}$$

where $\Omega = 2\pi\nu_{rot}$ is the angular rotation frequency and phase zero is at the time of magnetic maximum.

For a dipole magnetic field $P_\ell(\cos \alpha) = \cos \alpha$, and equation 1.1 becomes

$$B_{eff} \propto \, H_p \cos \alpha \tag{1.3}$$

Substituting equation 1.2 into equation 1.3 we get

$$B_{eff} \propto \, H_p \cos \, i \cos \beta + H_p \sin \, i \sin \beta \cos \Omega \, t \tag{1.4}$$

Thus the field varies with the rotation period about a zero point proportional to $\cos \, i \cos \beta$ and an amplitude proportional to $\sin \, i \sin \beta$. It follows that studies of magnetic variations of

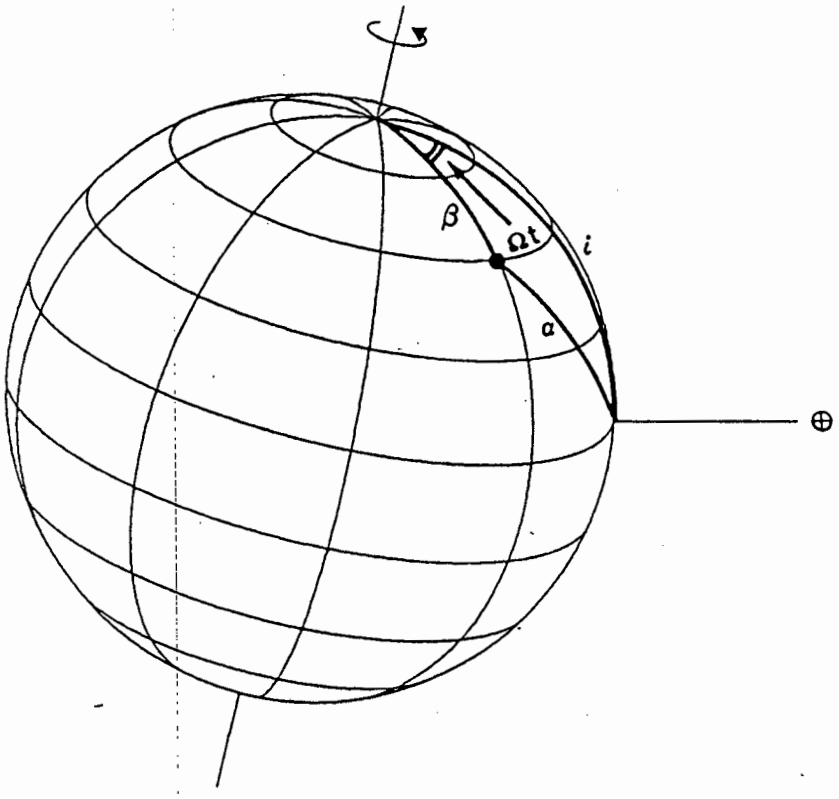

Figure 1.1: The geometry of an oblique rotator. The angle β (magnetic obliquity) is the inclination of the magnetic axis to the rotation axis, which is itself inclined to the line-of-sight by angle i. The angular rotation frequency is $\Omega = 2\pi\nu_{rot}$. Phase zero is taken to be at the magnetic maximum (from Kurtz 1990).

an oblique rotator can constrain its i and β values. The magnetic field variations in Ap stars are often characterised by a parameter r = $B_{eff}(min)/B_{eff}(max)$ for $-1 \leq r \leq +1$. This, when applied to magnetic variations of the form of equation 1.4 gives $\tan i \tan \beta = \frac{1-r}{1+r}$. Thus measurement of r puts constraints on the i and β values.

Spectrum variations are explained by assuming that the elemental abundance anomalies are not uniformly distributed over the stellar surface. Many elements and ions are overabundant or deficient in spots or rings that are approximately centered on the magnetic poles. So these patches will come in and out of view as the star rotates. Thus when a particular spot comes into view the anomalous lines become stronger or weaker. As it moves out of view they become weaker or stronger. The oblique rotator does not specify the physical mechanism producing line strength anomalies.

The light variations are thought to result from spectrum variations. Enhanced continuum and line opacity in the ultra–violet results in flux being distributed to longer wavelengths. So changes in line blanketing results in flux variations in the visible.

1.3 The properties of rapidly oscillating Ap stars

1.3.1 Introduction

I give a brief history of how the rapidly oscillating Ap stars were discovered. I then discuss those properties of the roAp stars that are relevant to the aims and objectives of this thesis. Before I go on, I introduce a class of pulsating stars called δ Scuti stars.

The δ Scuti stars occupy a region in the lower instability strip (where it crosses the main sequence among the A stars). They pulsate in low–overtone radial and non–radial p modes, with periods in the range 30 minutes to 6 hours. Their pulsation amplitudes in V range from a few thousandths of a magnitude to 0.8 mag. Pulsation in the δ Scuti stars is driven by the κ mechanism operating in the He II ionization zone. The diffusion hypothesis has been used to distinguish between δ Scuti stars and Ap stars. In the Ap stars, because they are slow rotators, diffusion occurs and causes helium to drain out of the He II zone, resulting in a non–pulsating Ap (or Am) star. The diffusion is inhibited by meridional currents in a rapidly rotating star. Such a star (where diffusion is inhibited) results in a chemically normal star that could become a δ Scuti star. It is this near exclusion between Ap stars and δ Scuti stars that led to the discovery of the roAp stars.

There has been a long–standing argument about the effective temperature of HD 101065. This is because of its exceedingly complex spectrum which makes it difficult to estimate its temperature and luminosity. Don Kurtz and Gary Wegner believed HD 101065 to be an Ap star because of the discovery of spectra that are qualitatively similar to that of HD 101065 in Ap stars HD 51418 (Jones *et al.* 1974) and HR 465 (Hartoog *et al.* 1973), and the discovery of the strong magnetic field (-2.2 kG) in HD 101065 (Wolff & Hagen 1976). If HD 101065 were an Ap star, then it should not pulsate, according to the diffusion arguments I mentioned above. So Kurtz tested HD 101065 for pulsations first by using two comparison stars (differential photometry). The appearance of the light curve suggested that oscillations were occuring on a short time–scale. When he observed using continuous integrations (high speed photometry) he discovered rapid oscillations of period 12.14 minutes in HD 101065. Since then, more roAp stars have been discovered, and at present there are 28 known roAp stars. A listing of all known roAp stars with their summarised properties is shown in Table 1.1 taken from Martinez (1996).

The roAp stars are high overtone, low degree non–radial p mode pulsators with periods between 5.6 and 15 minutes. Their pulsation semi–amplitudes are under 8 mmag in Johnson B.

I would like to list the major tools that are used in investigating the properties of roAp stars:

- The oblique pulsator model. This is used for determining the rotation periods and constraining the geometries of the star and is also valuable for mode identification. This tool is only useful where rotational frequency splitting is observed in the pulsation amplitude spectrum. This often involves collecting good quality data through multi–site campaigns. I discuss this in detail in section 1.3.2.

- Some techniques of asteroseismology that are applicable to roAp stars, the primary one being the asymptotic relation (Tassoul 1980, 1990) for high overtone, low order pulsators. This is used mainly for mode identification and potentially can be used as a mass and age indicator. The $T_{\rm eff}$ and the frequency spacing of the various independently excited modes enables asteroseismological luminosities of roAp to be determined (Martinez 1993) (this is discussed in section 1.3.3).

- The O–C diagrams for determining the nature of frequency variations observed in some roAp stars (HR 3831, α Cir, HD 134214, HD 137949, HD 101065, HR 1217 and HD 12932). Table 1.1 shows references to the latest analyses of these stars. An O–C diagram is a plot of the observed pulsation phase minus the phase calculated on the

Table 1.1: A summary of the properties of p mode spectra of the roAp stars (reproduced from Martinez 1996).

HD *HR*	V	ΔB [a] mmag	ν [b] μHz	N_ν [c]	$\Delta\nu$ [d] μHz	P_{rot} d
6532	8.4	5	2402	1		1.944973
9289	9.4	3.5	1585	>3?	20 or 30	?
12932	10.2	4	1436	1		?
19918	9.3	2.8	1510	2	30 ± 1 d^{-1}	?
24712	6.0	8	2688	6	34	12.4572
1217						
42659	6.8	0.8	1736?	> 1?		?
60435	8.9	8	1043–1433	> 10?	25.8	7.6793
80316	7.8	1.5	2252	1		inconclusive
83368	6.2	8	1428	1		2.851982
3831						
84041	9.3	2	1113	4?	31	3.69
86181	9.3	4.6	2688	> 1?		?
101065	8.0	13	1373	3	58	?
119027	10.0	2	1914	5	26	?
128898	3.2	5	2442	5	25	4.4790
5463						
134214	7.5	7	2950	1		?
137949	6.7	3	2015	> 1?	40?	?
150562	9.8	1.5	1559 or 1547	> 1?		?
161459	10.3	2.4	1390	> 1?		?
166473	7.9	1.4	1881 or 1892	3?	36?	?
176232	5.9	1.2	1436	3	50	?
7167						
185256	9.9	3	1630	> 1?		?
190290	9.9	2.3	2270	2	40	?
193756	9.2	1.7	1284	1		?
196470	9.7	1.4	1544	> 1?		?
201601	4.7	2	1365	4	30	> 70 yr
8097						
203932	8.8	1.6	2805	4?	33	?
217522	7.5	2.6	1200	3	15	?
218495	9.4	2.3	2240	1		?

[a] This is the typical peak-to-peak variation for a night when the star is "up" in amplitude.
[b] For multi-periodic stars the frequency of the mode with the highest amplitude is listed.
[c] This column lists the number of modes observed/suspected in a given star.
[d] This column lists the *observed* frequency spacing (i.e. no values multiplied by 2).

Table 1.1: continued ..

HD *HR*	Harmonics	Mode changes	Frequency changes	Distorted dipole	Well studied	Reference
6532	√	×	×	√	√√√	Kurtz96
9289	×	?	?		√	Kurtz94b
12932	√	×	√		√√	Marti94e
19918	√	×	×		√√	Marti95
24712	×	√	√		√√√	Kurtz89a
1217						
42659	×	?	?		×	Marti94c
60435	×	√	×		√√	Matth87
80316	×	×	?		×	Kurtz90b
83368	√	×	√	√	√√√	Kurtz94
3831						
84041	×	√	?		√	Marti93
86181	×	?	?		×	Kurtz94c
101065	√	×	√		√√√	Marti90
119027	×	√	?		√	Marti93a
128898	√	×	√		√√	Kurtz94a
5463						
134214	×	×	√		√√	Kreid94
137949	√	×	√		√	Kurtz91
150562	×	?	?		×	Marti94c
161459	√	?	?		×	Marti91
166473	√?	?	?		√	Kurtz87
176232	×	?	?		√	Helle90
7167						
185256	×	?	?		×	Kurtz95
190290	×	?	?		×	Marti91
193756	×	?	?		×	Marti91
196470	×	?	?		×	Marti91
201601	×	√	×		√√	Marti96
8097						
203932	×	√	×		√	Marti90a
217522	×	√	?		√√	Kreid91a
218495	√	?	?		×	Marti91

Helle90 = Heller & Kramer, 1990, MNRAS, 244, 372; **Kreid91a** = Kreidl et al., 1991, MNRAS, 250, 477; **Kreid94** = Kreidl et al., 1994, MNRAS, 270, 115; **Kurtz87** = Kurtz & Martinez, 1987, MNRAS, 226, 187; **Kurtz89a** = Kurtz et al., 1989, MNRAS, 240, 881; **Kurtz90b** = Kurtz, 1990, MNRAS, 242, 489; **Kurtz91** = Kurtz, 1991, MNRAS, 249, 468; **Kurtz94** = Kurtz et al., 1994, MNRAS, 268, 641; **Kurtz94a** = Kurtz et al., 1994, MNRAS, 270, 674; **Kurtz94b** = Kurtz et al., 1994, MNRAS, 271, 421; **Kurtz94c** = Kurtz & Martinez, 1994, IBVS, 4013; **Kurtz95** = Kurtz & Martinez, 1995, IBVS, 4209; **Kurtz96** = Kurtz et al., 1996, MNRAS, in press; **Marti90** = Martinez & Kurtz, 1990, MNRAS, 242, 636; **Marti90a** = Martinez et al., 1990, MNRAS, 246, 699; **Marti91** = Martinez et al., 1991, MNRAS, 250, 666; **Marti93** = Martinez et al., 1993, MNRAS, 263, 273; **Marti93a** = Martinez et al., 1993, MNRAS, 260, 9; **Marti94c** = Martinez & Kurtz, 1994, MNRAS, 271, 118; **Marti94e** = Martinez et al., 1994, MNRAS, 271, 305; **Marti95** = Martinez et al., 1995, MNRAS, in press; **Marti96** = Martinez et al., 1996, MNRAS, in press; **Matth87** = Matthews et al., 1987, ApJ, 313, 782;

basis of constant frequency as a function of time. The following observations can be made about such plots:

1. If the frequency and phase are constant, then the O–C is a horizontal straight line.
2. If too small a frequency is used then the O–C diagram is a straight line with negative slope.
3. If too big a frequency is used then the O–C diagram is a straight line with positive slope.
4. If the frequency is constant, but the phase changes discontinuously, the O–C lies along horizontal lines with discrete changes in zero points at the discontinuities.
5. If frequency or phase (or both) are continuously variable, the O–C diagram is non–linear. It is not possible to distinguish between continuously variable phase and continuously variable frequency in the O–C diagram, however. To distinguish one has to look at the physics of the situation.

Some of the possible physical causes of the frequency changes are stellar evolution (Heller & Kawaler 1988) which results in a quadratic curve in the O–C diagram, and the Doppler shift caused by binary motion which results in cyclic variation in the O–C. A circular orbit shows a sinusoid in the O–C diagram. Heller & Kawaler (1988) noted from the asymptotic relation for high overtone p mode pulsators that frequency changes due to stellar evolution can be measured. They also noted that frequency spacing is an age indicator, thus they show that measuring the secular frequency changes could identify the evolutionary stage of star. Note that this assumes high over–tone p mode pulsators, so it should be applicable to roAp stars. However, for all the roAp stars which show frequency changes, the nature of such changes is such that either the frequency changes are cyclic as in HR 3831 (Kurtz *et al.* 1994a), α Cir (Kurtz *et al.* 1994b) and HD 134214 (Kreidl *et al.* 1994), or for those that have secular frequency changes (such as that observed in HD 101065 (Martinez & Kurtz 1990)) the changes are several orders of magnitudes greater than those predicted by Heller & Kawaler's models. Stellar evolution should give rise to a constant rate of change in the pulsation period.

- Kurtz & Medupe (1996) have proposed a technique that enables one to study level effects on the pulsational temperature amplitude of roAp stars with dipole pulsation modes. This is the subject of this thesis. This technique arises out of an idea proposed

by Matthews (1990) that the pulsation amplitude as a function of wavelength of roAp stars gives a measure of the empirical T(τ), an idea which I show to be incorrect in section 3.2.1.

The tools mentioned above are discussed in detail in the following subsections.

1.3.2 The Oblique Pulsator Model

This thesis deals with stellar pulsations, and therefore it is necessary to introduce some of the terminology I am going to use before I proceed.

Non–radial stellar oscillations

If a non–rotating, non–magnetic star in hydrostatic equilibrium experiences small non–radial perturbations, its displacement is given by:

$$\xi_{n,\ell,m} = A_n(r)\, Y_\ell^m(\theta,\phi)\, e^{-i2\pi\nu t} \tag{1.5}$$

where $A_n(r)$ is the displacement amplitude as a function of stellar radius, Y_ℓ^m is the appropriate spherical harmonic and ν is the pulsation frequency. The coordinates θ (the co–latitude) and ϕ (the longitude) refer to the stellar surface. The spherical harmonic is expressed in terms of the Legendre polynomial $P_\ell^m(\cos\theta)$ as follows:

$$Y_\ell^m(\theta,\phi) = (-1)^m \sqrt{\frac{(2\ell+1)(\ell-m)!}{4\pi\,(\ell+m)!}} P_\ell^m(\cos\theta)\, e^{i\,m\phi}. \tag{1.6}$$

The indices n, ℓ, m, which characterise each pulsation mode are integers. I describe them below:

1. The overtone n gives the number of nodes in the radial direction (not true for centrally condensed stars). Stars that pulsate in high frequency p modes (to be discussed below) are characterised by high n values. A mode for which $n = 0$ is called a fundamental mode, $n = 1$, the first overtone, $n = 2$, the second overtone *e.t.c.*

2. The spherical index ℓ (also called the degree) gives the total number of the surface nodal lines. When there are no nodal lines on the stellar surface, $\ell = 0$ and the star pulsates radially. The ℓ value takes on $\ell = 0, 1, 2, ...$

3. The azimuthal order m is the number of nodal lines that are parallel to the lines of longitude on the stellar surface. The value of m runs from $-\ell$ to $+\ell$.

The angular dependence of the variation in luminosity ($\frac{\Delta L}{L}$) and other physical variables (density $\frac{\Delta \rho}{\rho}$ and pressure $\frac{\Delta p}{p}$) is the same as in equation 1.5.

The pulsation frequency of a non–rotating star depends on n and ℓ and is $(2\ell + 1)$–fold degenerate. This degeneracy is lifted by rotation so that the frequency which appears to be single for a non–rotating star will be split into $2\ell + 1$ components, each given by (Ledoux 1951)

$$\nu_m = \nu_o + m(1 - C_{n\ell})\nu_{rot}, \tag{1.7}$$

where ν_o is the frequency of a pulsating non–rotating star, and $C_{n\ell}$ is a constant that depends on the equilibrium structure of the star and on the pulsation mode. The rotation frequency is given by ν_{rot}.

Pulsations are also classified according to the restoring force. The dominant restoring forces are gravity and pressure for a star in hydrostatic equilibrium. At high frequencies the pressure oscillations dominate and the resulting pulsation modes are called p modes. The p modes consist of standing acoustic waves. The g modes develop when gravity as a restoring force dominates at low frequencies.

The analysis of the pulsation amplitude spectra of some roAp stars show equally spaced multiplets and pulsation amplitude modulation (see Kurtz 1982 for the initial analysis of HD 24712, HR 3831 and HD 137979). An attempt to explain this frequency splitting in terms of the rotationally perturbed m–modes (equation 1.7) has been rejected (Kurtz 1982, 1990) on the grounds that the measured $C_{n,\ell}$ are too small compared to the ones calculated from the pulsation models. Shibahashi & Saio 1985 determined that $10^{-2} \leq C_{n,\ell} \leq 10^{-3}$ for the roAp stars. The values that have been measured for $C_{n,\ell}$ are $C_{n,\ell} \leq 6 \times 10^{-4}$ for HR 1217 (Kurtz *et al.* 1989) and $C_{n,\ell} \leq 2 \times 10^{-5}$ for HR 3831 (Kurtz *et al.* 1992). The fact that the time of pulsation maximum and magnetic maximum are coincident suggests that $C_{n,\ell} = 0.0$, otherwise they must drift apart on a time scale proportional to $\frac{1}{C_{n,\ell}\Omega}$.

A possible mechanism that can produce amplitude modulation with the rotation frequency is constant amplitude pulsation superimposed on a variable background. This is possible in roAp stars since their mean light varies with the rotation phase (see section 1.2). However, Kurtz (1982) shows that the mean light in B varies by about 6% for HD 24712 (and by 1% in HR 3831), whereas the pulsation amplitude varies (in HD 24712) by a factor of about 5. Thus, this mechanism cannot explain the observed amplitude modulation.

The Oblique Pulsator Model

A better model that fits the data well is the oblique pulsator model suggested by Kurtz

(1982). This model assumes an oblique rotator, and that each pulsation mode can be described by a single spherical harmonic with its pulsation axis aligned with the magnetic axis. Thus, as a star rotates the pulsation amplitude will be modulated as the magnetic (pulsation) axis points in different directions. Figure 1.2 demonstrates this clearly.

When the effects of rotation and magnetic field are ignored, the luminosity variations due to a non–radial mode of degree ℓ are given (from equation 1.5) by:

$$\frac{\Delta L}{L} \propto P_\ell(\cos\alpha)\cos(\omega t + \phi) \tag{1.8}$$

where $\omega = 2\pi\nu$ is the angular pulsation frequency, and α is the inclination of the pulsation (magnetic) axis with respect to the line–of–sight. $P_\ell(\cos\alpha)$ is the associated Legendre polynomial. For a dipole mode $(\ell, m) = (1, 0)$ and $P_\ell(\cos\alpha) = \cos\alpha$. Using equation 1.2 I find that

$$\frac{\Delta L}{L} \propto A_{-1}\cos[(\omega - \Omega)t + \phi] + A_o\cos[\omega t + \phi] + A_{+1}\cos[(\omega + \Omega)t + \phi], \tag{1.9}$$

where

$$A_o = \cos i \cos\beta, \tag{1.10}$$

$$A_{-1} = A_{+1} = \frac{1}{2}\sin i \sin\beta. \tag{1.11}$$

Equation 1.9 indicates that an oblique dipole mode pulsator gives rise to a frequency triplet with a spacing that is equal to the rotation frequency. The central frequency component is at ω and the rotational sidelobes are at $\omega \pm \Omega$. In general, the oblique pulsator model predicts that a mode of degree ℓ will be split into $(2\ell + 1)$ components.

In Ap stars a parameter used to characterise magnetic fields is $r = \frac{B_{eff(min)}}{B_{eff(max)}}$ so that for an oblique rotator $\tan i \tan\beta = \frac{1-r}{1+r}$. A similar parameter is defined for an oblique pulsator $r_{puls} = \frac{1-\frac{A_{+1}+A_{-1}}{A_o}}{1+\frac{A_{+1}+A_{-1}}{A_o}}$. There is a good agreement between the measured values of r and r_{puls} in a few cases where this has been done. Figure 1.2 also shows that a phase reversal occurs at quadrature for a dipole oblique pulsator, indeed this has been observed in HR 3831 and HD 6532 (Kurtz 1990). The problem with this simplified oblique pulsator model is that it predicts that A_{-1} and A_{+1} are equal, whereas it has been observed that this is not true in general for those roAp stars on which the oblique pulsator model has been applied. Another problem is to explain the alignment of the magnetic field and pulsation axes, this was just an *ad hoc* assumption motivated only by observations.

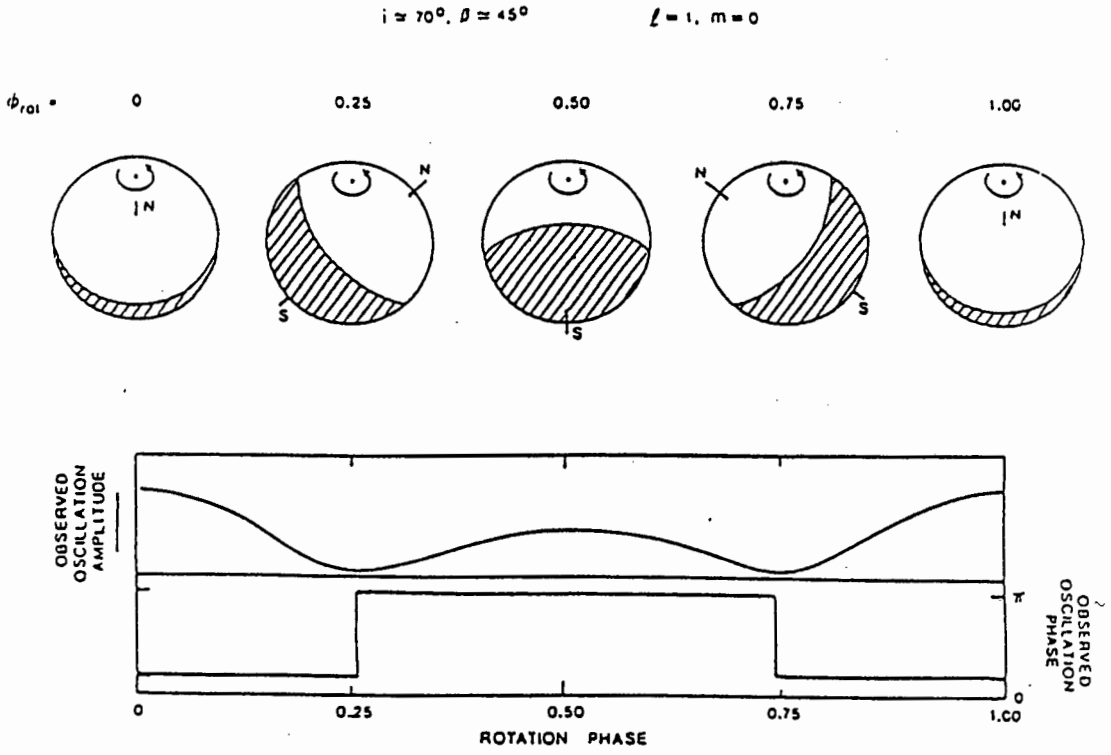

Figure 1.2: This schematic diagram traces an roAp star pulsating in a dipole mode through one rotation cycle. The upper part shows the actual geometry at various rotation phases. The variation of the amplitude with rotation phase ϕ_{rot} is plotted underneath the sketch. Notice that at quadrature, $\phi_{rot} = 0.25$ and $\phi_{rot} = 0.75$, the amplitude is minimum. When one of the pulsation poles is facing the observer the amplitude is a maximum. There is a π radians phase reversal at quadrature where there is polarity reversal in the magnetic field. The shaded portion of the disk represents that portion of the star varying in anti-phase to the other hemisphere of the dipole mode. The north and south poles of the pulsation (magnetic) axis are shown by N and S (from Matthews 1991).

Dziembowski & Goode (1985, 1986) generalised the oblique pulsator model to include the effects of the magnetic field and rotation. They showed that the pulsation axis locks to the magnetic axis naturally if the perturbation to the eigenfrequencies by the magnetic field dominates the perturbation due to rotation. Their results will be given here, without going into detail about the derivations. If the magnetic perturbation to the (ℓ, m) mode is $\omega_{|m|}^{(1)mag}$, then the perturbed frequency is given as:

$$\omega = \omega^{(0)} + \omega_{|m|}^{(1)mag} \tag{1.12}$$

where $\omega^{(0)}$ is the unperturbed frequency in the rest frame of the star. Dziembowski & Goode (1985) give the following

$$\omega_{|m|}^{(1)mag} \propto \frac{\ell(\ell+1) - 3m^2}{4\ell(\ell+1) - 3} K^{mag}, \tag{1.13}$$

where K^{mag} is a $|Y_\ell^m|^2$ -weighted integration over the P_2 distortion caused by the magnetic field. The calculated luminosity variation for an $(\ell, m) = (1, 0)$ mode (Kurtz & Shibahashi 1986) is:

$$\begin{aligned} \frac{\Delta L}{L} \propto\ & \frac{1}{2}\sin i \sin\beta \left(1 - \frac{C_{n,\ell}\Omega}{\omega_1^{(1)mag} - \omega_0^{(1)mag}}\right) \cos[(\omega^{(0)} + \omega^{(1)mag} - \Omega)\, t + \phi] \\ & + \cos i \cos\beta \cos[(\omega^{(0)} + \omega_0^{(1)mag})\, t + \phi] \\ & + \frac{1}{2}\sin i \sin\beta \left(1 + \frac{C_{n,\ell}\Omega}{\omega_1^{(1)mag} - \omega_0^{(1)mag}}\right) \cos[(\omega^{(0)} + \omega^{(1)mag} + \Omega)\, t + \phi]. \end{aligned} \tag{1.14}$$

Equation 1.14 reduces to equation 1.9 when the effect of the magnetic field is neglected ($\omega_{|m|}^{(1)mag} = 0$) and when the Coriolis force is neglected as well ($C_{n,\ell} = 0$). What is noticeable is the fact that the amplitudes of the sidelobes are not equal, in agreement with observations. The amplitudes are given as:

$$A_{-1}^1 = \frac{1}{2}\sin i \sin\beta \left(1 - \frac{C_{n,\ell}\Omega}{\omega_1^{(1)mag} - \omega_0^{(1)mag}}\right) \tag{1.15}$$

$$A_0^{(1)} = \cos i \cos\beta \tag{1.16}$$

$$A_{+1}^1 = \frac{1}{2}\sin i \sin\beta \left(1 + \frac{C_{n,\ell}\Omega}{\omega_1^{(1)mag} - \omega_0^{(1)mag}}\right) \tag{1.17}$$

Once again the angles i and β are constrained by

$$\frac{\left(A_{+1}^{(1)} + A_{-1}^{(1)}\right)}{A_0^{(1)}} = \tan i \tan\beta. \tag{1.18}$$

One can also show that

$$\frac{(A_{+1}^{(1)} - A_{-1}^{(1)})}{(A_{+1}^{(1)} + A_{-1}^{(1)})} = \frac{C_{n,\ell}\Omega}{(\omega_1^{(1)mag} - \omega_0^{(1)mag})}. \tag{1.19}$$

Equation 1.13 and 1.19 combine to give the following expression of K^{mag}

$$K^{mag} = \frac{-5\,C_{n,\ell}\Omega}{3}\frac{(A_{+1}^{(1)} + A_{-1}^{(1)})}{(A_{+1}^{(1)} - A_{-1}^{(1)})}. \tag{1.20}$$

K^{mag} is a measure of the magnetic field, hence the amplitudes of the rotational sidelobes are a measure of the magnetic field strength. The measurements of K^{mag} for various modes in a single star enable the internal structure of the magnetic field to be modelled.

In summary, the oblique pulsator model has provided valuable information about the roAp stars. It helps constrain the geometrical and magnetic properties of these stars and allows the rotation periods to be easily measured. The most valuable information (as far as asteroseismology of roAp stars and this thesis is concerned) is that it provides an alternative technique (to Balona & Stobie's 1979b technique) for pulsation mode identification.

A technique for mode identification for non–radial pulsators was developed by Balona & Stobie (1979b). It involves determining the spherical index ℓ from the phase difference between the light and colour curves $\Delta\phi\,(B-V,V) = \phi(B-V) - \phi(V)$, for example. Although this technique has been applied successfully to β Cep, 53 Per, δ Scuti, Cepheid and ZZ Ceti variables, it fails dismally when applied to roAp stars (Watson 1988). The roAp stars where the application of Balona and Stobie's technique has been attempted (unsuccessfully) are HR 3831 (Kurtz 1982), HD 101065 (Kurtz 1980; Kurtz & Wegner 1979), α Cir (Kurtz & Balona 1984; Weiss & Schneider 1984), HD 6532 (Kurtz & Kreidl 1985) and HD 24712 (Weiss 1986).

The Spotted Pulsator Model

For completeness I shall mention a model that was proposed as an alternative to the oblique pulsator model, namely the spotted pulsator model.

The spotted pulsator model was suggested by Mathys (1985) as an attempt to show that it is not necessary to assume that the pulsation axis is aligned to the magnetic axis in order to describe the frequency spectrum and amplitude modulation of HR 3831. Mathys (1985) points out that the surface inhomogeneities may cause an inhomogeneous distribution in the

ratio of the flux to radius variations, f, and in the phase lag ψ between the flux and radius variations. The contribution to luminosity variation is due to two factors; the flux variations and the surface area variations. The quantity f measures the relative importance of the flux variations compared to the surface area variations. Mathys showed that by varying f and ψ over the surface, within reasonable limits, the spotted pulsator model can describe the amplitudes in the frequency spectrum of HR 3831 with a single dipole mode aligned with the rotation axis.

The spotted pulsator model failed two observational tests. The first was the observation by Matthews *et al.* (1988) that the radial velocity in HR 1217 is amplitude modulated in phase with the light amplitude. The oblique pulsator model predicts exactly this, whereas the spotted pulsator does not. It is possible to have radial velocity amplitude modulation (by beating of the frequencies) in a spotted pulsator, if the star is multi–periodic (HR 1217 has six pulsation frequencies). However, Matthews *et al.* observed for 5 hours on each of the two nights, which should have averaged over many of the beat cycles of HR 1217 's six frequencies. The second piece of evidence in favour of the oblique pulsator model is the fact that the time of pulsation maximum in HR 1217 (which coincides with the time of magnetic maximum) differs from the time of the mean light minimum by 3σ (Kurtz *et al.* 1989) and by 5σ for HR 3831 (Kurtz *et al.* 1992). In the spotted pulsator model the pulsation maximum should coincide with the mean light extremum because the variations in f and ψ are caused by the surface inhomogeneities.

1.3.3 Asteroseismology

We have seen how the amplitude spectra of the roAp stars can be used to determine their geometrical properties. Here we discuss a field of study devoted to using pulsation frequencies to probe the atmospheres and interiors of stars, in the same way that geophysicists model the earth's interior structure by tracing the refracted paths of the pressure waves travelling through the earth's interior.

Asteroseismology is an extension of helioseismology which started when Leighton, Noyes & Simon (1962) set out to study the velocity patterns of gases on the solar surface by measuring Doppler shifts in solar absorption lines. Instead of finding random Doppler shifts (in line with the chaotic changes in brightness of the solar granulation), they discovered short lived wave patterns on the surface all having a characteristic period of 5 minutes. The "five–minute" solar oscillations remained a mystery for a long while until Ulrich (1970) and Leibacher &

Stein (1971) independently proposed that the "five–minute" oscillations are a manifestation of sound waves trapped inside the acoustic cavities within the atmosphere and the interior of the sun.

The extension of helioseismology to oscillations of stars other than the sun is not easy. This is because stars are far away so we only receive integrated light from them, no disk–resolved information. Only modes of low degree will produce variations large enough to be seen in integrated light or velocity. And even for these low degree modes we can only measure their amplitudes and frequencies. Despite these limitations a great deal of information can still be obtained from studies of frequencies and amplitudes (especially of multi–periodic stars). I shall show one such application (for high overtone pulsators) after discussing acoustic cavities in detail.

I shall go on to describe how an acoustic cavity might be set up in a stellar interior. The speed and direction of sound waves in a medium are dependent primarily on the temperature, composition, mass motions and density of the medium. In particular, the higher the temperature, the higher the speed of sound. Therefore, it is conceivable that pressure waves penetrating obliquely into the atmosphere will be refracted backwards towards the surface. This happens because as the waves go deeper into the atmosphere they are going into high temperature regions. Consequently the deeper part of the wavefront travels faster than the trailing part. On their way towards the upper part of the photosphere the waves follow paths of steeply decreasing density. The sharp decrease in density near the surface reflects the waves back. The waves thus trapped trace a series of arcs along the circumference (beneath the surface). They interfere constructively with themselves to produce a standing wave. The surface oscillations we see are a manifestation of these standing waves. Figure 1.3. demonstrates how an acoustic wave is set up.

For any given cavity there is an upper limit for its eigenfrequencies called the critical (or cut–off) frequency ν_{crit}. Shibahashi & Saio (1985) give an expression for the critical frequency for the existence of a standing wave. They attribute this to finite pressure scale heights (and since scale heights are proportional to temperatures) hence to non–zero surface temperature. Any standing wave with frequencies higher than the critical frequency will not be reflected at the upper boundary of the acoustic cavity, but will dissipate into the higher atmospheric regions and become evanescent. Shibahashi & Saio (1985) calculated ν_{crit} for standard A star models of various chemical composition and masses. They derived that $\nu_{\rm crit} < 2\,{\rm mHz}$ for roAp stars. Many of the roAp stars have pulsation frequencies greater than 2 mHz. The possible reason for this discrepancy is that the models Shibahashi & Saio used are homogeneous, and do not include the effects of magnetic fields. The strong magnetic pressure decreases the gas

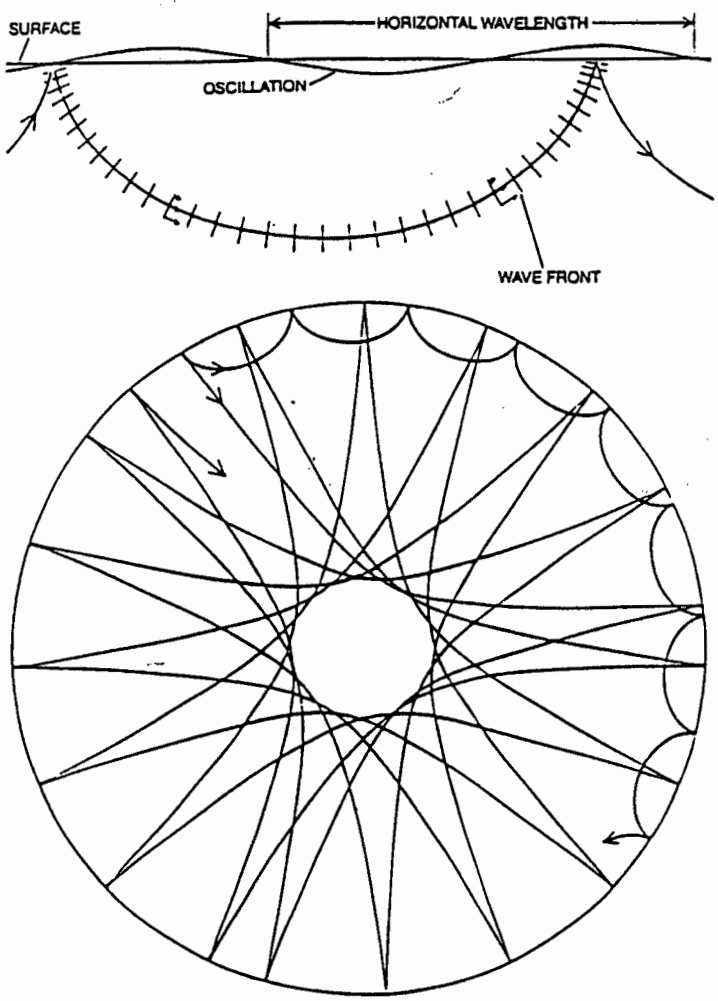

Figure 1.3: The boundaries of a stellar acoustic cavity are defined by the reflection layer near the stellar surface and the inner refraction layer. The upper part of this diagram demonstrates how the wave is refracted as it traverses regions of different temperatures. The horizontal wavelength is defined as well. The horizontal wavelength and period of the surface oscillations depend on the period of the internal standing wave and the depth of the cavity. Modes of high ℓ values are confined to shallow acoustic cavities. Modes of low ℓ values penetrate into deeper regions. (From Leibacher *et al.* 1990).

pressure and hence lowers the surface temperature. The strong magnetic tension will impede convective motion with the result that the heat flux will be inhomogeneous on the stellar surface. The net effect of these two phenomena is to produce large scale cool regions over each of the magnetic poles. This will increase the critical frequencies. Another effect which could increase the critical frequency is line blanketing by over–abundant elements at the magnetic poles. It increases the temperature gradient, so that the surface layers are cooler than for normal stars. Dolez *et al.* (1988) find that models with enhanced He driving at the magnetic poles have some excited modes with frequencies higher than their critical frequencies. They caution that the lower surface temperature suggested by Shibahashi & Saio for HR 1217 might not be necessary to explain the observed frequencies. This all calls for better model atmospheres of Ap stars. An important point to notice about the ν_{crit} arguments is that they suggest that the Ap stars may have abnormal atmospheric structure. This together with abnormal atmospheric abundances might explain the line strength anomalies and other Ap phenomena.

The roAp stars are high overtone and low degree (p mode) pulsators, and as such their eigenfrequencies can be described by the asymptotic relation of Tassoul (1980, 1990):

$$\nu_{n\ell} \approx \Delta\nu\,(n + \ell + \epsilon) + \delta\nu, \tag{1.21}$$

where ϵ is a constant that depends on the equilibrium structure of the star, and $\delta\nu$ is a second order term. $\Delta\nu$ is the uniform spacing of the eigenfrequencies and is given by

$$\Delta\nu = \left(2\int_0^R \frac{dr}{c(r)}\right)^{-1}, \tag{1.22}$$

where c(r) is the local speed of sound, so that $\Delta\nu$ is the inverse of the time taken by the sound wave from the surface to the core and back to the surface. The value of $\Delta\nu$ obtained for the sun is $135\,\mu$Hz and the values for roAp stars are $30\,\mu\text{Hz} \leq \Delta\nu \leq 70\,\mu$Hz. The smaller values of $\Delta\nu$ for the roAp stars compared to the sun are consistent with the larger radii typical of roAp stars.

The consecutive overtones (n, $n+1$) of modes having exclusively even or odd ℓ values have frequency separation $\Delta\nu$, and modes with alternating even and odd ℓ values will be spaced by $\frac{\Delta\nu}{2}$ according to equation 1.21. The spacing $\Delta\nu$ is sensitive to radius and mass and can be used to derive asteroseismological luminosities if the T_{eff} is known (Martinez 1993).

The second order term $\delta\nu$ in equation 1.21 lifts the degeneracy that exists for modes (n, ℓ) and $(n \pm 1, \ell \mp 2)$ by a small frequency spacing $\delta\nu$, which is much less than $\Delta\nu$. The physical

meaning of this is that modes (n, ℓ) and $(n \pm 1, \ell \mp 2)$ appear to have the same structure outside the stellar core, but will have different structure inside the core as is shown in Figure 1.4. The second–order term is sensitive to the sound speed gradient inside the star. The sound speed gradient is determined by the molecular mass gradient in the core. As H gets converted to He in the stellar core the molecular mass gradient changes, so the sound speed gradient changes as the star evolves. Thus $\delta\nu$ is an age indicator.

1.3.4 The Matthews' technique

Classical pulsators show a decrease in pulsation amplitude with wavelength which is consistent with that of a pulsating black–body (Matthews 1996). However, within few years of discovery of the roAp stars, multi–colour photometry (Weiss & Schneider 1984) showed that the pulsation amplitudes of roAp stars decline rapidly with increasing wavelength, more so than for classical pulsators. The Matthew's technique was suggested as an attempt to explain this rapid decline. The wavelength dependence of the pulsation amplitude for a black–body radiator is derived in chapter 3.

The Matthews' technique was motivated by the following observations:

1. In all of the roAp stars where mode identification has been successfully done, they have been found to pulsate in dipole modes (Kurtz 1990; Martinez 1993, 1996). As is shown in chapter 3, this makes it easy to model the pulsation of roAp stars, because dipole mode light variations are due entirely to temperature variations.

2. Irrespective of the inclination α of the dipole pulsation mode with respect to the line–of–sight, limb–darkening has the effect of increasing the pulsation amplitude. This does not apply for $\alpha = 90°$ where the two hemispheres of the dipole mode vary in anti–phase to each other and (since they contribute equally on the visible disk) produce a net amplitude of zero. Our analytical results in chapter 3 illustrates this point well. Matthews *et al.* (1990) supposed (reasonably so) that if limb–darkening has strong dependence on wavelength, the pulsation amplitude also has a strong dependence on wavelength. In particular, if limb–darkening drops steeply from the shorter wavelengths to longer wavelengths, then the observed pulsation amplitude will do like–wise. It needs to be qualified that this can be true only if limb–darkening is a big effect in pulsations. I shall show in chapter 3 that this is not the case.

Matthews *et al.* (1990) thus sought to explain the precipitous decline of the amplitude with wavelength by weighting the dipole mode with the strongly wavelength dependent limb–darkening. They reported a steeper dependence of limb–darkening coefficients on wavelength

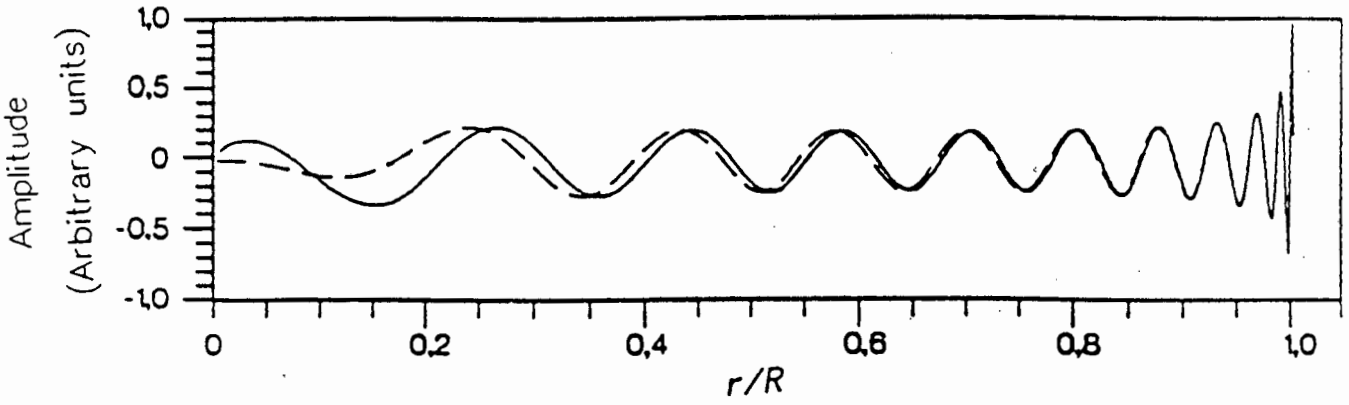

Figure 1.4: An example of the structures of modes ($n = 20, \ell = 1$) and ($n = 19, \ell = 3$). They look the same outside the stellar core, but are different inside the core. The second–order term is a measure this difference. (Taken from Belmonte *et al.* 1991).

for HR 3831 than that of the sun. A steeper limb–darkening dependence on wavelength implies a steeper $T(\tau)$ gradient. This result could not only explain the sharp decline of amplitude with wavelength, but was also consistent with the results of Shibahashi & Saio (1985) who suggested a steeper $T(\tau)$ in order to explain why some roAp stars have eigenfrequencies higher than the acoustic cut–off frequency (discussed in section 1.3.3).

Matthews *et al.* (1990) measured limb–darkening coefficients for HR 3831 by measuring the pulsation amplitudes at various wavelengths, and comparing them with the results of a pulsating black–body model without limb–darkening. Their data were obtained from multi–colour photometry. The models involved numerical simulation of the light variations of a dipole mode inclined to an observer by an angle α. Matthews *et al.* sampled the visible hemisphere of the star with a grid in latitude θ and longitude ϕ. Thus, the visible surface is divided into pixels whose contribution to the observed flux are weighted by the projected area in the plane of the sky. The local flux variation was determined from the Planck function at temperature minimum and temperature maximum, convolved with the response function of the desired filter bandpass. A limb–darkening law of the following form was applied to each pixel:

$$\frac{I(\theta)}{I(0)} = 1 - \beta_\lambda(1 - \cos\theta), \tag{1.23}$$

where θ is the angle measured from the centre of the visible disk to the limb, β_λ is the limb–darkening coefficient as a function of wavelength (its values range from 0 to 1), and $I(\theta)$ is the surface intensity as a function of position on the visible stellar disk. The flux contribution of each pixel was summed across the visible disk to obtain the net luminosity variation amplitude.

The success of this technique could lead to advances in the understanding of the atmospheric structure of roAp stars. It could provide a check for Ap model atmospheres and hence enable a more reliable determination of parameters such as effective temperatures and surface gravities, which are currently still difficult to determine accurately for Ap stars. Improved model atmospheres that could arise from this work would also make abundance analyses for Ap stars more accurate. The main source of continuous opacity can be deduced (as was done for the sun by Pierce & Waddell 1961) from the temperature gradient measurements. The effects of other physical processes such as convection and NLTE (which are poorly understood for Ap stars) could be investigated through comparison of the empirical $T(\tau)$ with those obtained from model atmospheres.

It was these exciting prospects that prompted my supervisor and me to attempt to apply the above-mentioned technique to some large amplitude roAp stars. We were interested in stars

which have the dipole pulsation mode as the dominant mode of pulsation in addition to being large amplitude pulsators. In this thesis we shall show that limb–darkening cannot account for the observed rapid decline of the amplitude with wavelength, since limb–darkening is only a small effect. We shall subsequently show that $T(\tau)$ cannot be determined empirically, but that the amplitude *vs* wavelength data give us information about ΔT (the polar pulsational temperature semi–amplitude) as a function of atmospheric depth if $T(\tau)$ is known *a priori* (from model atmospheres).

It is also the aim of this thesis to determine $\Delta T(\tau)$ as suggested by Kurtz & Medupe (1996) and to improve on their results which are based on a black–body pulsator and Wien approximation. In this thesis I include numerical pulsation models based on realistic treatment of stellar intensities. I collected the new data on HR 3831 at various rotation phases in order to investigate the effects of rotation on the observed pulsation amplitudes as a function of wavelength. I then show how this affects our derived $\Delta T(\tau)$.

I shall proceed to describe the properties and the suitability of our candidates to the application of the technique suggested by Kurtz & Medupe (as of now referred to as Kurtz & Medupe's technique) in the following sections.

1.4 The candidates

1.4.1 Introduction

For the successful application of the Kurtz & Medupe's technique one needs stars with relatively large optical amplitudes. Since we wanted to investigate a long wavelength baseline (covering the optical and infrared regions where the amplitudes are expected to be low) large optical amplitude stars were selected in the hope of getting amplitude in the infrared. We also selected single mode stars whose eigenfrequency spectrum is not complicated. Other independently excited modes produce beating effects, making it difficult to interpret the observed amplitudes. We show in the next few subsections that all of our candidates satisfy these requirements to a large extent.

1.4.2 HR 3831 (HD 83368)

HR 3831 (HD 83368), classified by Houk (1978) as Ap SrCrEu, is the best studied of all the known roAp stars. The properties of this star often make it the first star in the roAp group on which new techniques are tried. It is bright $V = 6.168$, and is amongst the larger amplitude roAp stars (semi–amplitude $\leq$ 4 mmag). Its pulsation amplitude spectrum is stable over 15 years and is relatively simple. Thus, it is used to demonstrate the oblique pulsator model (Kurtz 1990), and the Matthew's technique was first applied to it. I will show later that it is ideal for the application of Kurtz & Medupe's technique.

HR 3831 is a visual binary with a separation of 3.29 arcsec. Hurly & Warner (1983) found $V = 6.25$, $B - V = 0.25$ and $U - B = 0.12$ for HR 3831A and $V = 9.09$, $B - V = 0.64$ and $U - B = 0.15$ for HR 3831B. HR 3831B has been classified as G2V and from measurement of its parallax, its distance has been found to be about 66 pc. Kurtz *et al.* (1994a) estimate the radius of HR 3831A to be $R = 1.9 \pm 0.1\, R_{\odot}$. As of now any reference of HR 3831 refers to HR 3831A.

A polarity–reversing magnetic field that ranges from +780 to -740 G over a rotation period of $P_{rot} = 2.851982 \pm 0.000005\, d$ (Kurtz *et al.* 1992) has been measured for this star. Kurtz *et al.* (1992) also found a significant phase lag between the times of pulsation and magnetic extrema and the time of mean–light extremum. This argues in favour of the idea that roAp star are oblique pulsators rather spotted pulsators (see section 1.3.2). Rotational velocities have been measured by Carney & Peterson (1985) who obtained ($v \sin i = 33 \pm 3\,\mathrm{km\,s^{-1}}$) and more recently by Mathys (1993) ($v \sin i = 32.6 \pm 2.6\,\mathrm{km\,s^{-1}}$), in agreement with each other.

Martinez (1993) gives the following Strömgren indices: $V = 6.168$, $b-y = 0.159$, $m_1 = 0.230$, $c_1 = 0.766$, $\beta = 2.825$, δm_1 = -0.024, δc_1 = -0.062, from which he estimates $T_{\rm eff} = 7950\,\mathrm{K}$.

I summarise what is known about the pulsations of this star below:

- It is a single mode star, no other modes have been detected down to a semi–amplitude of 0.1 mmag. This single mode is rotationally modulated so that the principal frequency show a septuplet, the first harmonic is split into a quintuplet, the second harmonic into a triplet. A third harmonic appears to be a single (Kurtz *et al.* 1993).

- The principal frequency is variable with a frequency amplitude of $0.12\,\mu$Hz on a time scale of 1.6 years (Kurtz *et al.* 1994a). This variability is not due to the Doppler shift caused by binary motion. The radial velocity of this star shows no variability. Nor can

the frequency variability be due to beating of unresolved modes since they would have to cause amplitude modulation which is not observed. Kurtz *et al.* (1994a) suggested cyclic modulation of the magnetic field as a possible cause of the variations. Frequency variations (amplitude $0.5\,\mu$Hz and correlated with the solar cycle) have been observed for the solar p modes (Elsworth *et al.* 1990; Libbrecht & Woodard 1990; Bachmann & Brown 1993).

- Its pulsation amplitude varies with rotation from zero to just under 4 mmag through a Johnson B filter. The times of pulsation amplitude maximum and magnetic extrema coincide.

HR 3831 is a good candidate for the application of Kurtz & Medupe's technique because it has relatively high amplitude in B. It has a single mode. The presence of other modes would produce beating effects, making our analysis difficult. The dominant pulsation mode is the dipole mode. Its short rotation period makes it ideal for investigating the effect of rotation on Kurtz & Medupe's technique. From a practical point of view the short rotation period allows one to include phases of maximum pulsation amplitude even during a short observing run.

1.4.3 HD 128898 (α Circini)

HD 128898, discovered by Kurtz & Cropper (1981) to be an roAp star, is the brightest of all the known roAp stars with Johnson $V = 3.191$. This fact makes it attractive for spectral analysis; it is the only roAp star for which a spectral synthesis abundance analysis has been done (Kupka *et al.* 1996).

HD 128898 is a visual binary with a separation of 15.6 arcsec. Sinachopoulos (1989) finds the following Strömgren indices: α Cir A : $V = 3.191$, $b - y = 0.120$, $\beta = 2.821$ and α Cir B : $V = 8.237$, $b - y = 0.589$, $\beta = 2.587$. Thus the light from α Cir A (which is the star we are interested in and shall henceforth refer to as α Cir) dominates when the combined pair is observed. The close separation of the pair makes it mandatory to include both stars in the same aperture to avoid degradation of the data.

Magnetic measurements for this star have been carried out by Wood & Campusano (1975), Borra & Landstreet (1975; 1980) and Mathys (1991). Borra & Landstreet's 1980 measurement is the most accurate so far; $H_{eff} = -300 \pm 60\,G$. Only upper limits for the longitudinal (of 0.5 kG) component of the field have been measured. A constant quadratic field of 7.5 kG

was measured by Mathys. So far, rotational modulation of the magnetic field has not been detected.

The results that follow are based on the multi-site observing campaign launched by Kurtz *et al.* (1994b) as an attempt to resolve the long standing question of the rotation period, P_{rot}, of α Cir. Lavagnino (1960) reported $P_{rot} \approx 1$ day from radial velocity measurements that were subsequently found to be spurious. More recently Kurtz *et al.* (1993) also suggested $P_{rot} \approx 1$ day but expressed the need for multi–site observations to check if this was not a systematic effect caused by daily alias problems. Kurtz & Balona (1984) reported two significant frequencies separated by $2.6\,\mu$Hz in their data obtained from South African Astronomical Observatory (SAAO) and Cerro Telolo Inter–American Observatory (CTIO) contemporaneously. They assumed the two frequencies (which were later confirmed by Kurtz *et al.* (1993)) were independently excited modes with second order spacing $\delta\nu_{n,\ell} = 2.6\,\mu$Hz from the asymptotic relation alluded to in section 1.3.3 , equation 1.21 .

Shibahashi & Saio (1985) used the results of Kurtz & Balona (1984) on their A–star models to show that $\delta\nu_{n,\ell} = 2.6\,\mu$Hz is likely to be due to $\ell = 0$ and $\ell = 2$ modes, *i.e* the principal pulsation mode is radial. A dominant radial mode in the presence of dipole magnetic field could suggest that the magnetic field is not an important factor for mode selection (contrary to what has been found in other roAp stars). Kurtz *et al.* (1993) found from their frequency analysis that a single radial mode could not explain their pulsation amplitude *vs* rotation phase, and pulsation phase *vs* rotation phase curves. This motivated them to do multi–site observations of this star.

The high quality multi-site data Kurtz *et al.* (1994b) gathered from the SAAO and Mount John University Observatory (MJUO) revealed a frequency triplet, with the principal frequency $\nu_1 = 2442\,\mu$Hz. Rotational sidelobes are separated from the principal frequency by $2.6\,\mu$Hz. Members of the triplet are all in phase. Four other independently excited modes (separated from the principal frequency by multiples of $25\,\mu$Hz) were visible. This is shown in a schematic amplitude spectrum in Figure 1.5.

Figure 1.5 is a signature of an oblique dipole pulsator. From it Kurtz *et al.* (1994b) were able to derive the rotation period of 4.463 ± 0.010 days. By reanalysing the B data spanning the years 1981 and 1993 they obtained $P_{rot} = 4.4790 \pm 0.0001$ days, well in agreement with predictions of the oblique pulsator model. Another interesting finding in their data is that the pulsation phase is constant over the rotation period. This, within the context of the oblique pulsator, indicates that the rotational inclination i and the magnetic obliquity β are such that only one magnetic (pulsation) pole is seen all the time.

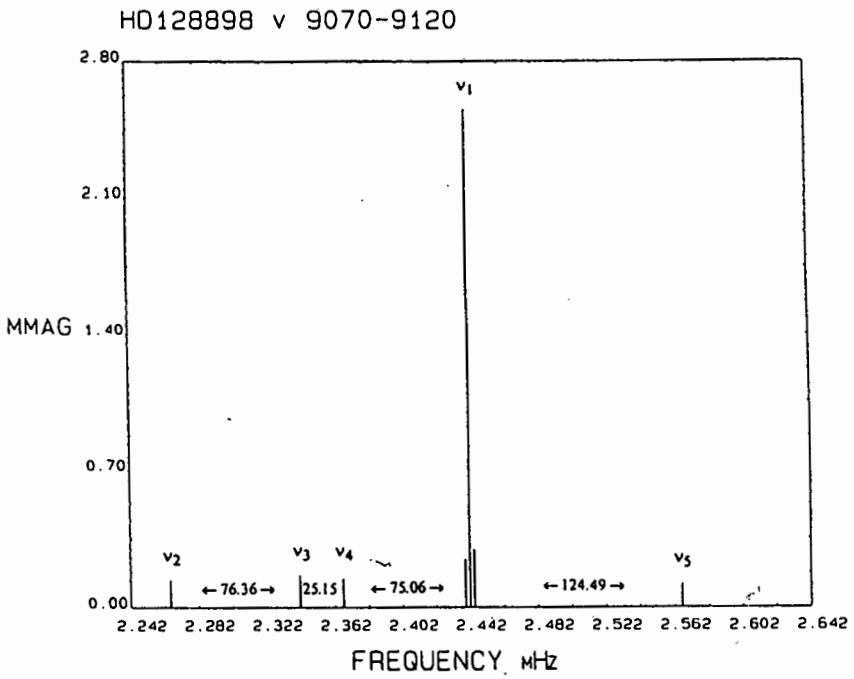

Figure 1.5: A schematic plot of the Strömgren u frequency spectrum of α Cir reproduced from Kurtz *et al.* (1994b). ν_1 is the principal frequency, shown around it are the rotational sidelobes. ν_2, ν_3, ν_4 and ν_5 are independently excited modes. The first harmonic of ν_1 is off the scale at 4884 μHz

Kurtz & Martinez (1993) derived $T_{eff} = 8000\,K$ from the observed combined Strömgren indices. Kupka *et al.* (1996) used spectrum synthesis and equivalent width technique to derive $T_{eff} = 7900 \pm 200\,K$. They also derived $\log g = 4.2$. I shall adopt Kupka *et al.*'s results in all of our calculations involving α Cir.

In summary, are we justified in applying the Kurtz & Medupe's technique on α Cir? A definite "yes" is the answer. The Johnson B amplitude of the principal frequency is high enough for long wavelength base-line work to be done on it. Kurtz *et al.* (1994b) have shown convincingly that the principal pulsation mode is dipolar. They have also demonstrated that the presence of other modes (whose amplitude is very small compared to that of the principal mode) does not affect the principal mode significantly. Their amplitude *vs* rotation phase diagram is not greatly affected by the removal or inclusion of the secondary frequencies. The added bonus is that model atmosphere parameters for α Cir are better determined than for all other roAp stars, thanks to Kupka *et al.* (1996) and to Kupka & Piskunov (1996). This

is a strong case !

1.4.4 HD 134214

This star, discovered by Kreidl (1985) to be an roAp star, has the shortest principal period (of 5.65048 minutes) of all the currently known roAp stars (Kreidl *et al.* 1994). It is singly periodic which makes it an ideal candidate for the Kurtz & Medupe's technique. However, because the star does not show rotational splitting in its eigenfrequency spectrum, the application of the oblique pulsator model to deduce its geometrical and magnetic properties is not possible. So the main disadvantage is that the geometry of this star is not known because even the rotation period is not known as yet. No amplitude modulation due to rotation has yet been measured for this star.

Singly periodic roAp stars were viewed as uninteresting, since the very absence of multi-mode frequency patterns means that asteroseismological studies cannot be made on them. The absence of frequency splitting means that the application of the oblique pulsator model (see section 1.3.2) to determine or constrain rotational and magnetic geometries is not possible. However, Heller & Kawaler (1988) predicted that evolutionary frequency changes may be detectable in the roAp stars with only 10 years of observations. This would be more noticeable in single mode roAp stars because of the absence of the complications of multi-periodicity, rotational amplitude and phase modulation. So far, frequency variations measured in roAp stars are orders of magnitude bigger than those predicted by Heller & Kawaler models. This, and Kurtz & Medupe's (1996) technique developed to observe level effects on the temperature oscillations of dipole mode pulsators, bring the single mode roAp stars back into the realm of scholarly interest.

HD 134214 shows cyclic variability in its pulsation frequency of $0.42\,\mu$Hz on a time scale of 248 days (Kreidl *et al.* 1994). The lack of radial velocity variation (Gautier Mathys in private communication (Kreidl *et al.* 1994)) suggests that the frequency variability is not due to Doppler shift caused by binary motion. The frequency variability is similar to that found in HR 3831 (Kurtz *et al.* 1994a), α Cir (Kurtz *et al.* 1994b) and the sun. These cyclic frequency variations are thus not due to stellar evolution but could be associated with magnetic effects.

Kurtz *et al.* (1991) found the pulsation amplitude of HD 134214 to be constant in B within errors in their 1985 and 1990 data sets. Kreidl *et al.* (1994) further confirmed this. The constant amplitude (see Figure 1 of Kreidl *et al.* (1994)) can be interpreted within the

context of the oblique pulsator model as an indication that either the star is pole on (i = 0) or that the magnetic obliquity is zero ($\beta = 0$). This could also indicate that the pulsation mode is radial ($\ell = 0$).

We do not know that the principal pulsation mode of HD 134214 is dipolar. The lack of frequency splitting makes it impossible to apply the oblique pulsator model to identify the pulsation mode (as was done for α Cir by Kurtz *et al.* 1994b). Kreidl & Kurtz (1986) attempted to apply Balona & Stobie's technique (discussed earlier) to HD 134214 to try to identify the pulsation mode, without success. However, since those roAp stars where mode identification has been done show dipole modes, I assume $\ell = 1$ for this star.

The observed Strömgren indices for HD 134214 are: $V = 7.464$, $b - y = 0.216$, $m_1 = 0.223$, $c_1 = 0.620$, $\beta = 2.774$, δm_1 = -0.029, δc_1 = -0.108 (Martinez 1993). From these, the effective temperature is estimated to be $T_{eff} = 7550K$. The schematic amplitude spectrum of this star is shown in Figure 1.6. The relatively large amplitude shown in Figure 1.6 and the absence of other frequencies makes HD 134214 very suitable for Kurtz & Medupe's technique.

1.4.5 HD 137949 (33 Lib)

HD 137949 was discovered to be a magnetic Ap star by Babcock (1958). In 1981 it was discovered to have short period oscillations of 8.27 minutes (Kurtz 1982), putting it in the roAp class. It is a magnetic variable (without polarity reversal) with the mean B_{eff} = 1570 ± 50 G and magnetic semi-amplitude of 200 ± 30 G (Kurtz 1982). The period of this variability is uncertain; estimates range from 7 to 23 days (Van den Heuvel 1971, Wolff 1975, Kurtz 1982). No definite mean light variations have been observed for this star, only an upper limit of 0.005 mag (peak-to-peak) in B or V.

Kurtz (1982) applied the oblique rotator model to the magnetic variation data to obtain $r \equiv B_{eff}(min)/B_{eff}(max) = 0.77 \pm 0.04$ from which he puts the constraints $i < 20°$ or $\beta < 20°$ on its geometry. He explained the lack of polarity reversal in terms of the rotation axis having an inclination such that only one magnetic pole is facing the observer (i.e $i + \beta < 90°$). The small amplitude in the magnetic field is explained in terms of small values of i or β. This also explains the lack of mean light variations and spectrum variations. He used $r_{puls} = \frac{1-2\frac{A_1}{A_0}}{1+2\frac{A_1}{A_0}}$ (the generalised oblique pulsator model was not yet developed then) for an oblique pulsator to derive the ratio of the amplitudes $A_1/A_0 = 0.06$. This, when used with the observed

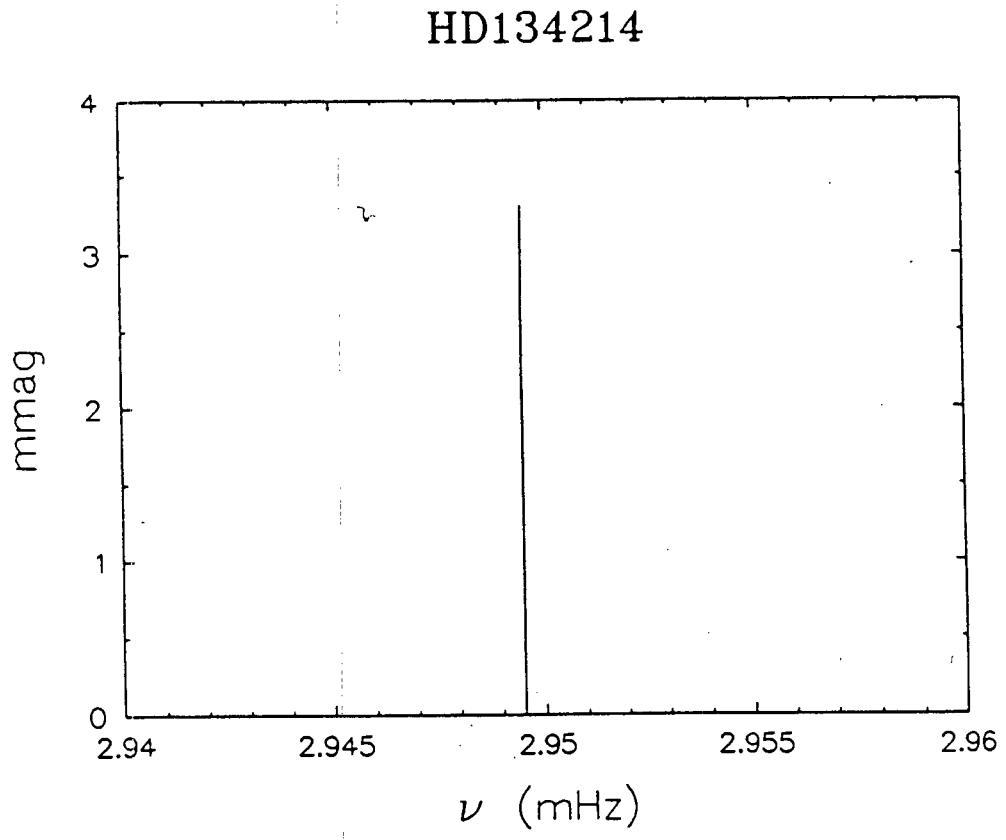

Figure 1.6: A schematic plot of the Johnson B eigenfrequency spectrum of HD 134214. This is taken from Martinez (1993).

amplitude of the principal frequency, gives $A_1 = 0.09$ mmag for the rotational sidelobes. The noise level in his 1981 data was sufficiently high that those rotational sidelobes, if present would not be detectable.

HD 137949 was observed again in 1987 using larger telescopes (Kurtz 1991). The data collected were less noisy than the 1981 data, but the noise was not low enough to show any rotational sidelobes of the principal frequency (if they are present). A reanalysis of the 1981 was done to refine the pulsation frequency of the 1981 data to $\nu_1 = 2014.821 \pm 0.003\,\mu$Hz. Analysis of the 1987 data gave $\nu_1 = 2014.781 \pm 0.001\,\mu$Hz which is significantly different from the ν_1 obtained from the 1981 data. This difference could be due to the presence of unresolved secondary frequencies. However, if this difference is real, it is two or three orders of magnitude larger than that expected from evolution ($\frac{d\ln\nu}{dt} = -9.9 \pm 0.7 \times 10^{-14}\,s^{-1}$) compared to $\frac{d\ln\nu}{dt} \approx 10^{-15} - 10^{-16}\,s^{-1}$ of Heller & Kawaler's predictions. All the roAp stars where the frequency changes have been observed show $\frac{d\ln\nu}{dt}$ several orders of magnitude larger that the predictions of Heller & Kawaler (1988). We can conclude that evolutionary frequency changes cannot be observed in roAp stars. The first harmonic of ν_1 was detected in the 1987 data. A secondary frequency $\nu_2 = 1975\,\mu$Hz still needs to be confirmed. A schematic amplitude spectrum is shown in Figure 1.7.

The observed Strömgren indices for HD 137949 are: $V = 6.673$, $b-y = 0.196$, $m_1 = 0.311$, $c_1 = 0.580$, $\beta = 2.818$, $\delta m_1 = $ -0.105, $\delta c_1 = $ -0.236 (Martinez 1993). From these, the effective temperature is estimated to be $T_{eff} = 8000$ K.

This star might be multi-periodic (with other secondary frequencies still unresolved with the available data) but, if so, their amplitudes relative to that of the principal frequency are so small that the pulsations are dominated by the principal frequency ν_1. The application of the oblique pulsator model on the amplitude spectrum of HD 137949 is still not possible as no rotational sidelobes of either the principal frequency (or ν_2) have been detected. So mode identification is still not possible for this star. HD 137949 is thus suitable for the Kurtz & Medupe's technique if we assume its principal frequency to be a dipole mode.

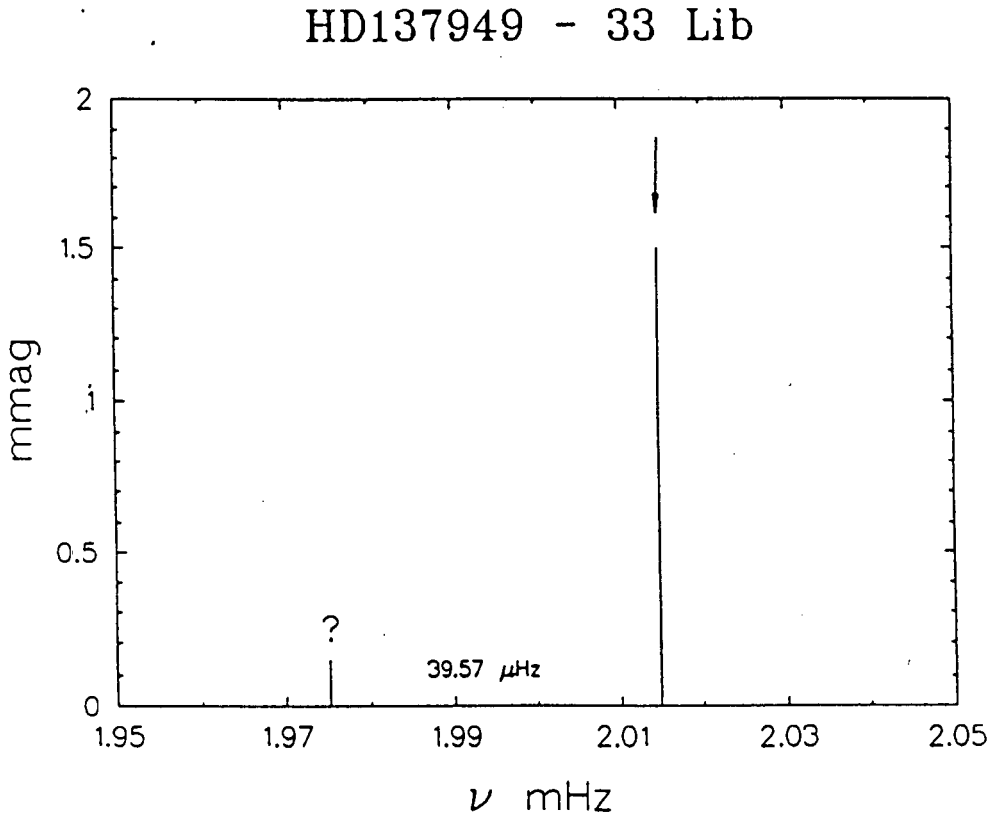

Figure 1.7: A schematic plot of the eigenfrequency spectrum of HD 137949. The arrow indicates that a harmonic exists for that frequency. The question mark indicates that the frequency is questionable, it still needs to be confirmed. This is taken from Martinez (1993).

1.4.6 HD 101065 (Przybylski's star)

HD 101065 was discovered by Przybylski (1961) to be one of the most peculiar stars in the sky. Its spectrum is so complex that for a long time no consensus existed on its basic atmospheric parameters. I showed in section 1.3.1 how arguments about its T_{eff} led to the discovery of the class of the rapidly oscillating Ap stars. Another contentious issue has been the question of whether the iron peak elements are deficient or not (Przybylski 1963, 1966; Wegner & Petford 1974; Przybylski 1977a,b; Cowley *et al.* 1977; Kurtz & Wegner 1979). Its absolute magnitude is also uncertain. Measurements of its trigonometric parallax by Churms (Kurtz & Wegner 1979) yields an upper limit of $\pi \leq 0.022$ arcsec. This only constrains the absolute magnitude to $M_V \leq 4.7$.

That this star is an extreme Ap star was shown by the discovery of qualitatively similar spectra in the known magnetic Ap stars HD 51418 (Jones, Wolff & Bonsack 1974) and HR 465 (Hartoog, Cowley & Cowley 1973), and the strong magnetic field of -2.2 kG by Wolff & Hagen (1976). The discovery of rapid oscillations in this star (Kurtz 1978) in common with 27 other Ap stars (that form the roAp stars) confirms that this is an Ap star.

The main problem, however, is that the data on spectrum, mean light and magnetic field variations of this star have been so sparse, that even at present the rotation period has not been determined (Martinez & Kurtz 1990). I shall come back to the question of the rotation period when I discuss the pulsation frequency analysis of this star. Spectral variations have not been observed with any conclusive results. A detailed comparison of the 1974 and 1975 coudé plates by Cowley *et al.* (1977) suggests that if the spectrum varied substantially, it must have returned to the same phase in one year. Wolff & Hagen (1976) and Wegner & Petford (1974) did not find any spectrum variations when they compared their data with Warner's (1966) line list. Wolff & Hagen (1976) took one Zeeman spectrogram in April 1974 and another two in March 1975 and could not find any significant variations in the magnetic field strength. Mean light variations (of either long term or short term nature) have also not been definitely observed. The *uvby* observations by Heck, Manfroid & Renson (1976), Renson, Manfroid & Heck (1976) and Heck, Mathys & Manfroid (1987) appear to exclude systematic mean light variations on a time–scale of a week. Przybylski (1977c) reported small changes in brightness (in Johnson V) over a period of eight years. However, he noted that his observations were insufficient to enable him to make a definite conclusion about the nature of the brightness variations.

Pulsation frequency analyses of HD 101065

This discussion is based on the paper of Martinez & Kurtz (1990 MK). In it they presented data collected in 1988. They frequency analysed those and earlier data by Kurtz (1978, 1980, 1981). Kurtz (1980) obtained a principal frequency of $\nu_1 = 1372.9 \pm 1.3\,\mu$Hz and three other secondary frequencies (ν_2, ν_3, ν_4). Kurtz (1981) reported long–term amplitude modulation which he used to show that the secondary frequencies were real. MK confirm this modulation but could still not assign a period to it. They suggested that several years' worth of data are required in order to be able to characterise this long–term variability.

MK observed a four–day amplitude modulation in their data. They could not tell whether this modulation period was the actual rotation period or not. They could not check against the spectrum, magnetic and mean light observations for this star as there is little of that data, and the little that is available is not of high quality. The lack of frequency splitting in the frequency spectrum means that one cannot use the oblique pulsator model to determine the rotation period. They also investigated the pulsation phase as a function of rotation phase and did not see any π–radian phase shift occuring on a four–day time scale. This does not exclude the $\ell = 1$ mode, however. HD 128898 (Kurtz *et al.* 1994b) shows this behaviour; it is thought that this is because the geometry of the star is such that only one pulsation pole is visible. A longer rotation period in HD 101065 can also explain this behaviour.

MK combined the nightly light curves into weekly data sets for the observations spanning the years 1978 to 1988, the aim being to have better frequency resolution that may reveal any frequency splitting consistent with the prediction of the oblique pulsator model. Frequency analyses of these data sets give $\nu_1 = 1372.8660 \pm 0.0013\,\mu Hz$. The two secondary frequencies seen in Kurtz's (1980) data are also observed at $\nu_2 = 1369.9260 \pm 0.0013\,\mu$Hz and $\nu_3 = 1315.0340 \pm 0.0013\,\mu$Hz. The first harmonic of ν_1 was also detected at $2\nu_1 = 2745.7355 \pm 0.0013\,\mu$Hz, they could not confirm a frequency at $\nu = 1367.5\,\mu$Hz reported by Kurtz (1980). Note that the separation of ν_1 and ν_2 is $3.2\,\mu$Hz. This separation can be identified with the amplitude modulation frequency discussed above. Thus ν_2 could possibly be a rotational side–lobe of ν_1, in which case ν_3 is an independently excited mode. No rotational sidelobes were found around ν_3 indicating that either ν_3 is a radial mode $\ell = 0$, or that the amplitudes of the rotational side–lobes around ν_3 are too low to be seen above the noise level, or that the rotation period is much longer than four days. A search for the second rotational sidelobe at $\nu_1 + (\nu_1 - \nu_2)$ was unsuccessful. From this they rejected a four day rotation period.

The consistent asymmetry of the ν_2 and ν_3 alias patterns suggest the presence of further frequencies which are inadequately resolved from the one day aliases of ν_2 and ν_3, and have amplitudes too low to be seen above the noise when the data are pre–whitened by ν_1, ν_2 and ν_3. Two new frequencies spaced by $\approx$ 3 nHz around ν_1 were discovered (forming a triplet). This spacing corresponds to a beat period of 10.6 years (close to the 10 year time–span of the data). However these frequencies are not resolved in terms of the 1.5/T criterion of Loumos & Deeming (1978), where T is the time–span of the data of the data set. Thus the values derived for these two frequencies are not reliable. The schematic frequency spectrum is shown in Figure 1.8.

There are two interesting features MK found in their data. The first one is the presence of the first harmonic of ν_3. If this is real it would be the first time that the first harmonic of a frequency other than the principal frequency has been detected in a roAp star. The second feature is that ν_1, ν_2 and ν_3 are found not to preserve their relative amplitudes. For example, MK find that $A_2 > A_3$ in one of their 1983 data set, and that $A_2 = A_3$ in their 1984 data sets. They could not tell whether this behaviour is caused by the real variations in the modes giving rise to ν_2 and ν_3 or it is the manifestation of beating with further unresolved frequencies.

In conclusion this star is still enigmatic, and mode identification is still not possible. Balona & Stobie's (1979b) technique has been shown not to work in roAp stars, and the lack of frequency splitting means the application of the oblique pulsator model is not possible. Another problem is that it will be difficult to create a realistic model atmosphere of this star, because of its exceedingly complex spectrum. In spite of these difficulties I think that HD 101065 meets the requirements for the application of Kurtz and Medupe's technique because its principal frequency has a relatively large amplitude compared to its secondary frequencies (figure 1.8). This means long wavelength base–line work can be done (in principle) and that the beating of other frequencies will not affect its amplitude greatly. I assumed the principal frequency is a dipole mode.

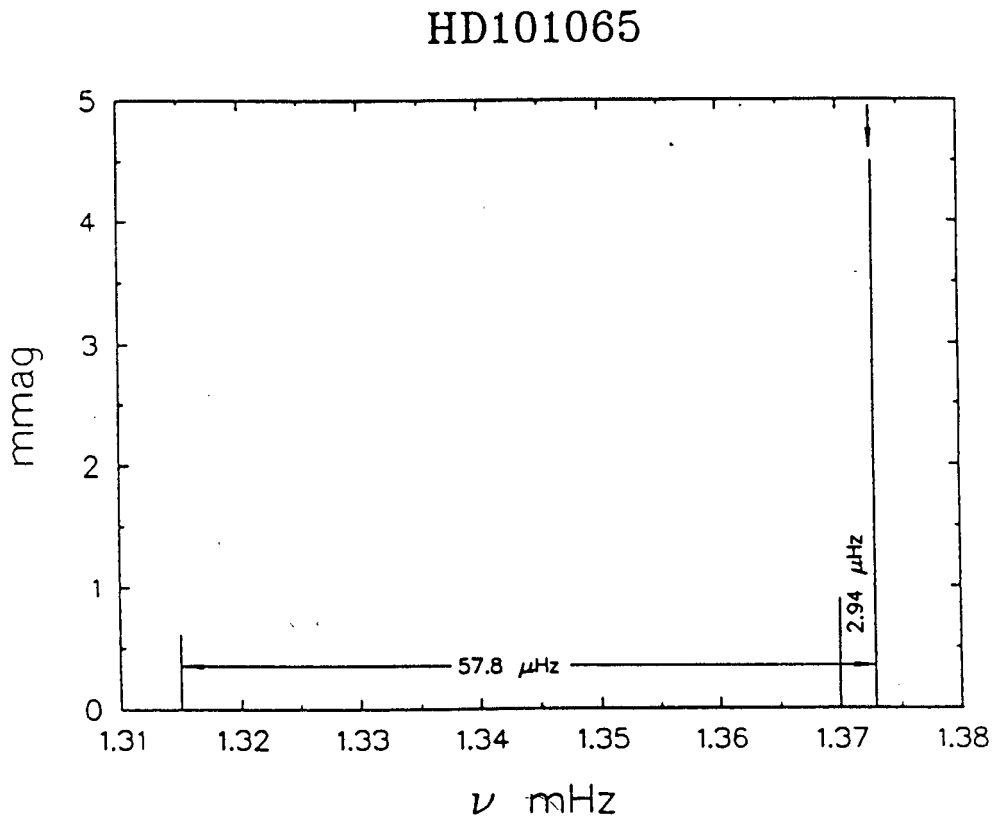

Figure 1.8: A schematic plot of the Johnson B eigenfrequency spectrum of HD 101065. The first harmonic is off–scale. (Reproduced from Martinez 1993).

Chapter 2

Data

2.1 Introduction

Our original idea was to make extensive simultaneous multi-colour photometric studies of HR 3831 to get as much coverage of the rotation phase as possible, the aim being to apply the Matthews' technique to HR 3831 at various rotation phases. To avoid poor sampling of the pulsation cycle (i.e few data points per pulsation cycle), and also because we needed infra–red data, three telescopes were used simultaneously.

Several observing campaigns were undertaken. The first observing campaign did not succeed because of bad weather conditions. Since observing time is a precious commodity (especially when more than one telescope is required), we later had to settle for a single telescope. During the second observing run HR 3831 was not well positioned for long time monitoring and we looked at other stars that have properties not very dissimilar to HR 3831, as is evident from the discussions in the previous chapter. Whenever conditions allowed, UBVRI colours were used, although sometimes we used the $uvby H\beta$, such as when the signal–to–noise ratio was too low in the R and I colours.

2.2 Instrumentation

We made use of four telescopes with four photo–electric photometers at the Sutherland station of the SAAO. Each of these instruments is briefly described below; detailed information about these and other instruments are found in the SAAO facilities manual (1994).

2.2.1 1.9–m Radcliffe telescope

The main purpose of using the 1.9–m telescope was to reduce the scintillation noise. Scintillation is caused by rapid small scale atmospheric temperature fluctuations occuring at various heights in the earth's atmosphere. These produce noise at all frequencies in the Fourier spectrum which sets lower limits of detectability of the star's oscillation amplitudes. In fact Kurtz (1984) showed by observing HD 101065 on the 0.5–m and 1.9–m telescopes that this telescope reduces scintillation noise (compared to the 0.5–m telescope) by a factor of 2.5. Matthews *et al.* (1990) only found an upper limit for their K amplitude which was well below their predicted value. The JHK amplitudes of roAp stars are expected to be very low, and it was hoped that by keeping the scintillation noise low, one might be able to detect and study the infrared amplitudes. Peter Martinez obtained upper limits for the infrared data he acquired with this telescope. I shall not use his data.

The Radcliffe telescope is the most automated telescope at the Sutherland site. The photometer used with this telescope is the MK III infrared photometer (henceforth called IRP). This uses two types of Dewars; the liquid nitrogen cooled InSb for JHKLM photometry, and the liquid helium cooled bolometer Dewar for MNQ photometry. Martinez used the InSb Dewar for his infrared measurements. Data acquisition and telescope nodding are controlled software running on the IBM PC–AT.

2.2.2 1.0–m Elizabeth telescope

Built by Grubb Parsons in 1964, this is the second largest telescope on site. It is suitable for lowering the scintillation noise. The St. Andrews Photometer (STAP) was used with this telescope. This is a two–channel photometer consisting of a blue sensitive tube and a red sensitive tube. The two channels cannot be used simultaneously, but sequentially. The blue tube is an EMI 6256 (S13 cathode) suitable for UBV measurements, the red tube is an EMI 9658 or EMI 9659 (extended S20) suitable for VRI measurements. Both tubes are housed in water–cooled boxes and maintained at $-10°$ C (the blue tube) and $-25°$ C (the red tube). The blue tube has lower dark count rate of 2 counts per second compared to 10 counts per second for the red tube. The dead–time coefficient (I discuss this in section 2.5.1) is $\tau = 70$ ns. The sensitivity of the red tube seems to be deteriorating, as I will show later. The count rates for both tubes are kept below $10^6 s^{-1}$. This translates to the following limiting magnitudes; $U = 5.4$, $B = 6.5$, $V = 5.8$ for the blue tube, and $V = 5.5$, $R = 5.5$ and $I = 3.8$. The acquisition software does not protect the tube from over–illumination. However it sends a warning signal when over–illumination occurs. If this happens it might

take a while (about 10 minutes) for the dark counts to stabilise. It is advisable for the observer to shut the dark-slide (immediately) and to monitor the dark counts after over–illumination occurs. No neutral density filters are provided for this photometer. The filter wheel is automated and is controlled by a PC, as is the channel change.

The STAP is controlled by an IBM–AT desk–top computer fitted with two custom–built interface cards, namely: the photometer interface and the time and display interface. The photometer interface provides 16 bit 100 MHz pulse counters and 16 TTL inputs and outputs to interrogate and control the photometer (*e.g* to control the filter wheel and so on). The time and display interface card reads time from the time service provided in each telescope dome and drives the vector graphics display. The vector graphics display allows visual inspection of the counts received every second and the accumulated count for the measurement in progress, and generally the status of measurements. It is thus invaluable for checking that everything is working well. Data are recorded on a 120 Mb hard disk drive of IBM–AT computer in the same format as it is displayed on the screen. An 80 column matrix printer is provided to keep a hard copy of the data (in case the data cannot be retrieved from the hard disk).

The telescope–photometer–filter response functions for the UBVRI system were not available. I shall therefore use the 0.5–m telescope UBVRI response functions. The STAP Strömgren response functions are shown in Figure 2.1.

2.2.3 0.75–m telescope

This telescope (built by Grubb Parsons company in 1974) was used with the University of Cape Town Photometer (UCTP). The UCTP is a general purpose single or dual channel photometer (we used it in the single channel mode). The UCTP is operated with an un-cooled Amperex 96DVP photo-multiplier tube with an S11 cathode. It has a relatively high quantum efficiency and low dark current. We used the UCTP to observe in UBV because it has a blue tube. A cooled GaAs (RCA 31034A) tube is also available for use (it has higher dark current). The dead–time coefficients measured for this photometer is $\tau = 70$ ns. The filter wheel can be controlled by automatic means for multi–colour photometry. The photometer allows the observer to offset–guide by eye or by an SBIG ST–4 CCD auto-guider. We chose to guide by eye, because it takes long to set up the SBIG ST–4 CCD auto-guider unlike the 1.0–m telescope auto-guider.

The computer hardware and software that control the UCTP photometer are the same as

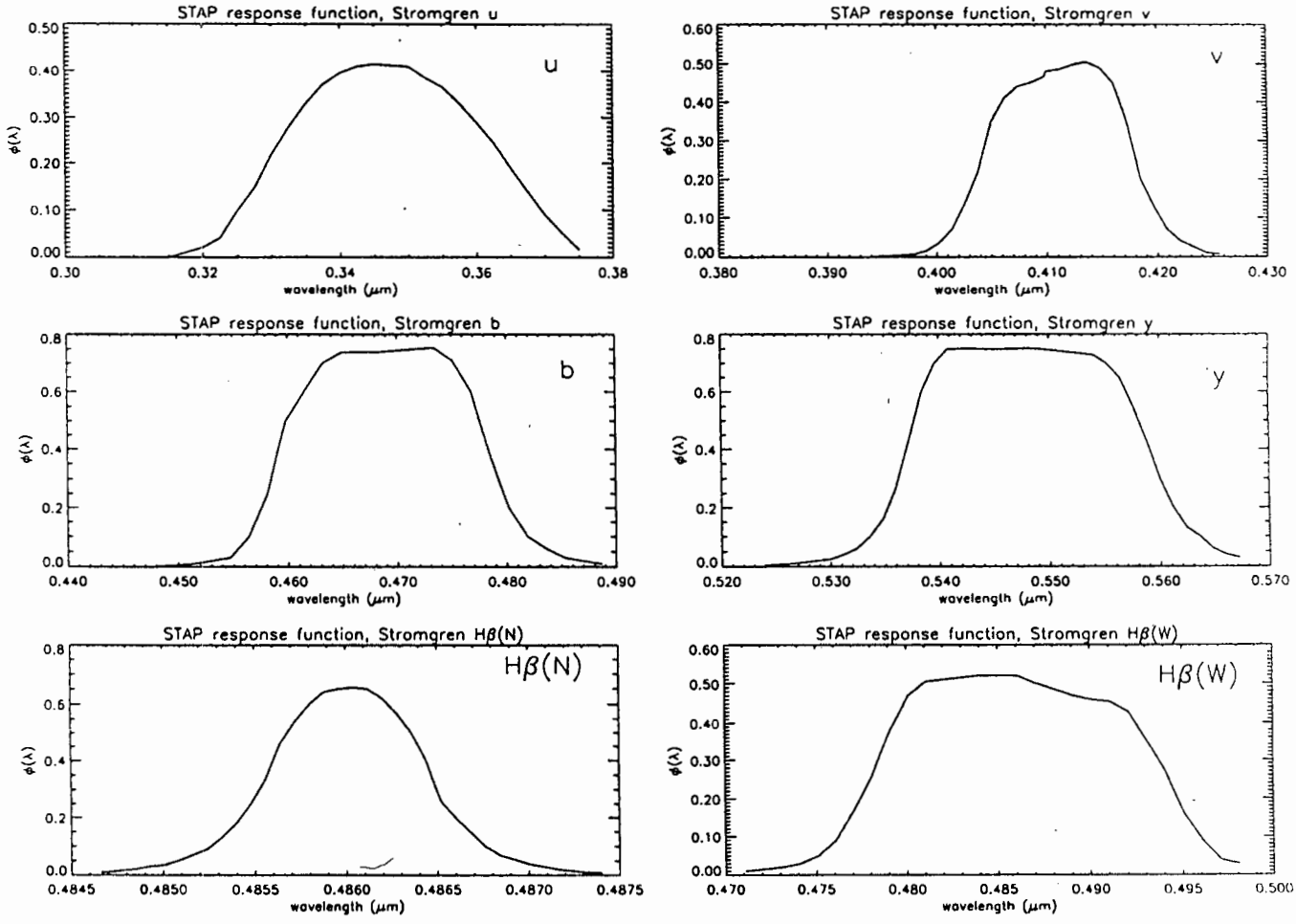

Figure 2.1: The response function for the STAP photometer for the $uvby\beta$ filters.

The computer hardware and software that control the UCTP photometer are the same as that already described for the STAP.

2.2.4 0.5–m Boller and Chivens Cassegrain telescope

This is the easiest telescope to operate on the Sutherland site. Although it does not have auto-guider facilities, it has excellent tracking so that the observer does not have to interrupt data collection at short time intervals to check guiding.

Attached to this telescope is the Modular Photometer (MP), which is fully described by Kilkenny *et al.* (1988). This instrument is dedicated to the 0.5–m telescope and is thus the most reliable photometer on site. The MP is a visual region single channel photometer of conventional design except that all major components are in a form of 'plug–in' modules. This makes it easy to change components, do instrument tests and do general maintenance. Backup modules for the mechanical and electronic units are available to be plugged–in in the event of a fault. This minimises the amount of instrument down time. The filter wheel is driven by a computer–controlled 200–steps–per–revolution stepping motor. This makes this photometer suitable for simultaneous multi–colour photometry.

The MP uses a Hamamatsu R943–02 Gallium Arsenide (Ga–As) photo-multiplier tube housed in a thermo-electrically cooled unit (to minimise the 'dark' current). The Ga–As tube allows the UBVRI colours to be measured with a single tube. This tube only allows stars of $B, V, R \geq 6.5\,\mathrm{mag}$, $U \geq 6.0\,\mathrm{mag}$ and $I \geq 5.5\,\mathrm{mag}$ to be observed. This is because for stars brighter than this the tube responds in an unpredictable way and can be easily damaged. For stars brighter than those limits neutral density filters are used. The tube is protected from over–illumination by the software that controls the MP. The software monitors the count rate continually and if the count rate exceeds the preset limit, the filter wheel is rotated half the distance between two consecutive filters so that the wheel blocks the star light path. An error message then appears on the computer screen. The dead time coefficient for the MP is $\tau = 40\,\mathrm{ns}$. The data acquisition program LUCY which is suitable for multi–colour photometry is described in section 2.3.

The response function for the MP photometer–filter system (for the filters we used) is shown in Figure 2.2.

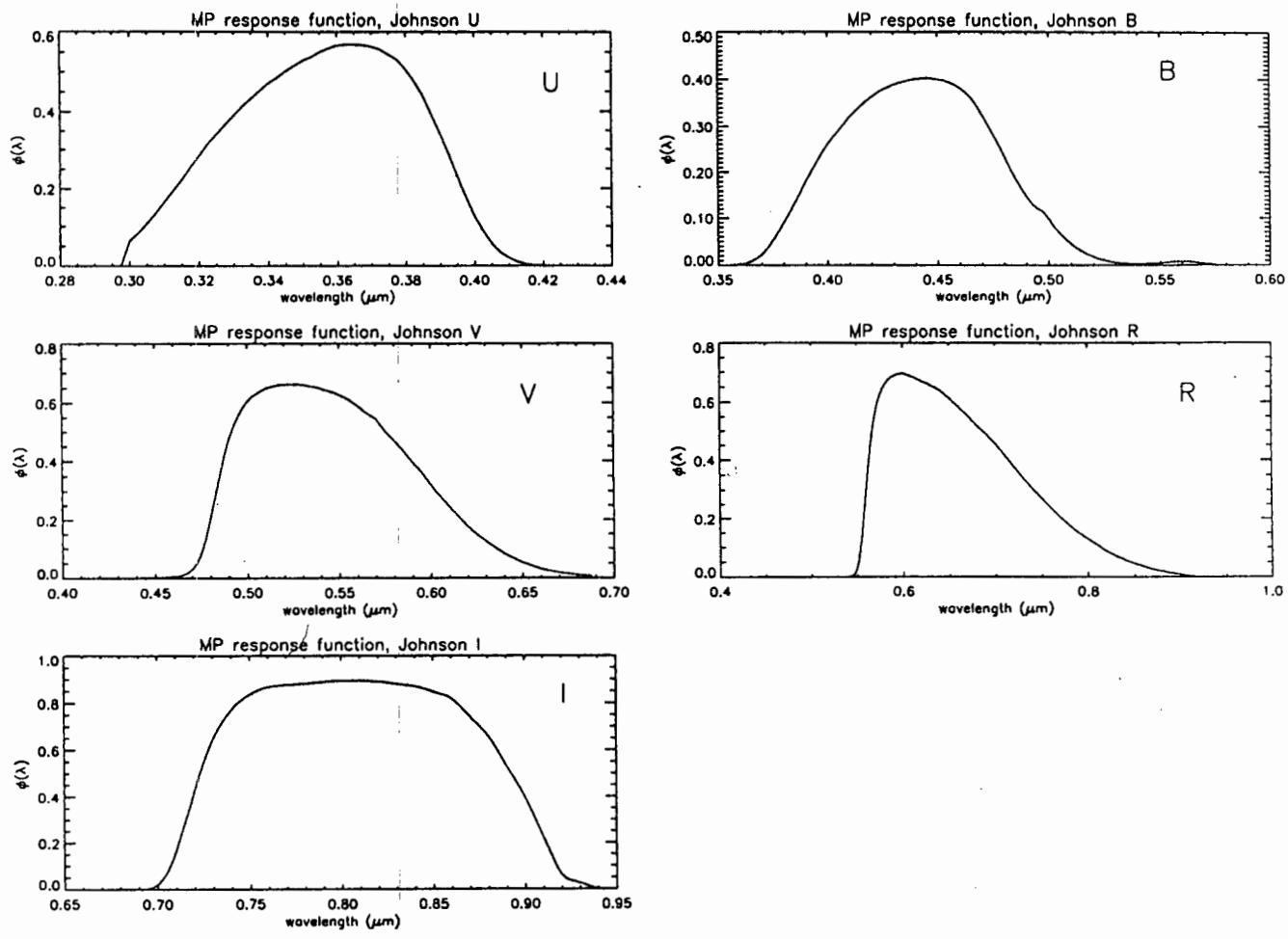

Figure 2.2: The response function for the MP photometer for the UBVRI filters. The UBV response functions above will be used whenever comparison of the model results with the data collected using the UCTP and STAP is made. This is because the response functions for both photometers were not available.

2.3 Observing campaigns

Simultaneous multi–colour observing campaigns were undertaken by myself and others at the initiation of this project for my MSc thesis. The list is given in Table 2.1.

Table 2.1: A list of observation campaigns since the initiation of the project. All of the observations were done at SAAO. Detectors used are put in parentheses.

date	**observer**	**instrument(s)**	**filters**	**results**
Feb 1995	D.W Kurtz	0.75 m (UCTP)	UBV	no
	M. Snowden	0.75 m (UCTP)	UBV	no
	P. Martinez	1.90 m (IRP)	JHK	no
	J. Matthews	0.50 m (MP)	R_c, I_c	no
	R. Medupe	0.50 m (MP)	R_c, I_c	no
May 1995	D.W Kurtz	0.75 m (UCTP)	UBV	yes
	P. Martinez	1.90 m (IRP)	JHK	null
	R. Medupe	0.50 m (MP)	R_c, I_c	yes
November 1995	R. Medupe	1.00 m (STAP)	$UBVR_cI_c$	no
February 1996	R. Medupe	1.00 m (STAP)	$UBVR_cI_c$,	yes
			$uvby\beta$	yes

The "no" results in the last column of Table 2.1 indicates that no data were obtained due to bad sky conditions, the "null" results indicates no pulsation signal detected, and "yes" means photometric data were obtained. The February 1995 campaign did not produce any usable data, no photometric nights. The marginally photometric nights combined with the poor performance of the STAP red tube rendered the November 1995 campaign data unusable. In May 1995, all the nights during which the four roAp stars were observed were photometric.

The two–week–long February 1996 campaign produced 9 usable nights out of 14. $UBVR_cI_c$ photometry was done on the first two nights. HR 3831 was too bright for the blue tube (especially in B and V) so for those two nights BVRI were observed with the red tube, U with the blue tube. It became evident that the red tube of STAP is very noisy. This prompted us to use narrow band filters ($uvby$) on the blue tube (to avoid over-illumination) but to continue using the R_cI_c filters on the red tube. After three nights, the problem with the red tube had become so severe that we decided to discontinue its use all together. So the R_cI_c filters were taken out and the Hβ_W and Hβ_N filters put on the blue tube.

2.4 Observations

Precautionary measures were taken both at the start of each observing night and during the course of observations to ensure good data were acquired. These precautions included checking the stability of the photo–tube by exposing it to the beta source, and checking the centering of the program star and the guide star (when the auto-guider was used) twice a night to avoid flexure problems. Flexure problems cause the program star and the guide star which were well aligned to become misaligned.

The photo-multiplier tube attached to the 0.5–m telescope shows a substantial increase in sensitivity when exposed to the first star of the night. To solve this problem the tube is exposed to a bright E–region standard star at the start of every observing night (in twilight). This exposure is continued until stability in the counts is achieved.

Sky measurements were taken at regular intervals of between 30 and 45 minutes to ensure proper monitoring of sky brightness variations. Extra care was exercised when there were rapid sky brightness variations, during moon–rise, moon–set, towards dawn, and just after evening twilight. Here sky measurements were taken at shorter time intervals of 10 to 15 minutes. It has been observed that when the moon is near the program star, as the dome is rotated, a discontinuity in the light curve develops. This is due to the reflection of moon–light on the internal parts of the telescope. This occured more frequently on the 1.0–m telescope than in others, probably because it has an open structure design. Proper handling of this discontinuity (as far as data reduction is concerned) is achieved by taking sky measurements just before rotating the dome, and another sky measurement just after.

The data were acquired using LUCY data acquisition program (Balona 1988). LUCY requires as input the colour equations, zero–points, extinction coefficients, star names and coordinates. These are used for on-line reductions. To specify the sequence of filters and the corresponding integration times, programs which contain integration time, flags to denote star or sky measurements and filter numbers are used. These programs can be arranged into a macro–program containing one or more programs. In our case, we included a star program (a program with flags set for star measurements) and a sky program (a program with flags set to sky measurements) in our macro–program. This allowed us to switch between the two programs whenever necessary. The results of each integration are displayed on the screen, stored on the hard disk drive of the PC and printed on the matrix printer (if so required). After every program a summary of the on–line reductions (Heliocentric Julian Date, magnitudes and colours) corresponding to the middle of integration is displayed on the screen.

This is invaluable for tracking errors in the instruments, the presence of clouds and can be used to check if the correct star is being observed.

All observations were obtained with 10 second integrations and 30 arcsec apertures. We found this aperture size to be optimal for avoiding light losses when the telescope tracking was not good or when the seeing is marginal or bad.

2.5 Data reduction and Analysis

All the raw light curves were visually inspected to remove any obvious bad data points. The possible sources of bad points in general are satellites, cosmic rays and meteors that pass in front of the telescope. Electrical interference from radios and other electrical appliances in the observing dome could contribute as well. The observing domes at SAAO are properly shielded from electrical interference. So at SAAO the main cause of bad points was very thin cirrus clouds that are not easy to see. Satellites, cosmic rays and meteors have very small probability of passing in front of the telescope and being detected, so I do not think they contribute.

I then applied the following corrections to the data, in order; dead–time correction, sky–subtraction and atmospheric extinction correction. An account of the corrections applied to the counts follows below.

2.5.1 Dead–time correction

Since the stars we observed are all bright objects (with Johnson $V < 8$), it is important to correct for dead–time losses. The following equation was used

$$N_o = N \exp(-\tau N) \tag{2.1}$$

where N_o is the observed count rate in counts per second, N is the corrected count rate also in counts per second. τ is the dead–time coefficient for the counting system. N in equation 2.1 is obtained by using Newton's method for finding roots of equations. By application of binomial expansion to equation 2.1 we can get the often used dead–time correction equation :

$$N = \left(\frac{N_o}{1 - \tau N_o}\right). \tag{2.2}$$

2.5.2 Sky–subtraction

Almost all observations were done on bright nights when the moon was up. This necessitated a regular monitoring of the sky brightness variations, especially near twilight, moon–rise and moon–set.

The sky counts were interpolated linearly to the times of star counts, to facilitate the subtraction of sky counts from the star counts.

2.5.3 Atmospheric extinction correction

The magnitudes we use throughout this thesis are not converted to the standard system. Standard stars (used to determine zero points and transformation coefficients) were not measured. Instead the zero mean magnitude was calculated in the following way

$$\frac{1}{N}\sum_i m_i = 0, \tag{2.3}$$

where m_i is the extra–atmospheric apparent magnitude for the ith data point.

Assuming only first order extinction we get

$$m_i = m_{obs_i} - \kappa'_\nu X, \tag{2.4}$$

where m_{obs_i} is the observed apparent magnitude, κ'_ν is the principal extinction coefficient in magnitudes per airmass, and X is the airmass. m_{obs_i} is given by

$$m_{obs_i} = -2.5 \log C_i + constant. \tag{2.5}$$

where C_i is the observed corrected counts per second, and the constant is the zero point.

Equation 2.4 becomes

$$m_i = -2.5 \log C_i + constant - \kappa'_\nu X. \tag{2.6}$$

Applying equation 2.3 we get

$$2.5 \log C_i = constant - \kappa'_\nu X. \tag{2.7}$$

Therefore, by applying the linear least squares fit to $2.5 \log C_i$ *vs* X one can get an estimate of the extinction coefficient. Then by substituting the estimated κ'_ν into equation 2.6 one applies the correction to each data point.

The times of the mid-points of observations were converted to Julian Dates, and heliocentric correction with an accuracy of 10^{-5} day applied to each data point.

2.5.4 Determining Amplitudes from measurements

The reduced data were then Fourier analysed, using the discrete Fourier transform technique as suggested by Deeming (1975) and modified by Kurtz (1985), in order to obtain the Fourier spectrum. The pulsation amplitudes and the phases were obtained by fitting (by linear least squares) a function of the following form

$$y = A_\nu \cos(2\pi\nu\,(t - t_o) + \phi) \tag{2.8}$$

given a particular frequency of interest ν in mHz. A_ν is the amplitude in mmag, and ϕ is the phase in radians. The amplitudes as function of wavelength obtained by application of this technique are shown in Table 2.2 for the May 1995 campaign, and Table 2.3 for the February 1996 campaign. The standard deviation σ measures the noise in the data. It includes all sources of noise as well as the intrinsic light variations of the star itself.

The consistently large σ values in $H\beta_N$ (see Table 2.3) are due to the edge deterioration of that filter. This effect is exacerbated when the seeing is not so good and the auto-guider cannot guide properly. Table 2.3 also includes the rotation phases for each observation. These are calculated from the following ephemeris (Kurtz *et al.* in preparation) for times of maximum pulsation amplitude:

$$JD_{max} = 2448312.23606 + (2.851976 \pm 0.00003)\,E. \tag{2.9}$$

Table 2.2 and Table 2.3 are summarised by the plots of prewhitened Fourier spectra shown in the next pages.

Table 2.2: A table of amplitudes obtained from a linear least squares fit to the May 1995 campaign data.

Star	ν	**Filter**	λ	σ	**A(obs)**
	mHz		Å	mmag	mmag
HD 101065	1.3728660	U	3670	4.14	7.43 ± 0.25
		B	4360	2.39	6.59 ± 0.14
		V	5450	2.29	3.01 ± 0.13
		R	6380	2.56	1.72 ± 0.12
		I	7970	2.23	0.53 ± 0.11
HD 128898	2.4419999	U	3670	3.81	2.71 ± 0.18
		B	4360	3.49	2.03 ± 0.15
		V	5450	3.17	1.06 ± 0.14
		R	6380	3.76	0.54 ± 0.15
		I	7970	3.35	0.41 ± 0.13
HD 134214	2.949574	U	3670	2.93	4.25 ± 0.16
		B	4360	2.15	4.13 ± 0.11
		V	5450	2.55	1.94 ± 0.13
		R	6380	2.35	1.27 ± 0.11
		I	7970	2.61	0.73 ± 0.12
HD 137949	2.014781	U	3670	2.59	1.37 ± 0.15
		B	4360	2.19	1.46 ± 0.13
		V	5450	2.09	0.82 ± 0.12
		R	6380	2.30	0.55 ± 0.12
		I	7970	2.50	0.24 ± 0.13

Table 2.3: A table of amplitudes for the February 1996 campaign on HR 3831. Notice the large σ values for the R and I. This is largely due to the problems with the red tube. $\nu = 1.42801257$ mHz.

Filter	λ	σ	**A(obs)**	**rotation phase**
	$\AA$	mmag	mmag	radians
U	3670	2.74	3.23 ± 0.22	0.57
B	4360	3.89	2.82 ± 0.33	0.57
V	5450	3.91	2.21 ± 0.32	0.57
R	6380	4.06	1.05 ± 0.33	0.57
I	7970	4.23	0.58 ± 0.33	0.57
U	3670	2.56	3.92 ± 0.20	0.93
B	4360	4.02	2.63 ± 0.32	0.93
V	5450	4.05	1.84 ± 0.32	0.93
R	6380	4.48	1.16 ± 0.36	0.93
I	7970	4.09	0.87 ± 0.33	0.93
u	3500	2.98	1.86 ± 0.26	0.62
v	4110	2.84	2.66 ± 0.24	0.62
b	4650	2.61	2.24 ± 0.22	0.62
y	5500	2.58	1.81 ± 0.21	0.62
R	6380	4.81	1.28 ± 0.40	0.62
I	7970	4.76	0.49 ± 0.40	0.62
u	3500	2.97	4.27 ± 0.23	0.97
v	4110	2.80	4.59 ± 0.22	0.97
b	4650	2.60	2.96 ± 0.20	0.97
y	5500	2.55	2.43 ± 0.20	0.97
R	6380	4.50	1.13 ± 0.35	0.97
I	7970	4.34	0.77 ± 0.34	0.97
u	3500	2.56	0.88 ± 0.21	0.32
v	4110	2.36	1.69 ± 0.18	0.32
b	4650	2.15	1.03 ± 0.17	0.32
y	5500	2.38	1.12 ± 0.19	0.32
R	6380	3.48	0.99 ± 0.28	0.32
I	7970	3.25	0.53 ± 0.27	0.32

Table 2.3: continued ..

Filter	λ	σ	A(obs)	rotation phase
u	3500	3.49	1.70 ± 0.48	0.42
v	4110	2.89	2.64 ± 0.40	0.42
b	4650	3.03	1.72 ± 0.42	0.42
y	5500	2.61	2.00 ± 0.37	0.42
$H\beta_W$	4860	2.63	1.38 ± 0.37	0.42
$H\beta_N$	4860	3.37	2.10 ± 0.43	0.42
u	3500	3.10	0.45 ± 0.31	0.75
v	4110	2.87	0.41 ± 0.28	0.75
b	4650	2.06	0.40 ± 0.20	0.75
y	5500	2.04	0.34 ± 0.20	0.75
$H\beta_W$	4860	2.23	0.36 ± 0.22	0.75
$H\beta_N$	4860	3.33	0.29 ± 0.34	0.75
u	3500	2.73	3.11 ± 0.23	0.08
v	4110	2.87	3.71 ± 0.24	0.08
b	4650	2.29	2.58 ± 0.19	0.08
y	5500	2.58	1.95 ± 0.22	0.08
$H\beta_W$	4860	2.76	2.19 ± 0.22	0.08
$H\beta_N$	4860	3.30	1.78 ± 0.28	0.08
u	3500	4.18	2.04 ± 0.48	0.16
v	4110	3.52	1.87 ± 0.39	0.16
b	4650	3.44	0.81 ± 0.39	0.16
y	5500	3.24	1.25 ± 0.35	0.16
$H\beta_W$	4860	3.06	0.88 ± 0.34	0.16
$H\beta_N$	4860	4.10	0.89 ± 0.49	0.16

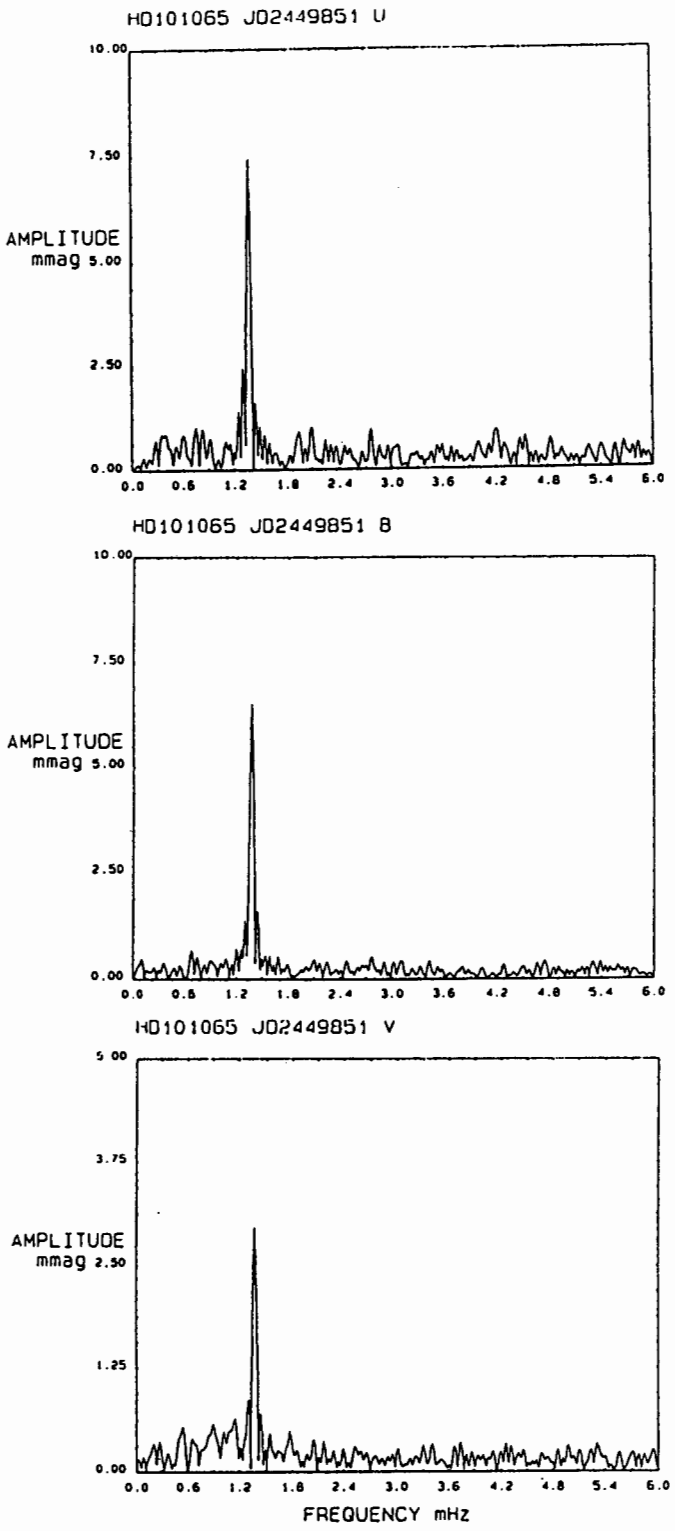

Figure 2.3: The Fourier spectra of HD 101065 showing the rapid decline of amplitude with increasing wavelength, continues on the next page.

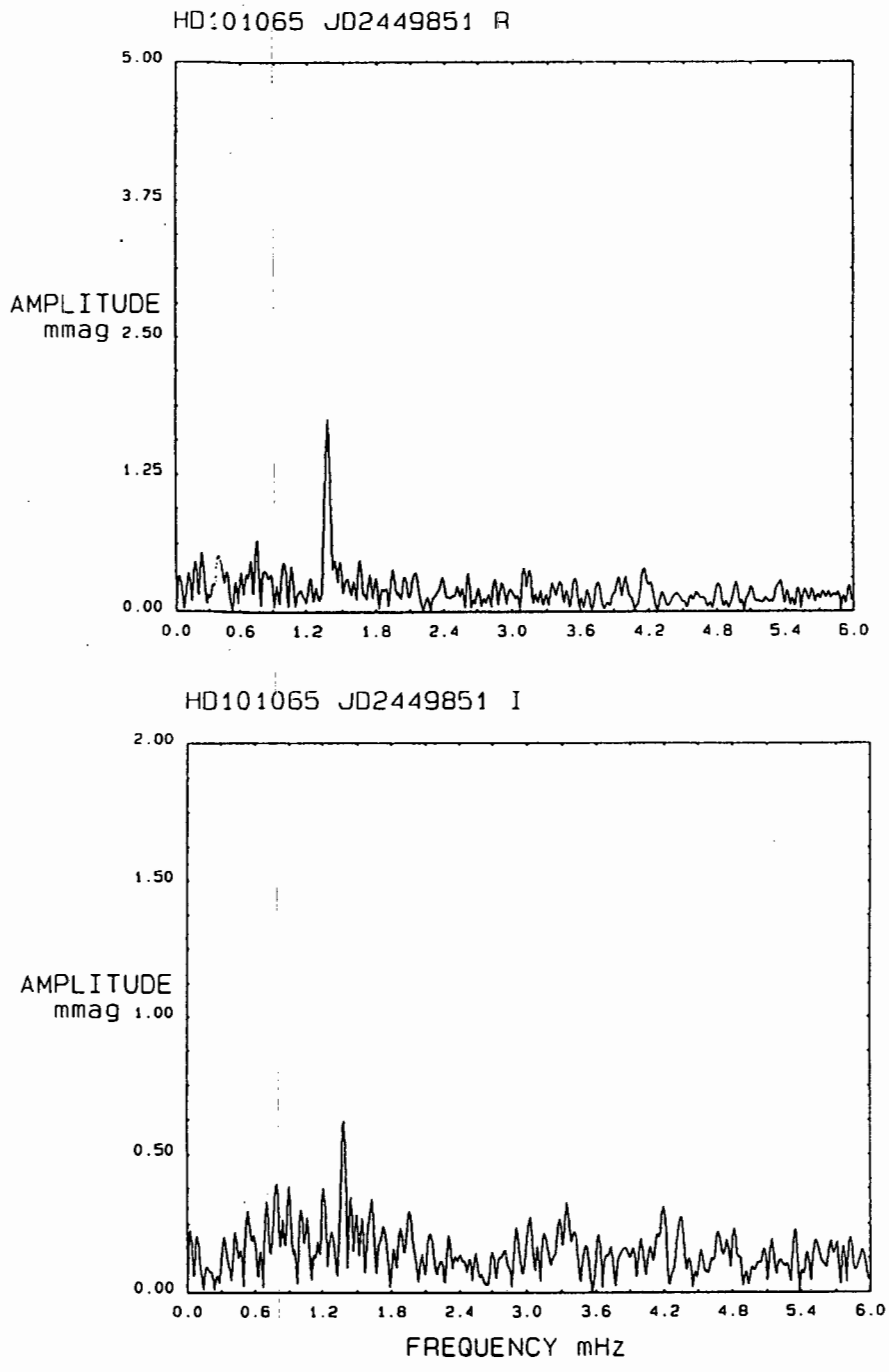

Figure 2.3: continues.

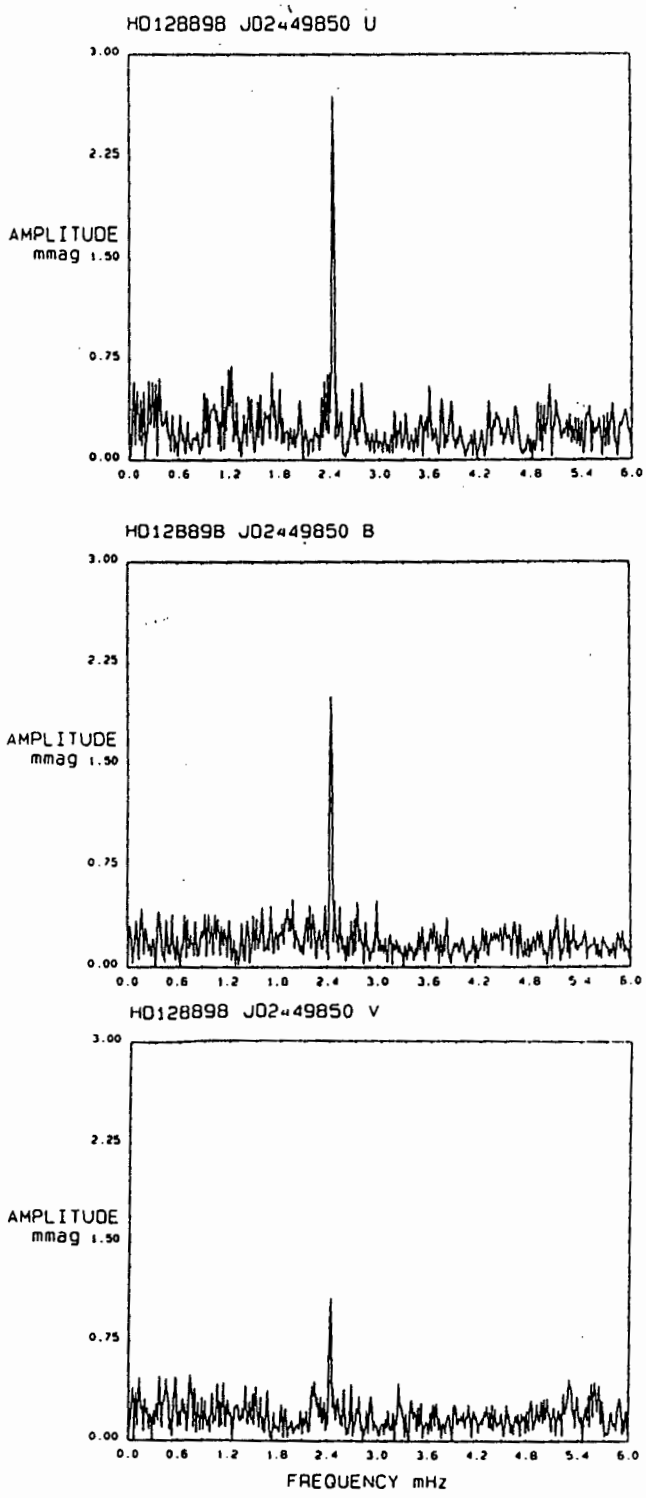

Figure 2.4: The Fourier spectra of HD 128898, the rest of the spectra are on the next page.

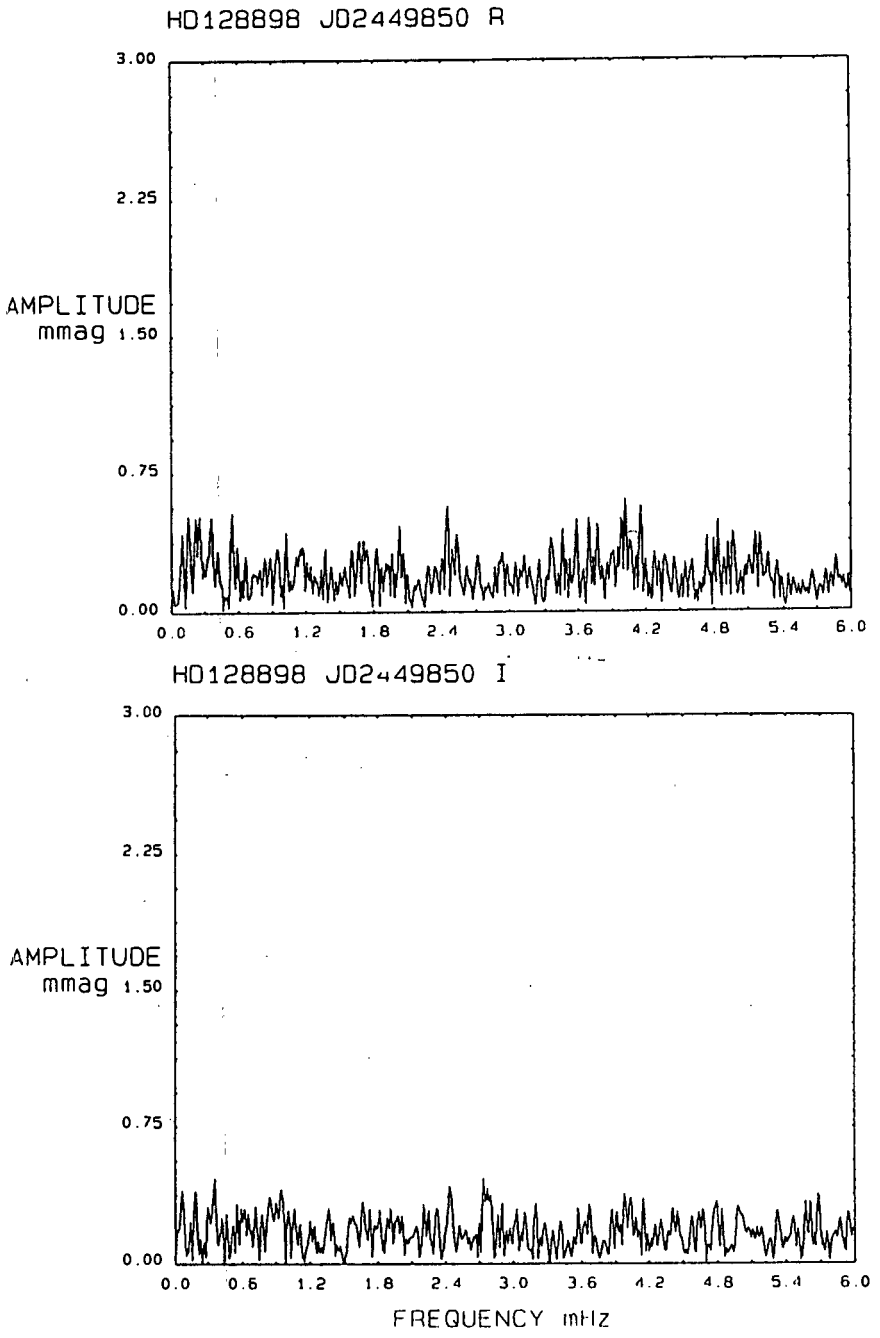

Figure 2.4: continues.

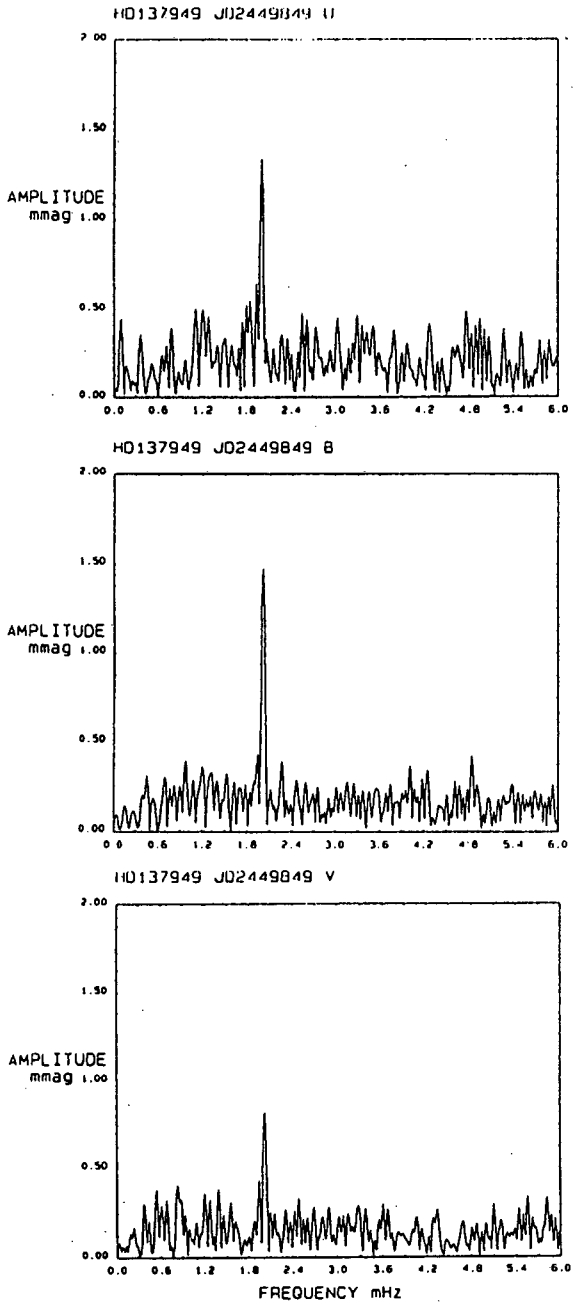

Figure 2.5: The Fourier spectra of HD 137949, see the rest on the next page.

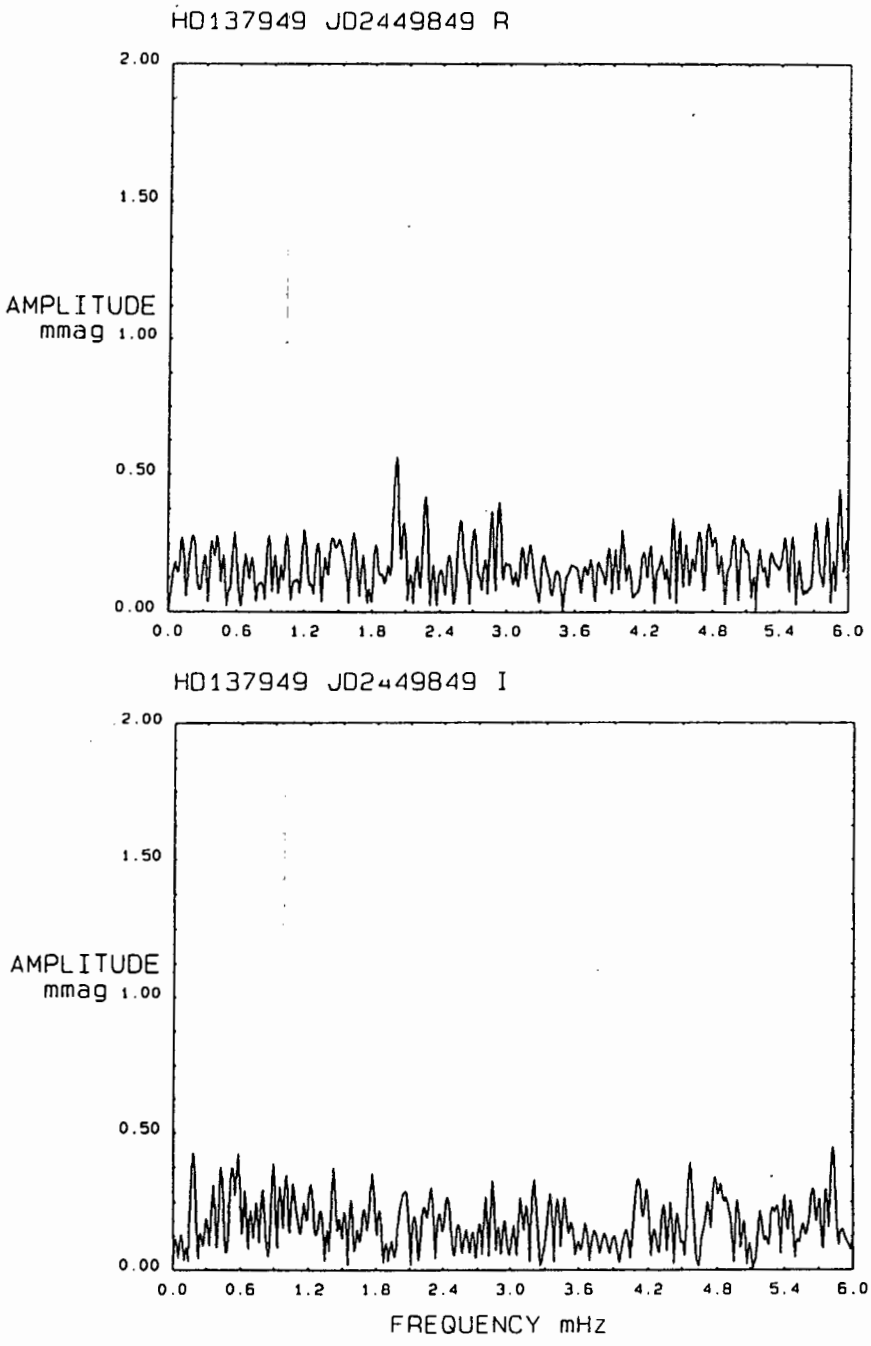

Figure 2.5: continues.

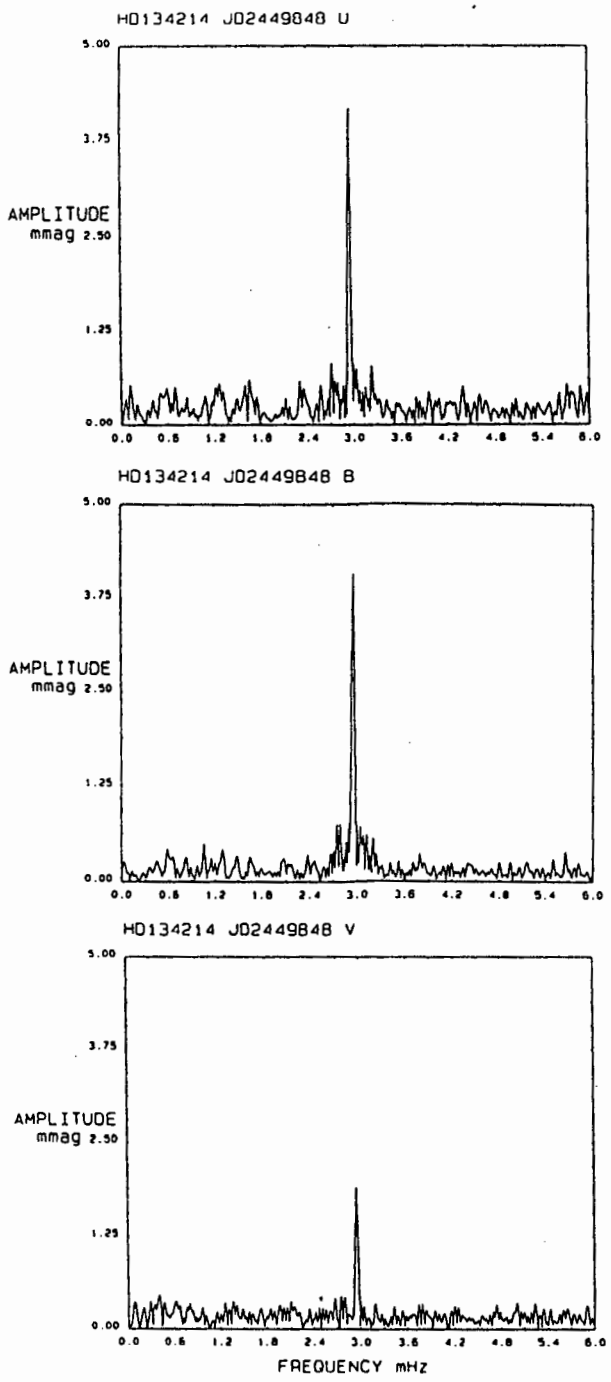

Figure 2.6: The Fourier spectra of HD 134214, see the rest on the next page.

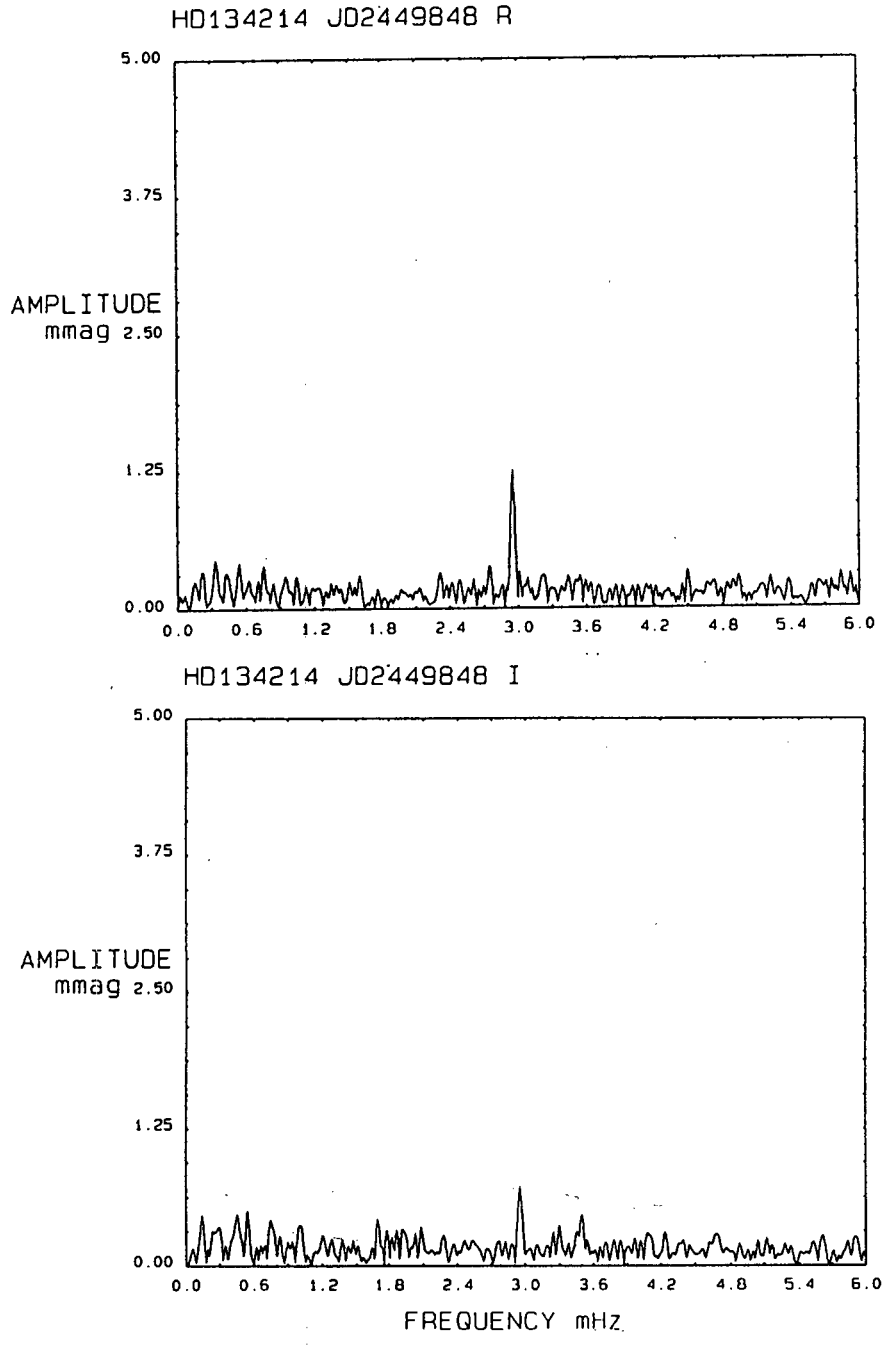

Figure 2.6: continues.

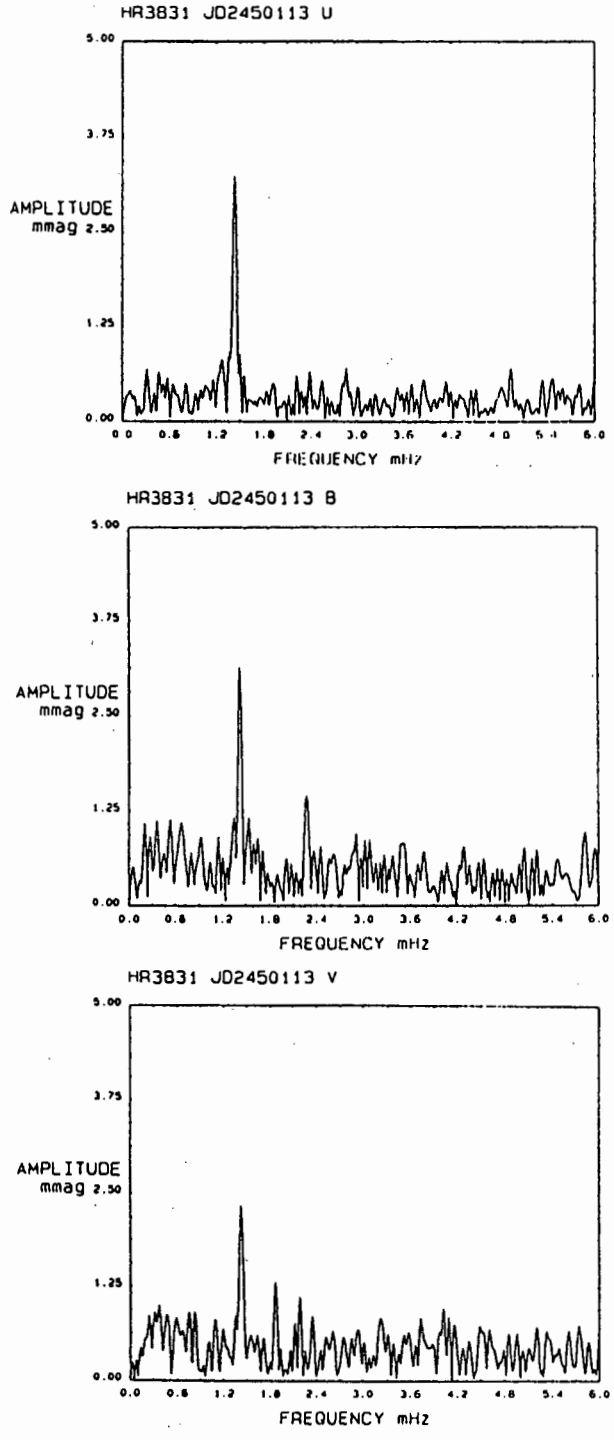

Figure 2.7: The Fourier spectrum of HR 3831 at phase 0.57. Notice the poor signal to noise ratio in the BVRI, I think it is due to the deterioration of the red tube. The rest are on the next page.

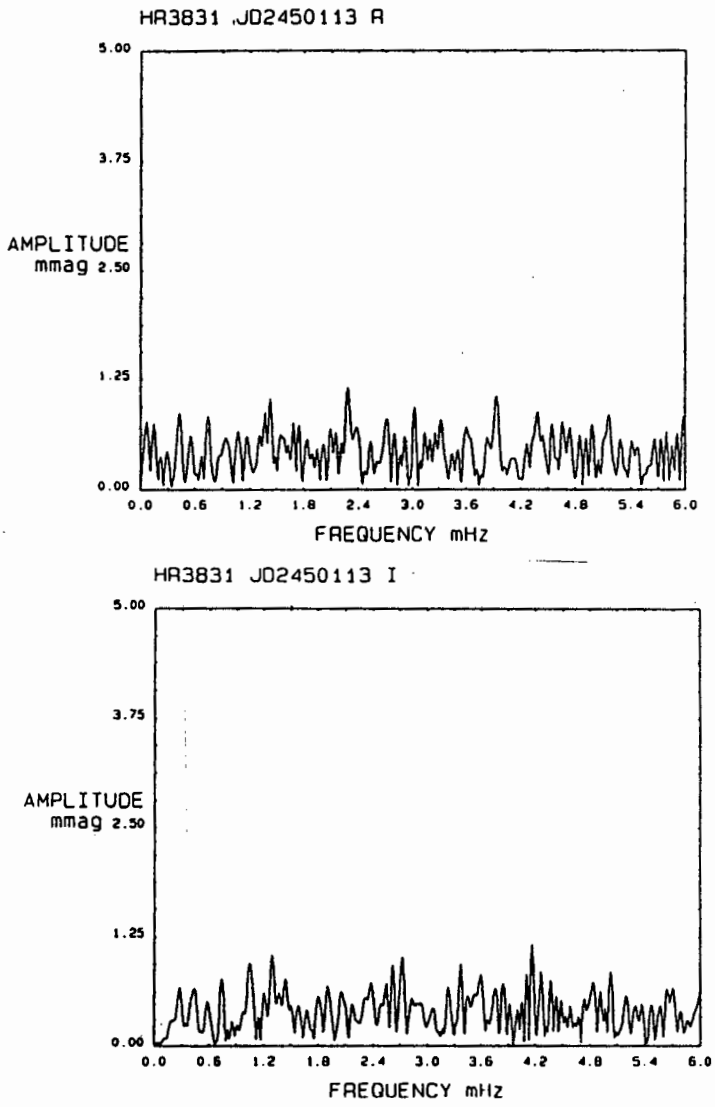

Figure 2.7: continues.

Chapter 3

The Pulsation Model

3.1 Introduction

All roAp stars for which pulsation mode identification has been done successfully show dipole mode in their principal frequencies (α Cir (Kurtz *et al.* 1994b) and HR 3831 (Kurtz *et al.* 1994a), for example). This is very useful because dipole mode light variations are particularly easy to model. Balona and Stobie (1979a) derived a linearised expression to describe the variation of the projected surface area for a non–radially pulsating star. The expression is given below:

$$\frac{\Delta A}{A_o} = \epsilon P_{\ell m}(cos\Theta_o)cos(\omega t + m\Phi_o)2(2p_\ell - q_\ell) \tag{3.1}$$

where

$$p_\ell = \int_0^1 \mu P_\ell d\mu \tag{3.2}$$

and

$$q_\ell = \ell \int_0^1 (P_{\ell-1} - \mu P_\ell) d\mu \tag{3.3}$$

$\mu = \cos\theta$, A is the projected surface area, ΔA is the variation of A from the equilibrium value, (Θ_o, Φ_o) denotes the direction of the observer, ϵ is arbitrary and $\ll 1$, $P_\ell = P_\ell(\mu)$ is the Legendre polynomial.

The values of p_ℓ and q_ℓ for $0 \leq \ell \leq 8$ as calculated by Balona and Stobie (1979a) are reproduced in Table 3.1. It is clear from the tabulated values that $\frac{\Delta A}{A_o}$ is zero for odd values of ℓ.

Table 3.1: Values of p_ℓ and q_ℓ as given by equations 3.2 and 3.3 respectively for various values of ℓ.

ℓ	p_ℓ	q_ℓ	$2p_\ell - q_\ell$
0	5.00E-1	0.00	1.00
1	3.33E-1	6.67E-1	0.00
2	1.25E-1	7.50E-1	1.75E-1
3	0.00	0.00	0.00
4	-2.08E-2	-4.17E-1	-1.00
5	0.00	0.00	0.00
6	7.81E-3	3.28E-1	-1.00
7	0.00	0.00	0.00
8	-3.91E-3	-2.81E-1	-1.00

In the same paper Balona and Stobie (1979a) show that the magnitude variation is given by:

$$\Delta m_\lambda = \Delta S_\lambda - 2.5\,(\log_{10} e)\frac{\Delta A}{A} \tag{3.4}$$

where ΔS_λ is the surface brightness variation and $S_\lambda = -2.5 log F_\lambda$, for the mean projected flux F_λ. It then becomes clear that for odd values of ℓ the light variations are due entirely to flux or temperature variation (ΔS_λ). Therefore for the $(\ell, m) = (1, 0)$ mode $\Delta m_\lambda = \Delta S_\lambda$, *i.e* brightness variations are entirely due to flux or temperature variations.

Two approaches have been adopted towards modelling the pulsation amplitude as a function of wavelength of the dipole mode in roAp stars. One is the simple analytical approximation, the results of which were reported by Kurtz & Medupe (1996), and the other, which is more realistic, is numerical modelling.

In the two approaches several simplifying assumptions are made which I list below:

1. The star is spherically symmetric. This is a reasonable assumption since most roAp stars are slow rotators. Rotation flattens the poles of a star thus making the shape spherically asymmetric. The corresponding distribution of temperature and luminosity over the stellar surface is non–uniform (Wolff 1983) with resulting changes on the emergent spectrum.

2. The equilibrium surface temperature is uniform over the stellar surface. It only varies with depth. This is strictly not a correct assumption because non–uniform element distribution on Ap star surfaces causes surface temperature variation.

3. LTE is assumed. This is reasonable since NLTE is mostly important for hot stars and low temperature stars with low gravities as mentioned by Kurucz (1979). The roAp stars are neither hot nor low gravity stars, so NLTE effects should be very small for these stars.

4. Limb–darkening of the form of equation 1.23 is adopted. This is a reasonable approximation for the sun and has been used in modelling other stars.

In both approaches, the idea is to determine the luminosity of the visible surface of the stellar disk at pulsation maximum, and compare it to the luminosity at pulsation equilibrium in order to determine the pulsation semi–amplitude. Each method is described in the next two sections.

3.2 Analytical approximation

The following discussion is based on the geometry shown in figure 3.1. Consider the surface element of area dA at angle θ as shown in figure 3.1. It is easily shown that

$$dA = R\,sin\theta\,d\phi\,R\,d\theta. \tag{3.5}$$

The unit normal to the surface dA is $\mathbf{n}$ and the unit normal in the direction of the observer is $\mathbf{u_z}$. Then the dot product

$$\mathbf{n} \cdot \mathbf{u_z} = \cos\theta \tag{3.6}$$

is the projection factor into the line–of–sight of the observer. Thus the projected surface area of the surface element is

$$dA_p = R^2 \cos\theta \sin\theta d\theta d\phi. \tag{3.7}$$

The intensity is weighted by the projected surface area in order to define

$$dl_\lambda = I_\lambda(\theta, \phi) dA_p, \tag{3.8}$$

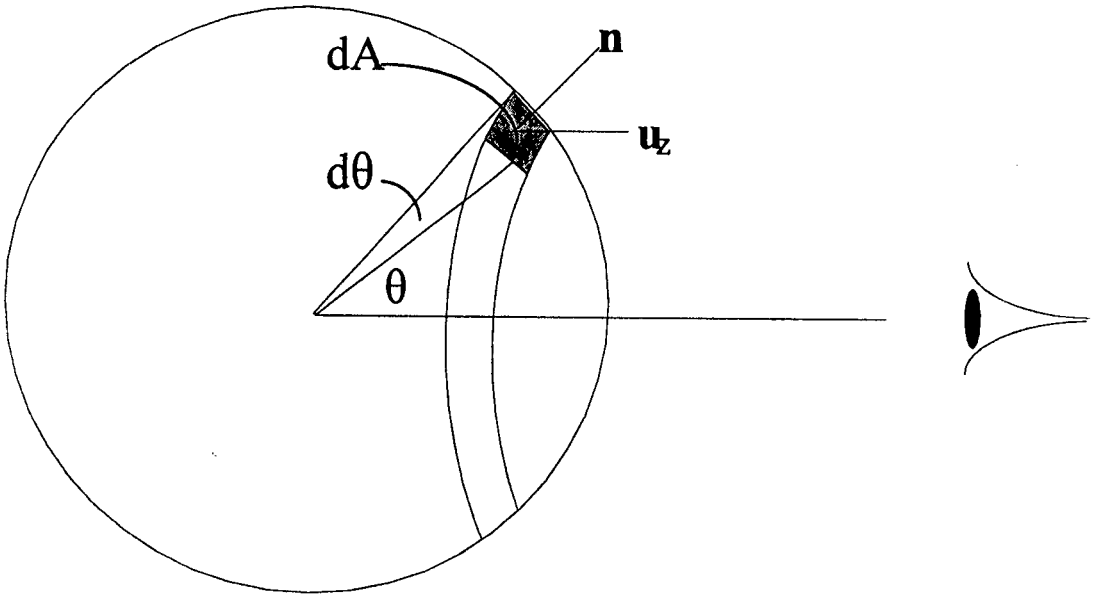

Figure 3.1: A sketch to show the geometry of a spherically symmetric star of radius R in equilibrium. The surface element area dA at co–latitude θ is shown. The pulsation and rotation axes are both pointing to the observer, *i.e* the pole–on case.

for each surface element dA, where $I_\lambda(\theta, \phi)$ is the limb–darkened monochromatic surface intensity given by this expression

$$I_\lambda(\theta, \phi) = I_{\lambda,o}(\theta, \phi)(1 - \beta_\lambda(1 - \cos\theta)). \tag{3.9}$$

The net observed surface flux is proportional to the integral of dl_λ over the visible surface of the star. The luminosity is then directly proportional to the net flux:

$$L_\lambda \propto \int_0^{2\pi} \int_0^{\frac{\pi}{2}} I_\lambda(\theta, \phi) \cos\theta \sin\theta d\theta d\phi \tag{3.10}$$

The contribution of the radius to the luminosity is subsumed in the proportionality of the above equation. On comparing with observations the intensity has to be convolved with the the response function of the detector (namely the telescope, filters and the photo–multiplier system). I assume here that observations were made with rectangular response functions so the intensity is constant across the filter and equal to the monochromatic intensity. The

width of the response function $\Delta\lambda$ is also subsumed in the proportionality of the above relation. The effect of this assumption is very small, as I show in the next section.

I then make an assumption that the star radiates like a black–body, so that the monochromatic intensity is given by :

$$I_{\lambda,o}(\theta,\phi) = \frac{2hc^2}{\lambda^5}\frac{1}{exp(\frac{hc}{\lambda kT(\theta,\phi)}) - 1} \tag{3.11}$$

The temperature is a function of θ and ϕ due to non-radial pulsation (and inhomogeneous surface distribution of elements, which I neglect). A better treatment for the intensity is done by using the intensity from the solution of the radiative transfer equation as is done numerically in the ATLAS9 model atmosphere program described in the next section.

For a star pulsating non–radially with the pulsation pole inclined at an angle α to the line of sight, the temperature oscillations about equilibrium temperature value T_o are given thus:

$$T(\theta,\phi) = T_o + \Delta T Y_\ell^m(\theta',\phi') = T_o\left(1 + \frac{\Delta T}{T_o}Y_\ell^m(\theta',\phi')\right) \tag{3.12}$$

ΔT is the maximum pulsational semi–amplitude of the temperature from the equilibrium value at the pulsation pole. $Y_\ell^m(\theta',\phi')$ is the spherical harmonic that describes non–radial pulsations. The co–ordinates θ' and ϕ' are measured with respect to the pulsation pole.

The fact that our observations covered the wavelength range $3500\,\text{Å} < \lambda < 8000\,\text{Å}$ and that the characteristic temperature (T_o) for roAp stars is about 8000 K implies that $164.2 \geq \exp\left(\frac{hc}{\lambda kT_o}\right) \geq 9.3 \gg 1.0$. This justifies our using the Wien approximation. The pulsation amplitudes of roAp stars are very small ≤ 10 mmag; this makes $\Delta\text{T} \ll 80\,\text{K}$. With $\text{T} \approx 8000\,\text{K}$ we get $\frac{\Delta T}{T} \leq 0.01 \ll 1$. Given the above estimates and the fact that $Y_\ell^m(\theta',\phi') \sim 1$ we are able to use a first order binomial expansion to find

$$I_{\lambda,o}(\theta,\phi) = \frac{2hc^2}{\lambda^5}\exp\left(-\frac{hc}{\lambda kT(\theta,\phi)}\right) = B_\lambda(T_o)\exp\left(\frac{hc}{\lambda kT_o}\frac{\Delta T}{T_o}Y_\ell^m(\theta',\phi')\right) \tag{3.13}$$

where

$$B_\lambda(T_o) = \frac{2hc^2}{\lambda^5}\exp\left(-\frac{hc}{\lambda kT_o}\right). \tag{3.14}$$

In the wavelength range of our observations $2.2 \leq \frac{hc}{\lambda kT_o} \leq 5.1$ so

$$\frac{hc}{\lambda kT_o}\frac{\Delta T}{T_o}Y_\ell^m(\theta',\phi') \ll 1 \tag{3.15}$$

Hence we can use the first order approximation $e^x \approx 1 + x$ for $x \ll 1$ to get

$$I_{\lambda,o}(\theta,\phi) = B_\lambda(T_o)\left(1 + \frac{hc}{\lambda k T_o}\frac{\Delta T}{T_o}Y_\ell^m(\theta',\phi')\right). \tag{3.16}$$

Equation 3.9 then becomes

$$I_\lambda(\theta,\phi) = B_\lambda(T_o)\left(1 + \frac{hc}{\lambda k T_o}\frac{\Delta T}{T_o}Y_\ell^m(\theta',\phi')\right)(1 - \beta_\lambda(1-\cos\theta)). \tag{3.17}$$

The luminosity (from equation 3.10) is then given by

$$L_\lambda \propto \int_0^{2\pi}\int_0^{\frac{\pi}{2}}\left(1 + \frac{hc}{\lambda\, k\, T_o}\frac{\Delta T}{T_o}Y_\ell^m(\theta',\phi')\right)(1 - \beta_\lambda(1-\cos\theta))\cos\theta\sin\theta\, d\theta\, d\phi \tag{3.18}$$

where $B_\lambda(T_o)$ has been subsumed into the proportionality.

To transform the pulsation mode from the pulsation axis to the line–of–sight we use the standard coordinate rotation rule:

$$Y_\ell^m(\theta',\phi') = \sum_{m'=-\ell}^{+\ell} A_{mm'}Y_\ell^{m'}(\theta,\phi) \tag{3.19}$$

where $A_{mm'}$ are elements of the coordinate transformation matrix which can be found in Edmonds (1957). (θ',ϕ') refers to the pulsation axis, and (θ,ϕ) to the line–of–sight. Hence, the dipole pulsation mode can be decomposed into $(\ell,m) = (1,-1),(1,0)$ and $(1,1)$ modes along the line–of–sight.

It can be shown (Kurtz & Shibahashi (1986)) that for the dipole mode the transformation is given thus

$$\begin{aligned} Y_{\ell=1}^{m=0}(\theta',\phi') \;=\; & -\frac{1}{4}\sqrt{\frac{3}{2\pi}}(1+\cos\alpha)\sin\theta e^{i\phi} \\ & +\frac{1}{2}\sqrt{\frac{3}{\pi}}\cos\alpha\cos\theta \\ & +\frac{1}{4}\sqrt{\frac{3}{2\pi}}(1+\cos\alpha)\sin\theta e^{-i\phi} \end{aligned} \tag{3.20}$$

where α is the inclination of the pulsation axis to the line–of–sight. Equation 3.18 involves integrating in ϕ from 0 to 2π and since

$$\int_0^{2\pi}\frac{1}{4}\sqrt{\frac{3}{2\pi}}(1+\cos\alpha)\left(\sin\theta e^{-i\phi} - \sin\theta e^{i\phi}\right)d\theta = 0, \tag{3.21}$$

there will be no ϕ dependence in equation 3.18. The $m = \pm 1$ modes are rotating about the line–of–sight, so they do not contribute to the observed luminosity variation.

Substituting the term that does not depend on ϕ in equation 3.20 into equation 3.18 and integrating over ϕ we get

$$L_\lambda \propto \int_0^1 \left(1 + \frac{1}{2}\sqrt{\frac{3}{\pi}}\frac{hc}{\lambda k T_o}\frac{\Delta T}{T_o}\cos\alpha\mu\right)(1 - \beta_\lambda + \beta_\lambda\mu)\mu\, d\mu \tag{3.22}$$

where $\mu = \cos\theta$. The pulsation semi–amplitude in intensity units, A_λ, is the ratio of the luminosity at pulsation maximum to the luminosity at equilibrium. A_λ is given by

$$A_\lambda = \frac{L_\lambda(\Delta T)}{L_\lambda(\Delta T = 0)}. \tag{3.23}$$

Using the above derived expression for L_λ we get

$$A_\lambda = \frac{\int_0^1 \left(1 + \frac{1}{2}\sqrt{\frac{3}{\pi}}\frac{hc}{\lambda k T_o}\frac{\Delta T}{T_o}\cos\alpha\mu\right)(1 - \beta_\lambda + \beta_\lambda\mu)d\mu}{\int_0^1 (1 - \beta_\lambda + \beta_\lambda\mu)\mu\, d\mu} \tag{3.24}$$

Evaluating the above equation explicitly we get the following results

$$A'_\lambda = \frac{1}{4}\sqrt{\frac{3}{\pi}}\left(\frac{4 - \beta_\lambda}{3 - \beta_\lambda}\right)\cos\alpha\frac{hc}{\lambda k T_o}\frac{\Delta T}{T_o}, \tag{3.25}$$

where $A'_\lambda = A_\lambda - 1$. The observed amplitude $A_{\lambda obs}$ in magnitudes is

$$\begin{aligned} A_{\lambda obs} &= 2.5\log(A'_\lambda + 1) \\ &= \frac{2.5\ln(A'_\lambda + 1)}{\ln 10} \\ &= 1.086\ln(A'_\lambda + 1) \end{aligned} \tag{3.26}$$

and since $\ln(1 + x) \approx x$ for small x we get

$$A_{\lambda obs} \approx 1.086 A'_\lambda \tag{3.27}$$

Substituting equation 3.25 into 3.27 we finally have

$$A_{\lambda obs} = 1.086\frac{1}{4}\sqrt{\frac{3}{\pi}}\left(\frac{4 - \beta_\lambda}{3 - \beta_\lambda}\right)\cos\alpha\frac{hc}{\lambda k T_o}\frac{\Delta T}{T_o}. \tag{3.28}$$

This important result deserves detailed discussion which we provide in the next section.

3.2.1 Discussion

The amplitudes from Tables 2.2 and 2.3 are normalised to 1 in B and plotted in Figure 3.2. The plot shows that the pulsation amplitude of the roAp stars drops by a factor between 4 and 12 from B to I. Also plotted in Figure 3.2 is the wavelength dependence of the amplitude as described by equation 3.28 for constant T_o and ΔT. We can deduce from the plot that the wavelength dependence of equation 3.28 alone can only explain the factor of 2 decline of the pulsation amplitude at longer wavelengths.

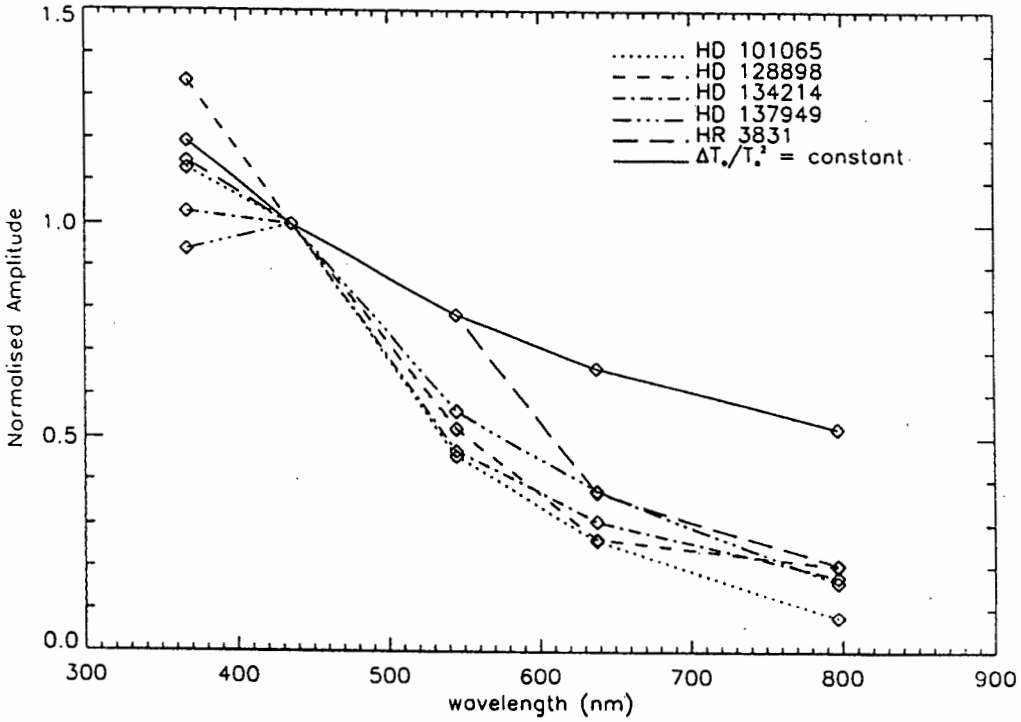

Figure 3.2: The observed amplitudes from Tables 2.2 and 2.3 normalised to 1 in B. The HR 3831 amplitudes are taken at the rotation phase 0.57. The solid line represents equation 3.28 with $\frac{\Delta T}{T_o^2}$ kept constant. The solar limb–darkening coefficients were used.

Equation 3.28 also shows the effect of limb–darkening on the observed amplitude. Changing the limb–darkening coefficient from 0 in I to 1 in B filters (the maximum range allowable), only increases the normalised amplitude by 0.125. This is too small an effect to explain the precipitous decline of amplitude with wavelength. The dependence of equation 3.28 on limb–darkening is shown in Figure 3.3. The first observation to make is that equation 3.28 indeed confirms the point made earlier that limb–darkening increases the pulsation

amplitude. The gradual increase of amplitude with increasing limb–darkening demonstrates

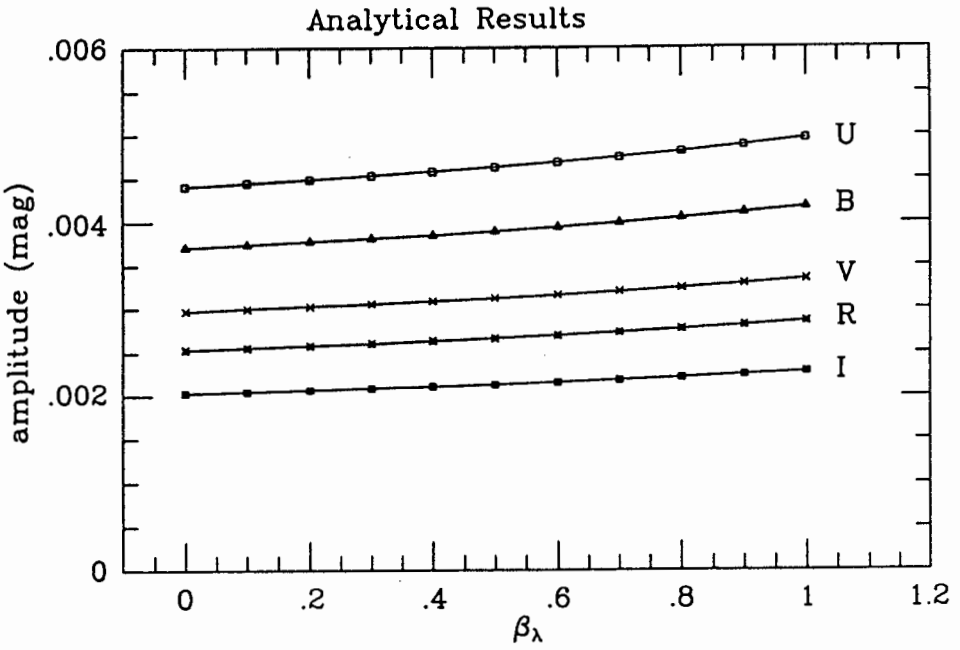

Figure 3.3: Equation 3.28 is used to show the dependence of amplitude on limb–darkening at various wavelengths. Parameters used are $T_o = 7900K$, $\alpha = 0.0$ and $\Delta T = 20K$.

that limb–darkening is only a small effect. This is a proof that the Matthew's technique does not work.

The observed amplitude thus depends strongly on T_o and ΔT. The opacity in Ap stars increases from B to V to R to I (in the continuum), therefore the temperature T_o decreases with increasing wavelength. Since temperature also depends on atmospheric depth z, there is a relation between z and wavelength λ. In fact, when one looks at longer wavelengths one looks higher in the atmosphere. The fact that the temperature decreases with increasing wavelength alone will have the effect of increasing the observed amplitude at longer wavelengths (according to equation 3.28), contrary to the observations. It must, therefore, be the strong decline of $\Delta T(\lambda, z)$ with increasing wavelength that causes the observed amplitude to decline sharply with wavelength. Thus, rather than giving information about limb–darkening (and thus $T(\tau)$), the pulsation amplitude as a function of wavelength observations enable one to see level effects in the temperature amplitude of the pulsation modes in the roAp stars. I conclude that by giving $T(\tau)$ as an input, one can determine the variation of ΔT

with λ and atmospheric geometric depth z. I shall pursue this goal in sections 3.4 and 3.5.

Equation 3.28 is a good approximation for the short wavelength observations. However, one expects it to describe data less well (by 10%) at longer wavelengths, largely because the Wien approximation is poorer at longer wavelengths.

The above result was obtained by assuming that the star we are looking at is a black–body radiator. This is not entirely true and so a better treatment of the intensity is necessary. We do this in the next section where intensity as a function of wavelength obtained from model atmospheres is used.

3.3 Numerical Modelling

3.3.1 Model description

We once again consider the visible surface of the star whose pulsation axis is inclined at an angle α to the line–of–sight. We then sample the visible surface with a grid such that the grid lines are parallel to the lines of longitude ϕ and latitude θ of the star as shown in Figure 3.4. Thus, the grid will have pixels of unequal area ΔA.

Consider one such pixel bounded by two latitude grid lines θ_i and θ_{i+1} and longitude grid lines ϕ_j and ϕ_{j+1}. The separation between two consecutive latitude grid lines (those parallel to lines of latitude) is $\Delta\theta$ and that for the longitude grid lines is $\Delta\phi$. Therefore $\Delta\theta = \theta_{i+1} - \theta_i$ and $\Delta\phi = \phi_{j+1} - \phi_j$. The area (projected onto the line–of–sight) of each pixel is then given by

$$\Delta A_p = R^2 \sin\theta \Delta\theta \Delta\phi \cos\theta \tag{3.29}$$

where R is the radius of the star. The contribution to the luminosity at a given pixel, convolved with the instrument response function $\phi(\lambda)$ is given by

$$l_{\lambda i}(T_o) = \int_{\lambda_1}^{\lambda_2} I_\lambda(\theta, T_o) \Delta A_p \phi(\lambda)\, d\lambda \tag{3.30}$$

$I_\lambda(\theta, T_o)$ is the limb–darkened intensity at temperature T_o, λ_1 and λ_2 are wavelength limits of the filter response function. Equation 3.30 gives the contribution to equilibrium luminosity of each pixel. The variation of $l_{\lambda i}$ with temperature is determined from model atmospheres for equispaced temperatures ranging from T_o to $T_{max} = T_o + \frac{\Delta T}{2}\sqrt{\frac{3}{\pi}}\cos\alpha$, for a dipole mode.

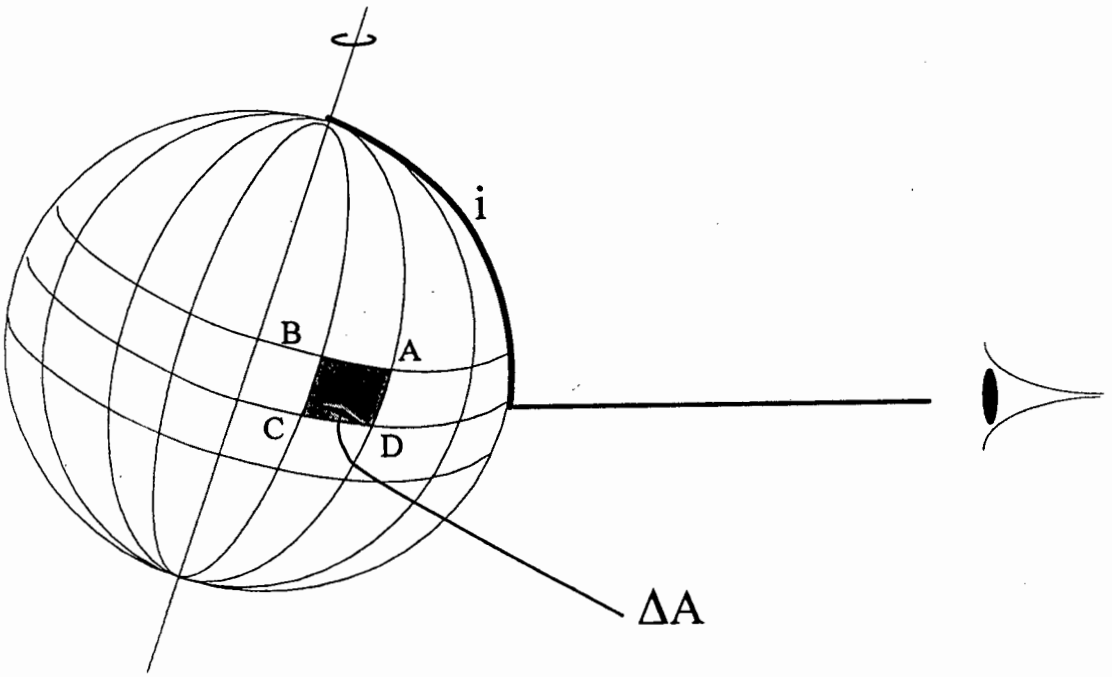

Figure 3.4: The surface of the star is sampled with a grid. The shaded area shows one of the pixels of area ΔA, bounded by A $(\theta_{i+1}, \phi_{j+1})$, B (θ_{i+1}, ϕ_j), C (θ_i, ϕ_j) and D (θ_i, ϕ_{j+1}). The dimensions of the pixel are AD $= \Delta\theta = \theta_{i+1} - \theta_i$ and BA $= \Delta\phi = \phi_{i+1} - \phi_i$. Angle i is the inclination of the rotation axis with respect to the line–of–sight. Any calculation at any given pixel is done at the centre of that pixel.

In section 3.2 we showed that temperature variations due to a star pulsating in a dipole mode, inclined at angle α to the line–of–sight is given by

$$T(\theta) = T_o \left(1 + \frac{\Delta T}{T_o} \frac{1}{2} \sqrt{\frac{3}{\pi}} \cos\alpha \cos\theta\right). \tag{3.31}$$

The value of $l_{\lambda i}$ at T(θ) is estimated by the linear interpolation scheme given below:

$$l'_{\lambda i}(T(\theta)) = l_{\lambda i}(T_j) + \frac{(l_{\lambda i}(T_{j+1}) - l_{\lambda i}(T_j))}{T_{j+1} - T_j}(T(\theta) - T_j) \tag{3.32}$$

for T(θ) falling between T_j and T_{j+1} in the i^{th} pixel. This gives us the perturbed value of $l_{\lambda i}$.

The $l_{\lambda i}(T)$ contributions at each pixel are added up and amplitude worked out from

$$A_{\lambda obs} = 2.5 \log \left(\frac{\sum_i l'_{\lambda i}(T(\theta))}{\sum_i l_{\lambda i}(T_o)} \right). \tag{3.33}$$

The summation is over the visible surface. A brief description of how model atmospheres were created is described below. This is followed by the actual implementation of the pulsation model and the model results.

3.3.2 Model atmospheres

Parameters such as intensity, opacity and density, that are to be used later in the chapter are obtained from model atmospheres. Model atmospheres were constructed using the ATLAS9 program run with the VAX FORTRAN 5.0 compiler, on the VMS version 6.2 environment.

Model atmospheres as calculated by ATLAS9 are made under the following assumptions and approximations:

1. Steady state atmosphere.
2. The energy flux is constant with depth in the atmosphere and equals $\sigma \, T_{\rm eff}^4$, where $\sigma = 5.6697 \times 10^{-5}$ erg cm^{-2} K^{-4}.
3. The surface of the atmosphere is homogeneous, the only variations are vertical, *i.e* variation with depth. So effects such as magnetic fields, starspots, cells, spicules and granules are ignored.
4. Plane parallel atmosphere. This is valid for stars with thin atmospheres relative to their radii. This assumption is thus valid for main sequence stars (and so valid for roAp stars as well), but inappropriate for supergiants.
5. Hydrostatic equilibrium is assumed, so there is no net acceleration and no relative motion of the layers of the atmosphere in the vertical direction. This is not valid for pulsating stars, but since the pulsation amplitudes for roAp stars are small it is a small effect.
6. The atomic abundances are constant throughout the atmosphere. We know about the surface inhomogeneities of elements in Ap stars, so this is not a valid assumption for roAp stars. This is a small effect since we are only interested in average properties of the atmospheres. This would be crucial for spectral analysis.

Models

All model atmospheres presented in this thesis include both radiative and convective zones, with the mixing length to scale height ratio of $\frac{\ell}{H} = 1.5$ in the convective zone. We also assume LTE, as it has been pointed out at the beginning of this chapter that NLTE effects are not significant in the atmospheres of roAp stars.

Opacity plays a crucial role if a realistic model is to be calculated. It is for this reason, and for the fact that we will use opacity to determine the relationship between atmospheric depth and wavelength, that we devote the next session to discussing how opacity is calculated in ATLAS9.

Opacity

ATLAS9 divides all possible absorption and scattering processes into twenty groups (see Kurucz 1970), and allows the user to select those groups that are relevant to the stars of interest. For our models we included continuous opacities for H I and H II, H^-, H_2^+, He I - He III, C I - C IV, N II - N V, O II - O VI, Ne I - Ne VI, Mg I, Al I, Si I, electron scattering and H Rayleigh scattering. The net continuous opacity is taken as the sum of all of these contributions $\sigma_\lambda^c + \kappa_\lambda^c$ in units of $\mathrm{cm^2\,g^{-1}}$, where κ_λ^c is the total continuous mass absorption coefficient (in units of $\mathrm{cm^2\,g^{-1}}$), and σ_λ^c is the total scattering coefficient, also in units of $\mathrm{cm^2\,g^{-1}}$.

Line opacities (ℓ_λ) in ATLAS9 are represented by the opacity distribution functions (ODFs). It is computationally impossible to represent all the lines of most stars at each frequency, because most cool stars have many absorption lines . It is rather unnecessary to use detailed point by point frequency variation of opacity in model calculations. This is because the structure of stellar atmosphere is determined by integrals of the radiation field over frequency at each depth, and not on monochromatic quantities as such.

Computationally ODFs are represented as step functions with steps of width w_i for each step i. ATLAS9 produces a table of all continuous opacities and line opacities ($\ell_{\lambda i}$) at each depth point for each distribution function step i and width w_i. This is presented at each of the sampled wavelength points. The monochromatic line opacity is then given by

$$\ell_\lambda = \sum_{i=1}^{N_\lambda} w_i \ell_{\lambda i} \tag{3.34}$$

where N_λ is the number of steps, the ATLAS9 ODFs have a fixed $N_\lambda = 12$.

So the total opacity κ_λ I use is

$$\kappa_\lambda = \kappa_\lambda^c + \sigma_\lambda^c + \ell_\lambda. \tag{3.35}$$

Two sets of ODFs are used, the high resolution ones used for calculating surface fluxes and intensities, and the low resolution ones for model calculation. The ODFs are linearly interpolated, using Kurucz's DFINTERP program (Kurucz 1993b), to get the appropriate ones for the required abundances.

Our models use scaled solar abundances. Kurucz's (1993a) model grids were used as inputs to ATLAS9, and converged to within 1% flux error, except at greater depths where the flux error was kept below the 3% level. In the next few pages we show the intensity distributions over wavelength for the various models. The α Cir model is the most realistic of all the models. The input parameters for this model are well determined by Kupka *et al.* (1995, 1996).

F. Kupka and his group are producing better Ap star model atmospheres. They produce their own ODFs according to the individual composition of stars (something which ATLAS9 lacks). Kurucz (1993a) has announced his new opacity sampling model atmosphere program (ATLAS12) which allows arbitrary abundances, and will enable improved model atmospheres of CP stars to be made. Unfortunately, it is not available yet. The intensity spectrum (central intensities) from the model atmosphere of α Cir, based on the abundances by Kupka (1995, 1996) is shown in Figure 3.5. Kupka & Piskunov (in preparation) concluded from their individual model of α Cir (Figure 3.5) that a chemical composition similar to that in Kupka *et al.* (1995, 1996), has more or less the same effect as scaling the solar composition by +0.2 dex. I produced the +0.2 dex, $T_{\rm eff} = 7900\,{\rm K}$, $\log g = 4.2$, $V_{\rm turb} = 2{\rm km\,s^{-1}}$ model using ATLAS9. The intensity spectrum for this model is shown in Figure 3.6. Comparison of the two models show that the scaling of the two spectra is the same, and that the continua (at wavelengths longer than 400 nm) match exactly. All absorption lines in the region $\lambda > 400\,{\rm nm}$ for both spectra are of the same strength. I do not include the part of the spectrum shortward of $\lambda = 400$ nm as F. Kupka is still working on it. The overall similarity of the two models (as far as the surface intensity spectrum is concerned) gives me the confidence that my models are on average correct.

The luminosities of roAp stars are not well known, and model atmospheres of these are difficult to construct (except α Cir). Therefore the surface gravities of these stars are not well determined. For the other four stars HD 134214, HR 3831, HD 137949 and HD 101065 I shall use $\log g = 4.2$. Since we expect line blanketing to be severe in HD 101065, I have decided to use higher abundances (of +0.5 dex) to make its model atmosphere. The intensity

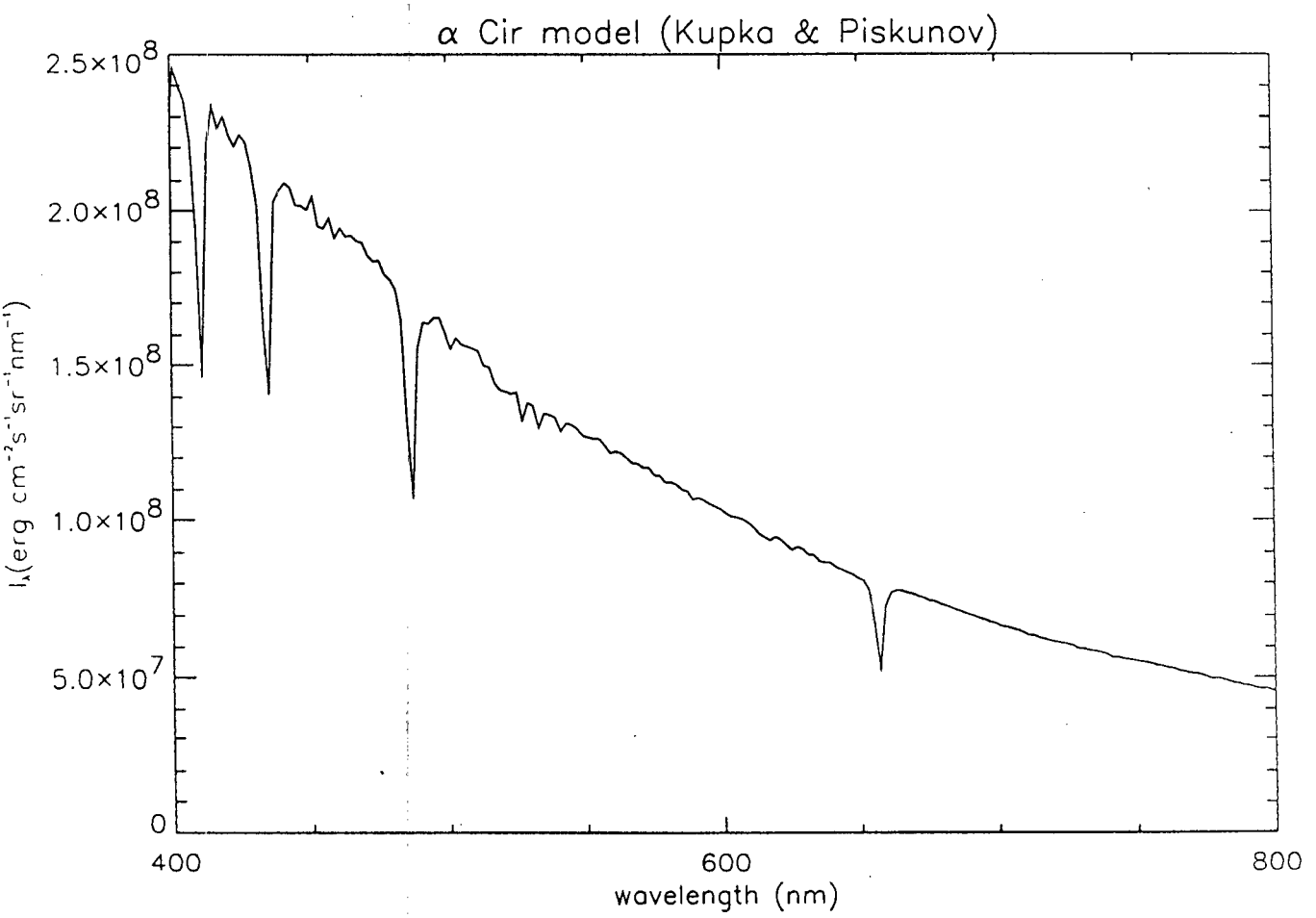

Figure 3.5: The intensity spectrum (in the optical region) of the model atmosphere of α Cir based on the abundances derived by Kupka *et al.* (1995, 1996), with $T_{eff} = 7900\,K$, $\log g = 4.2$, $V_{turb} = 1.5\,km\,s^{-1}$.

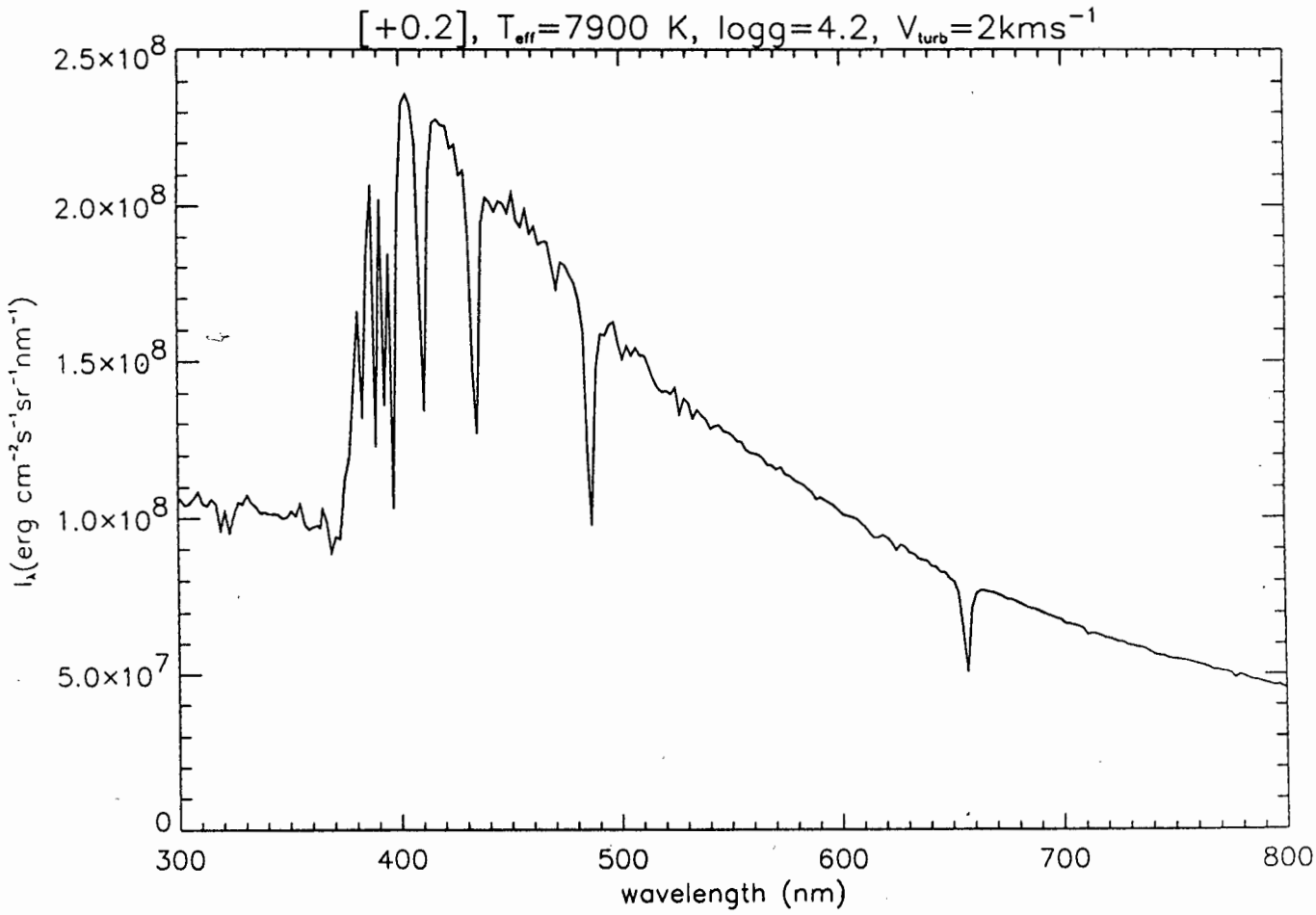

Figure 3.6: The model atmosphere of α Cir based on scaled solar abundance. The atmospheric parameters used are $T_{eff} = 7900\,K$, $\log g = 4.2$, $V_{turb} = 2\,km\,s^{-1}$ from ATLAS9. The comparison with Kupka & Piskunov (in preparation)'s model shows that this model is in agreement with theirs from the B to the I regions.

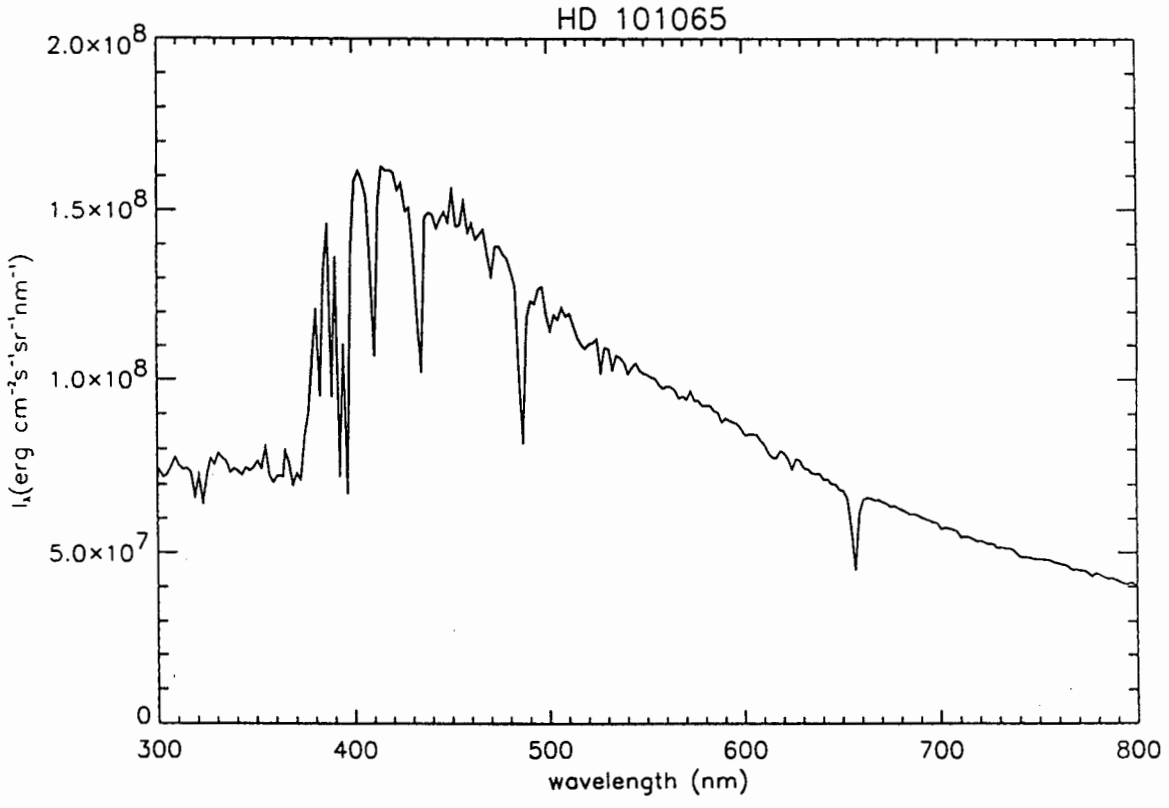

Figure 3.7: The intensity spectrum of the model [+0.5], $T_{eff} = 7400\,K$, $\log g = 4.2$ (HD 101065).

spectra for each of these stars are shown in the next few pages. The turbulent velocity used is $V_{turb} = 2\,kms^{-1}$.

3.3.3 Implementation of the numerical model

A grid of model atmospheres was created for temperatures ranging from T_o to $T_o + \Delta T$ in equal steps of temperature. This enables the determination of the relationship between the surface flux and temperature. Figure 3.11 shows the surface intensity as a function of temperature at the wavelengths of interest.

The linear functional relationship is confirmed by the black–body results shown in figure 3.12. The intensities from model atmospheres do not simply decrease with increasing wavelength as is the case with the black–body intensities (compare Figure 3.11 and Figure 3.12). The

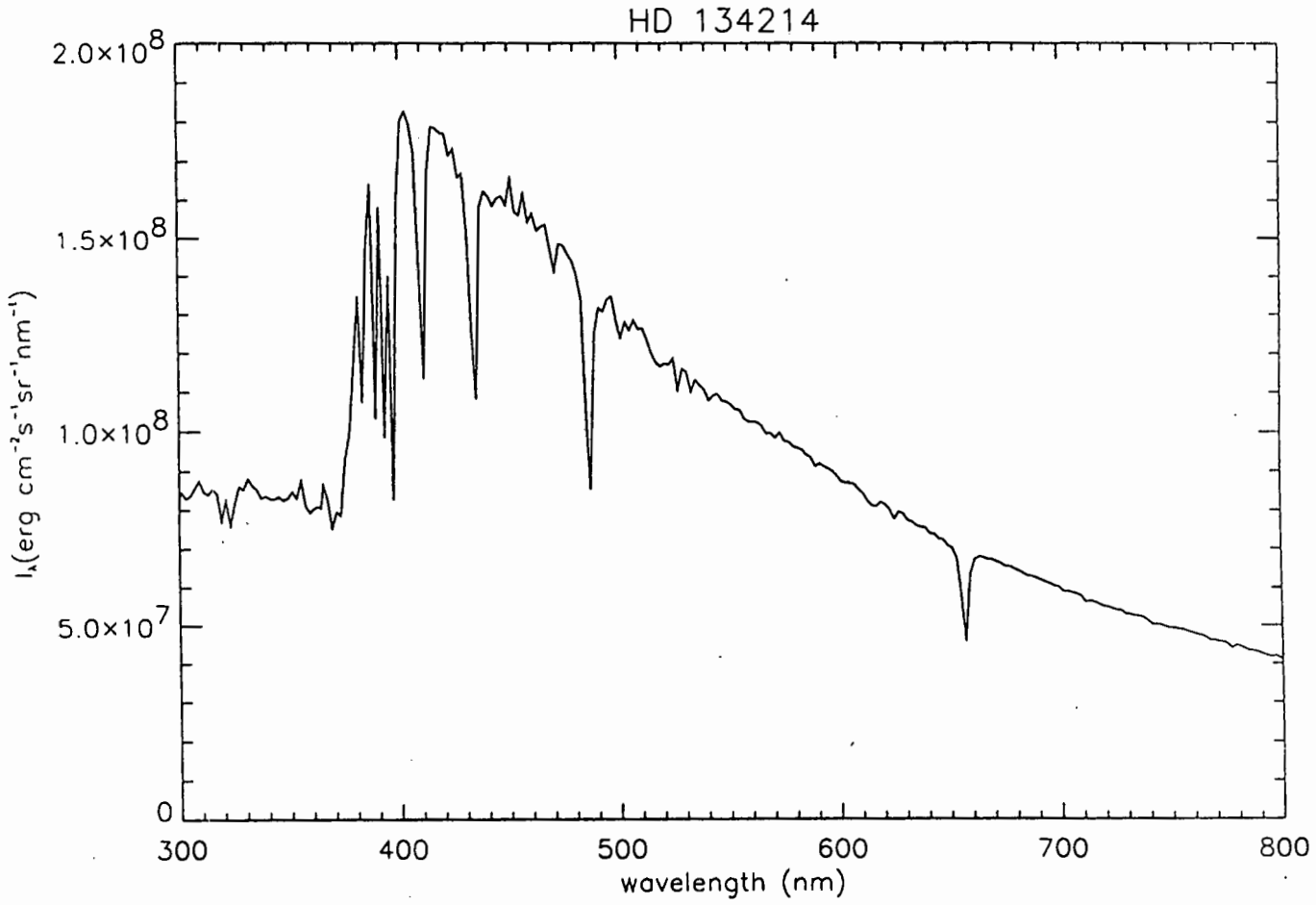

Figure 3.8: The intensity spectrum of the model [+0.2], $T_{eff} = 7550\,K$, $\log g = 4.2$ (HD 134214).

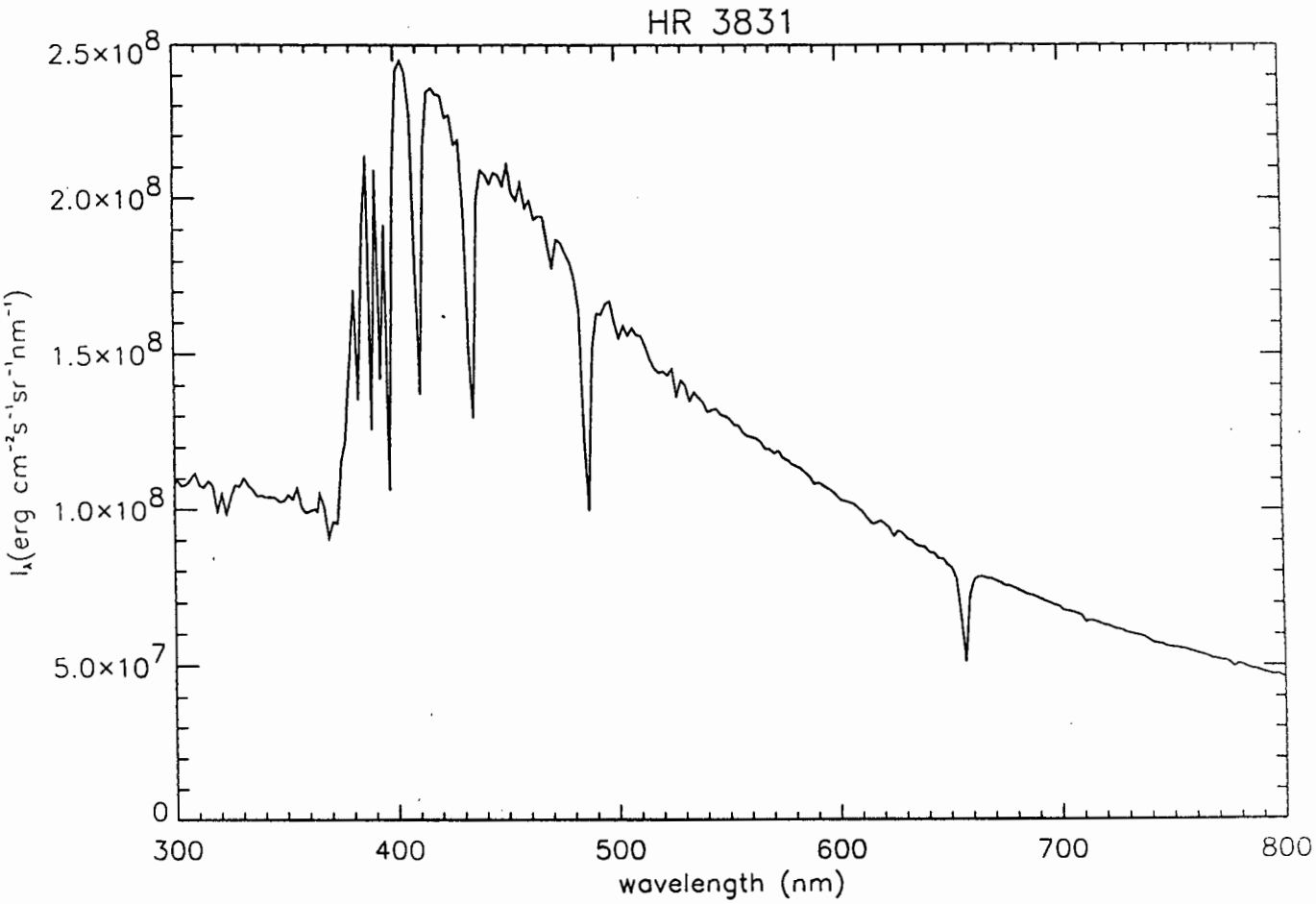

Figure 3.9: The intensity spectrum of the model [+0.2], $T_{eff} = 7950\,K$, $\log g = 4.2$ (HR 3831).

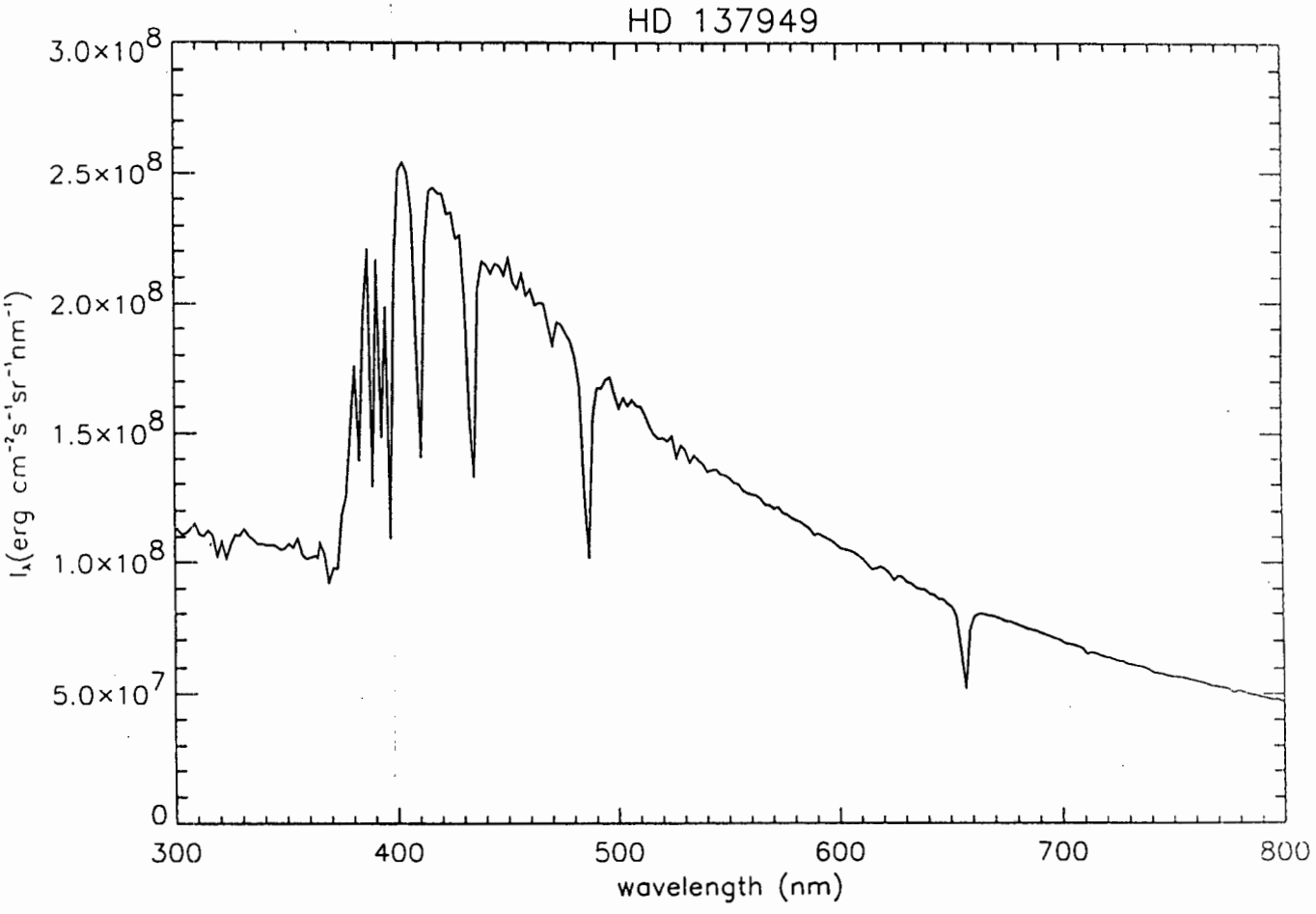

Figure 3.10: The intensity spectrum of the model [+0.2], $T_{eff} = 8000\,K$, $\log g = 4.2$ (HD 137949).

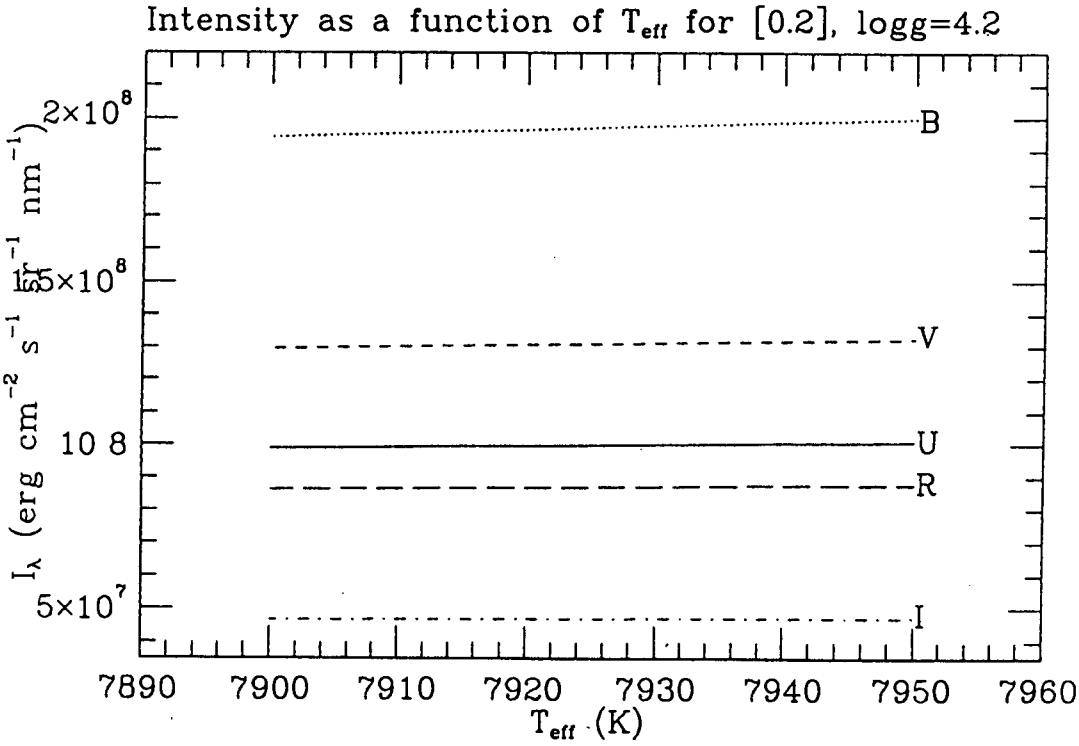

Figure 3.11: The intensity as a function of temperature obtained from model atmosphere grids with scaled abundance [+0.2] and log $g = 4.2$, and $V_{turb} = 2\,kms^{-1}$ at the wavelengths corresponding to the Johnson UBVRI colours.

U intensities are greatly affected by the Balmer discontinuity and are thus lower than the B intensities.

The $l_{\lambda i}$ values were calculated from limb–darkened intensities. Centre–of–disk intensities ($I_\lambda(\theta = 0)$) as a function of wavelength were obtained from ATLAS9. Limb–darkening was then introduced by multiplying centre–of–disk intensities with equation 1.23. This allowed us to use limb–darkening of our choice, enabling us to investigate its effect on our results.

In ATLAS9 surface intensities are sampled at unequally spaced wavelength points to allow better sampling of absorption (or emission) features on the spectrum. We were thus justified in using the simple trapezoidal integration method for working out fluxes from monochromatic intensities. So integration was approximated thus:

$$\int_a^b f(x)\,dx \approx \sum_{i=1}^{N} \frac{h_i}{2}(f(x_i) - f(x_{i-1})) \tag{3.36}$$

where $x_o = a$, $x_N = b$ and $h_i = x_i - x_{i-1}$.

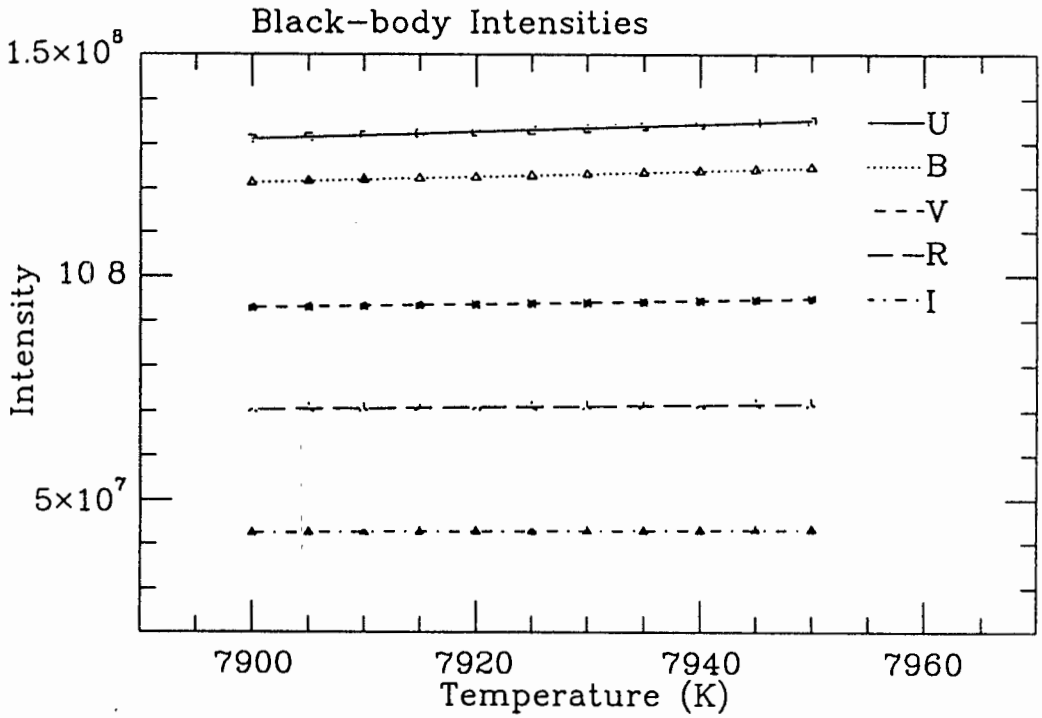

Figure 3.12: $B(T)$ as a function of temperature for comparison with figure 3.11. The scale is not the same because the model atmosphere includes the effects of opacity which the Planck function does not (see Kurucz (1979) on the effects of opacity on the energy distribution of stars).

The numerical model was checked against equation 3.28 by calculating the pulsation amplitude as a function of wavelength, using the solar limb–darkening coefficients with $\frac{\Delta T}{T_o^2}$ held constant. In Figure 3.13 I show this comparison, the amplitudes were normalised to 1 in Johnson B. There are differences which can be well explained. At the longer wavelengths the difference is $\approx$ 13%, consistent with the Wien approximation. It was indicated earlier that a 10% difference due to the Wien approximation is to be expected. The difference in the U can be attributed to the fact that Black–body intensities (which do not take into consideration the effects of line blanketing at the shorter wavelength regions of the star) were used in the derivation of equation 3.28. The intensities used in the numerical models are from line blanketed model atmospheres, and hence are better. However, one expects the U amplitudes to differ considerably from one roAp star to the next. The main point, however, is that the two models predict the same trend in the amplitude *vs* wavelength diagram. They predict a factor of two decline in amplitude from B to I for constant $\frac{\Delta T}{T_o}$; far less than what the data show.

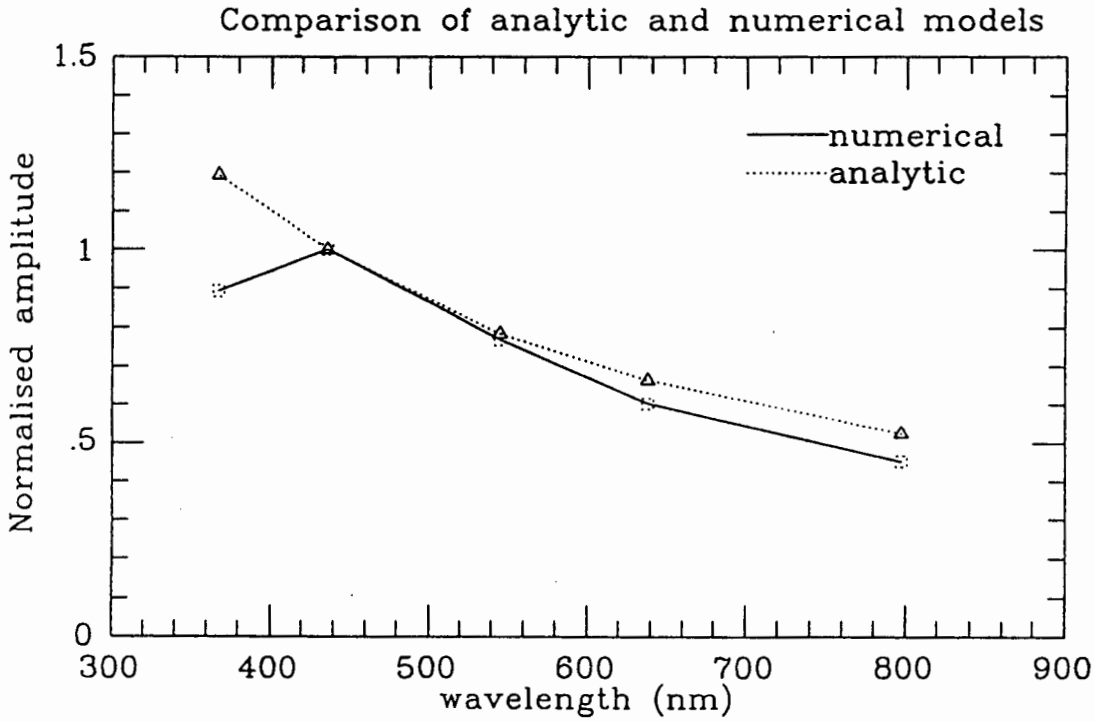

Figure 3.13: A comparison of the analytical results equation 3.28 and the numerical model. The main differences are in the U amplitudes and the R and I amplitudes. The long wavelength differences are mainly due to the Wien approximation. The differences in U are due to line blanketing and Balmer Jump effects. The two models are in agreement within these limitations.

3.4 Determination of the z *vs* λ relation

The pulsation model described in section 3.2 requires as input; amongst other things, temperature as a function of wavelength. However ATLAS9 only gives $T_o(\tau, z)$, $\rho(\tau, z)$ and $\kappa_\lambda(\tau, z)$ as its output. The τ is the optical depth, and z is the atmospheric depth, and ρ and κ_λ are density and mass absorption coefficient respectively. Thus there is a need to convert $T(\tau, z)$ to $T(\lambda)$. We have shown in section 3.2.1 how the fact that the opacity in roAp stars increases with increasing wavelength suggests that when one looks at longer wavelength, one actually looks higher in the atmosphere. Thus z and λ are related. It is the objective of this section to investigate the nature of this relation.

The optical depth that increases with depth z is defined in the following way:

$$\tau_\lambda = \int_0^z \kappa_\lambda(x)\rho(x)\,dx, \tag{3.37}$$

where κ_λ is the monochromatic mass absorption coefficient in $\mathrm{cm^2\,g^{-1}}$, and ρ is the mass density in $\mathrm{g\,cm^{-3}}$. If we assume we are seeing to the depth of $\tau_\lambda = \ln 2$ at all wavelengths, we can obtain the depth z corresponding to wavelength λ. Then the problem reduces to solving for z in the following equation

$$\int_0^z \kappa_\lambda(x)\rho(x)\,dx = \ln 2, \tag{3.38}$$

To compare with the observations we convolve the monochromatic optical depth with the detector response function. The final expression is given below:

$$\int_{\lambda_1}^{\lambda_2}\int_0^z \kappa_\lambda(x)\rho(x)\phi(\lambda)\,dx\,d\lambda = \ln 2 \tag{3.39}$$

where once again λ_1 and λ_2 are the wavelength limits of $\phi(\lambda)$. In appendix A I describe an improvement to the convolution of equation 3.38. This is a subject of future work.

The quantities $\kappa_\lambda(x)$, $\phi(\lambda)$ and $\rho(x)$ have no simple analytical forms, and so equation 3.39 cannot be solved analytically for z.

The geometric depth z is obtained numerically by reformulating the problem in the following way: Let us define a function f(z) such that

$$f(z) = \int_{\lambda_1}^{\lambda_2}\int_0^z \kappa_\lambda(x)\rho(x)\phi(\lambda)\,dx\,d\lambda - \ln 2 = 0. \tag{3.40}$$

Now the problem reduces to finding the roots of f(z). The numerical technique used to do this is the Newton's method of finding the roots of functions.

Equation 3.40 was evaluated for continuum opacities ($\kappa_\lambda(x) = \kappa^c_\lambda$) alone, and for continuum plus line opacities. The f(z) *vs* z plot for the continuum opacity is shown in Figure 3.14. Figure 3.15 is for the continuum plus line opacity case. Notice that when the line opacity is included the order of the zeroes of f(z) is different. The variation of total opacity (line+continuum) with wavelength is shown in the figures 3.19–3.22. These plots show that even though the continuum opacities increase from B to I wavelengths, the line opacity is strong in the B and V. The I filter also includes some of the lines. This a subject of future work; for the moment I shall use the continuum opacities only.

The results of the technique described in the previous paragraph are shown in Table 3.2. The temperature values T(z) from ATLAS9 were then interpolated to the z–values listed in Table 3.2 in order to get $T(\lambda)$. Table 3.2 is also used to convert the $\Delta T \cos\alpha\,(\lambda)$ obtained from the pulsation model to $\Delta T \cos\alpha\,(z)$ (see the next section). The temperature vs wavelength for the $T_{eff} = 7900\,K$, +0.2 dex, log $g = 4.2$ and $V_{turb} = 2\,kms^{-1}$ model is shown in Figure 3.16. The U and V temperatures are the approximately the same, this means that when one looks in the U and V, one is looking at the same geometrical depth in the atmosphere. The results for other stars are shown in figures 3.19–3.22.

Table 3.2: The relationship between wavelength and atmospheric geometric depth due to the dependence of total opacity on wavelength and atmospheric depth for all stars. The results for HR 3831 are for rotation phase 0.57.

filter	λ (Å)	**z** (km) α Cir	**z** (km) HD 134214	**z** (km) HD 101065	**z** (km) HR 3831	**z** (km) HD 137949
U	3670	1693	1596	1486	1709	1723
B	4360	1810	1666	1538	1832	1853
V	5450	1682	1546	1427	1704	1724
R	6380	1604	1475	1361	1625	1643
I	7970	1567	1440	1330	1588	1607

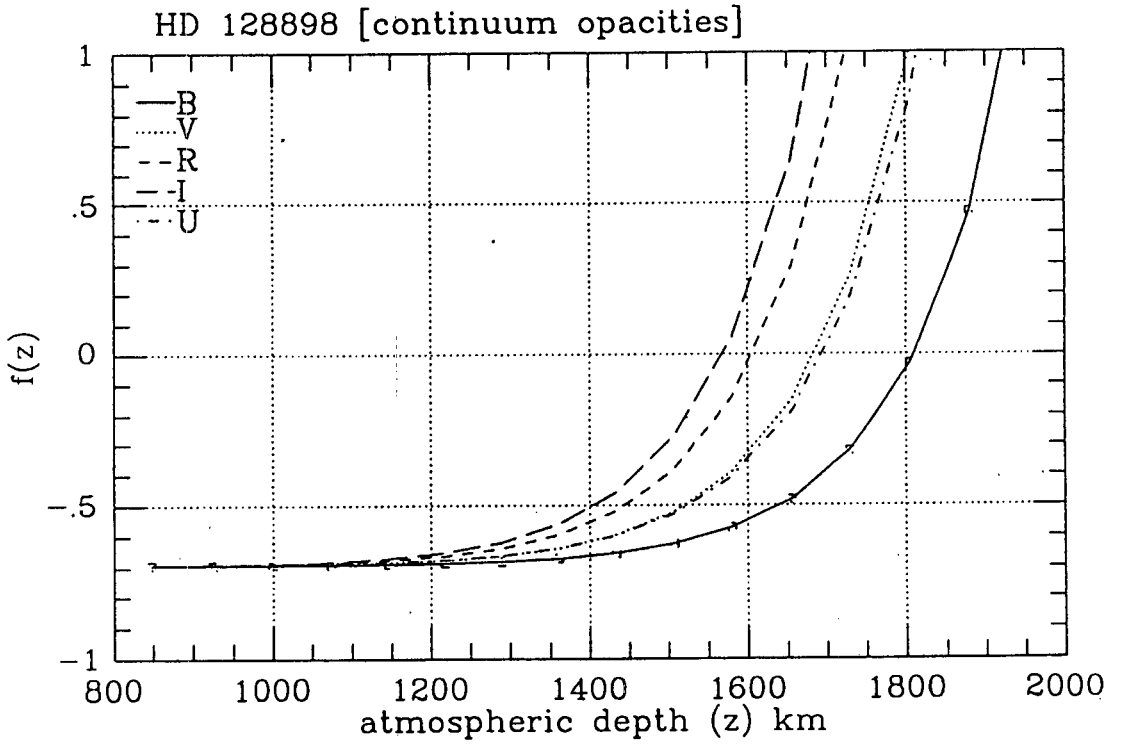

Figure 3.14: A plot of f(z) as a function of z for various wavelengths of observations, for the model $T_{eff} = 7900\,K$, +0.2 dex, log $g = 4.2$ and $V_{turb} = 2\,kms^{-1}$. The graph crosses the f(z)=0 axis at various z values in the expected wavelength order. Thus as one looks at longer wavelengths, one looks higher in the atmosphere. The opacity used in the calculations of f(z) includes continuum opacities only. This plot enables one to make the initial estimates on the roots of f(z). Newton's method refines those initial estimates.

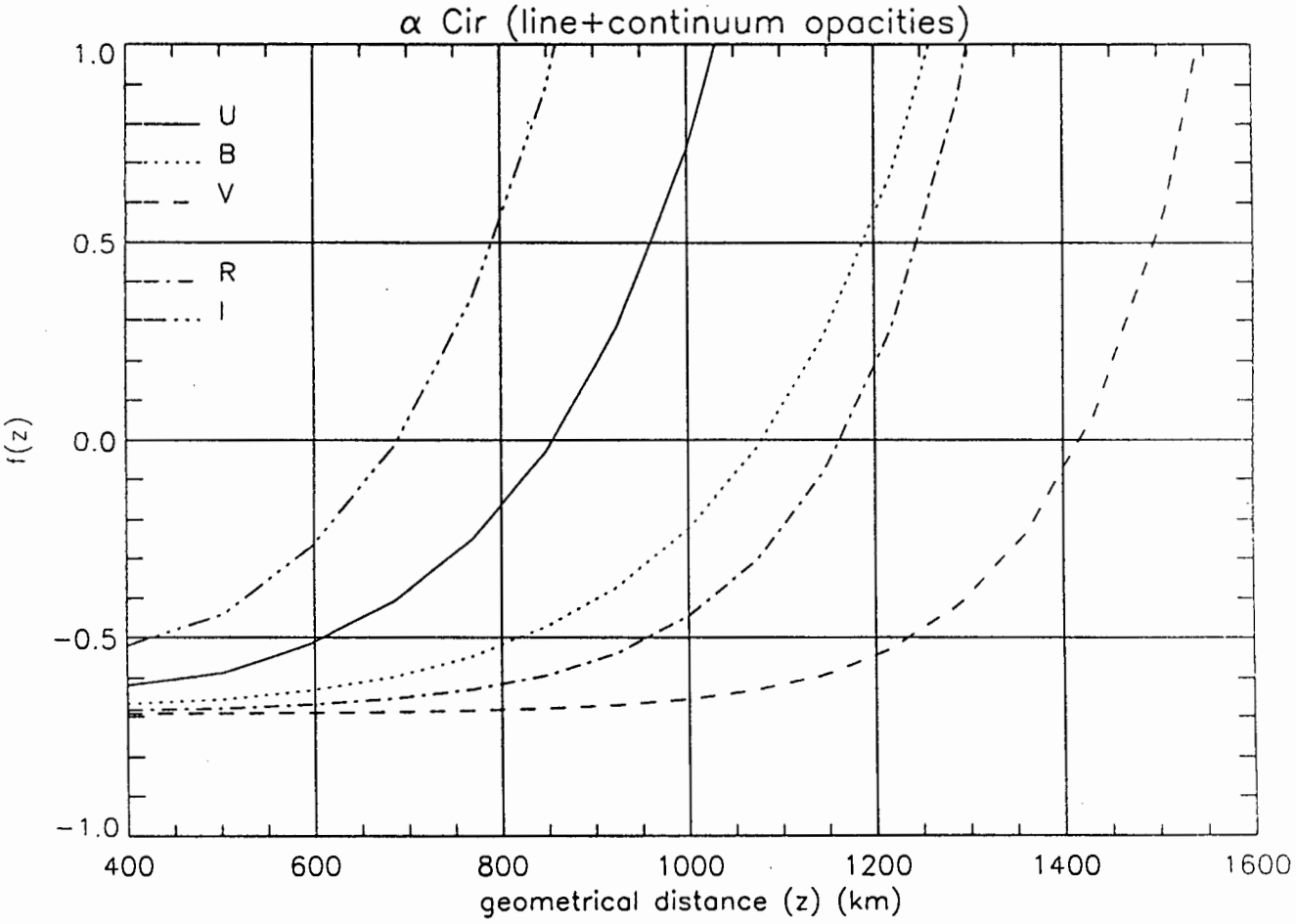

Figure 3.15: A plot of f(z) as a function of z for various wavelengths of observations, for the model $T_{eff} = 7900\,K$, +0.2 dex, log $g = 4.2$ and $V_{turb} = 2\,kms^{-1}$. Here the order is different, and this is because of the line opacity.

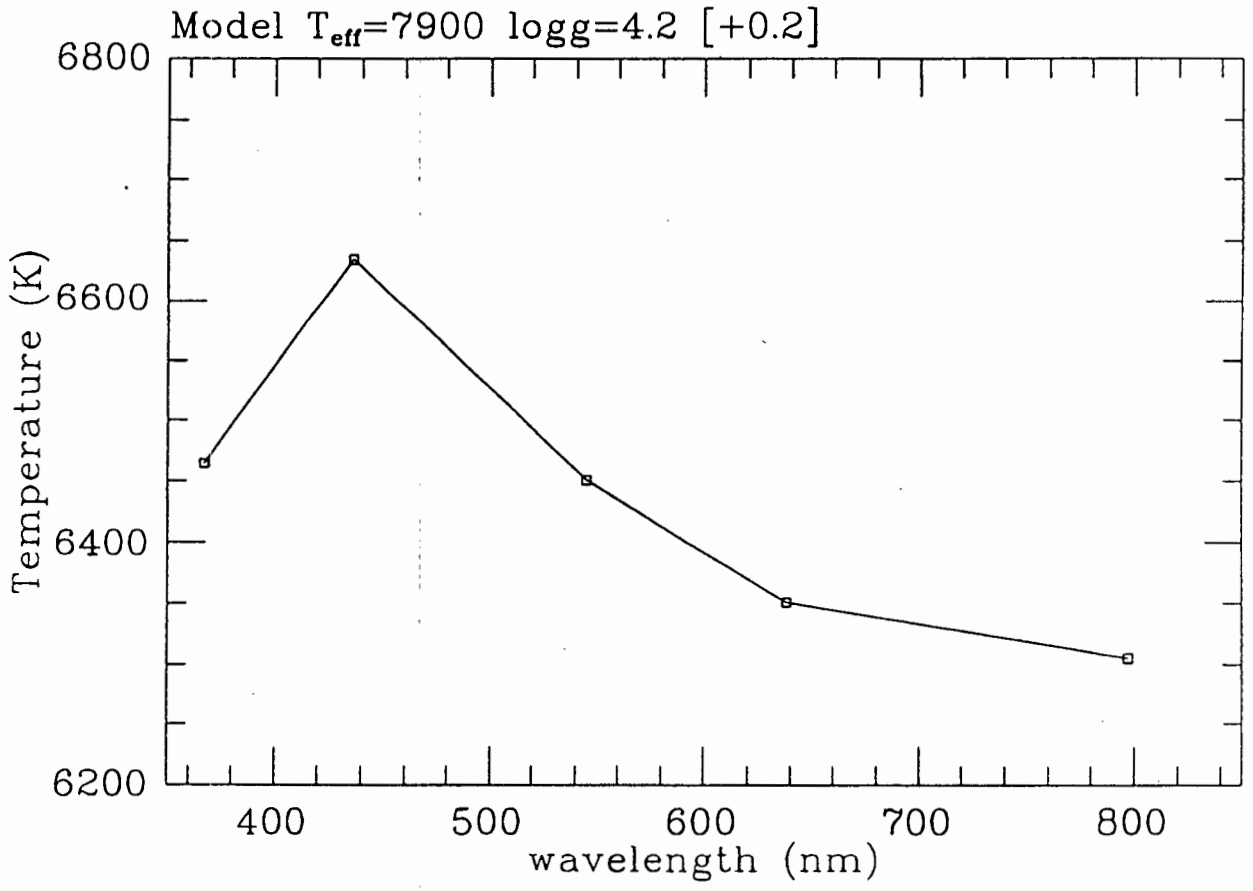

Figure 3.16: The temperature *vs* wavelength relation for $T_{eff} = 7900\,K$, +0.2 dex, log g = 4.2 and $V_{turb} = 2\,kms^{-1}$ model.

3.5 $\Delta T \cos\alpha$ *vs* atmospheric depth

The pulsation models (both numeric and analytic) described previously require $T(\lambda)$, limb–darkening (β_λ), inclination angle (α) of the pulsation mode and observed amplitude as input, if $\Delta T(\lambda)$ is to be the output. We shall use the $T(\lambda)$ values obtained in the last section and the solar limb–darkening coefficients to derive $\Delta T \cos\alpha$. The value of α was fixed since it is not a very well determined value for most of our candidates.

An empirical iterative procedure was devised in order to compare the observed amplitudes with those calculated from models to try to minimise the differences between the observed and calculated amplitudes. An initial guess of the $\Delta T(\lambda)$ was made based on the pulsating black–body and on the optical amplitudes of the roAp stars. A pulsating black–body at temperature maximum of $T_{max} = T_o + \Delta T$ will have a semi–amplitude of

$$\Delta m_\lambda = -2.5 \log \left(\frac{\exp(\frac{h\,c}{\lambda\,k\,T_o}) - 1}{\exp(\frac{h\,c}{\lambda\,k\,T_{max}}) - 1} \right) \tag{3.41}$$

for equilibrium temperature T_o, Planck's constant h, speed of light c and Boltzmann's constant k. No assumption was made about the nature of the pulsation (*i.e* whether it is radial or not, for example). So given any optical pulsation amplitude Δm_λ at any given wavelength λ, the temperature at pulsation maximum is given as

$$T_{max} = \frac{h\,c}{\lambda\,k} \left(\ln \left(10^{\frac{\Delta m_\lambda}{2.5}} \left(\exp(\frac{h\,c}{\lambda\,k\,T_o}) - 1 \right) + 1 \right) \right)^{-1}. \tag{3.42}$$

The initial estimate of ΔT is then obtained from

$$\Delta T = T_{max} - T_o. \tag{3.43}$$

The amplitude $\Delta m_{\lambda c}$ is then calculated from the pulsation model. I shall only present the results for which $\Delta m_{\lambda c}$ is calculated from equation 3.28. The results for when $\Delta m_{\lambda c}$ is calculated from the numerical models are not expected to be too different, since it has been shown in Figure 3.13 that the numerical calculations are in agreement with equation 3.28. This calculated amplitude will necessarily differ from the observed amplitude $\Delta m_{\lambda\,obs}$ by Δ, so that

$$\Delta = \Delta m_{\lambda c} - \Delta m_{\lambda\,obs}. \tag{3.44}$$

This means that the initial guess of ΔT differs from the "true" $\Delta T'$ by an "error" $\sigma_{\Delta T}$. The calculated amplitude is a function of ΔT, T, λ, β_λ, and α, so

$$\Delta m_{\lambda c} = \Delta m_{\lambda c}(\Delta T, T, \lambda, \beta_\lambda, \alpha). \tag{3.45}$$

The uncertainty in $\Delta m_{\lambda,c}$ due to uncertainties in ΔT, T, λ, β_λ, and α is given thus:

$$\begin{aligned}\sigma^2_{\Delta m_{\lambda,c}} &= \left(\frac{\partial(\Delta m_{\lambda c})}{\partial(\Delta T)}\sigma_{\Delta T}\right)^2 + \left(\frac{\partial(\Delta m_{\lambda c})}{\partial T}\sigma_T\right)^2 \\ &+ \left(\frac{\partial(\Delta m_{\lambda c})}{\partial \lambda}\sigma_\lambda\right)^2 + \left(\frac{\partial(\Delta m_{\lambda c})}{\partial \alpha}\sigma_\alpha\right)^2 \\ &+ \left(\frac{\partial(\Delta m_{\lambda c})}{\partial \beta_\lambda}\sigma_{\beta_\lambda}\right)^2,\end{aligned} \tag{3.46}$$

where the uncertainty in any observable x is denoted as σ_x. If we assume that we know all parameters well enough so that the only uncertainty is in the value of ΔT, we end up with

$$\sigma_{\Delta m_{\lambda,c}} = \frac{\partial(\Delta m_{\lambda c})}{\partial(\Delta T)}\sigma_{\Delta T}. \tag{3.47}$$

We take the difference between the observed amplitude and the calculated one, Δ, to be the uncertainty in $\Delta m_{\lambda,c}$, $\sigma_{\Delta m_{\lambda c}}$. Therefore,

$$\Delta = \frac{\partial(\Delta m_{\lambda c})}{\partial(\Delta T)}\sigma_{\Delta T}. \tag{3.48}$$

We then take

$$\frac{\partial(\Delta m_{\lambda c})}{\partial(\Delta T)} \approx \frac{d(\Delta m_{\lambda c})}{d(\Delta T)}. \tag{3.49}$$

Thus, the correction we must add to the ΔT value is:

$$\sigma_{\Delta T} \approx \left(\frac{d(\Delta m_{\lambda c})}{d(\Delta T)}\right)^{-1}\Delta. \tag{3.50}$$

$\frac{d(\Delta m_{\lambda c})}{d(\Delta T)}$ is estimated from Newton's formula for derivatives

$$\frac{d(\Delta m_{\lambda c})}{d(\Delta T)} \approx \frac{\Delta m_{\lambda c}(\Delta T + h) - \Delta m_{\lambda c}(\Delta T)}{h}, \tag{3.51}$$

where h is the the stepsize.

So the improved value of ΔT is

$$\Delta T' = \Delta T + \sigma_{\Delta T} \tag{3.52}$$

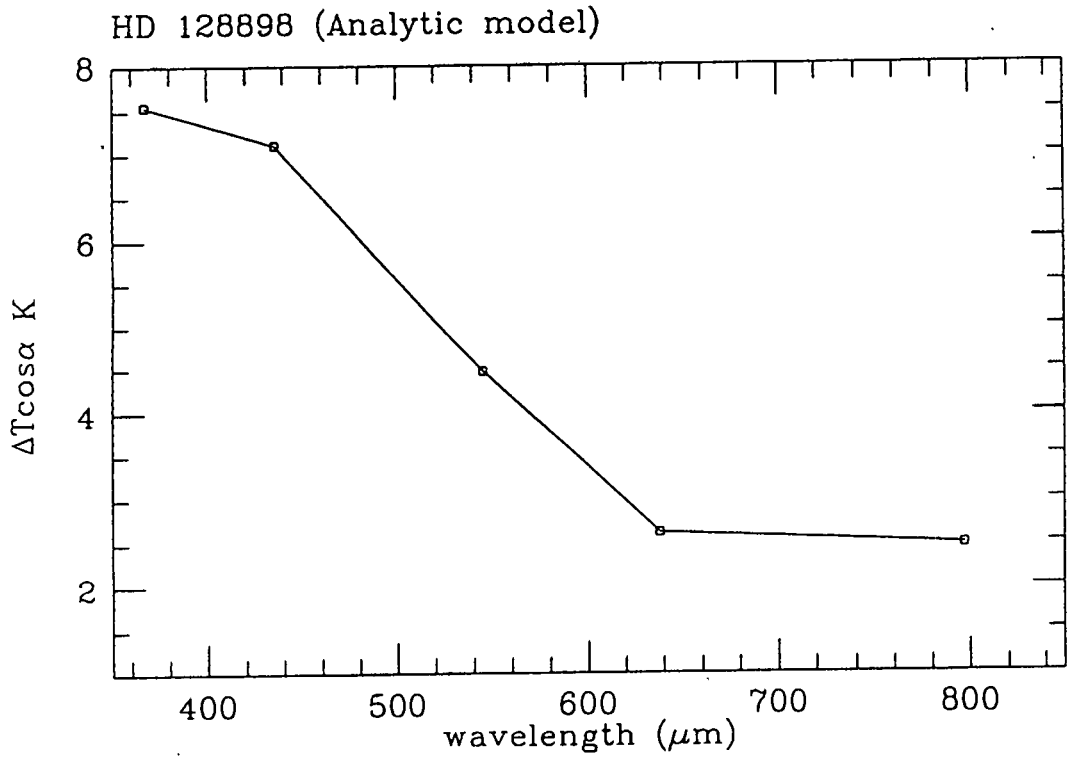

Figure 3.17: The $\Delta T \cos\alpha$ *vs* wavelength relation for α Cir at $\tau_\lambda = \ln 2$ obtained from application of the iterative technique described. The amplitudes are calculated from equation 3.28.

We iterate this scheme until we obtain arbitrarily small values of Δ. Figure 3.17 shows the results of applying this iteration to a model with $T_{eff} = 7900\,K$, +0.2 dex, $\log g = 4.2$ and $V_{turb} = 2\,\mathrm{kms}^{-1}$ (which I shall call the α Cir model). The amplitudes were calculated using the analytical results, equation 3.28. Table 3.2 was used to linearly interpolate the $\Delta T(\lambda)$ to $\Delta T(z)$. This is shown for α Cir in Figure 3.18. The $\Delta T \cos\alpha$ increases with depth for the Johnson BVRI. The U band does not follow the trend, and we suspect this is due to the high opacity in the U region of the spectrum. Since for the U band we are looking at more or less the same depth as in the V band, according to equation 3.28, the temperature semi-amplitude should be about the same as that of the V, but this is not the case.

The $\Delta T \cos\alpha$ as a function of atmospheric depth for HD 101065, HD 134214, HD 137949 and HR 3831 are shown in Figures 3.19–3.22 respectively. Also shown in each Figure is a plot of the total opacity as a function of wavelength, the derived $T(\lambda)$ and the $\Delta T \cos\alpha$ *vs* wavelength.

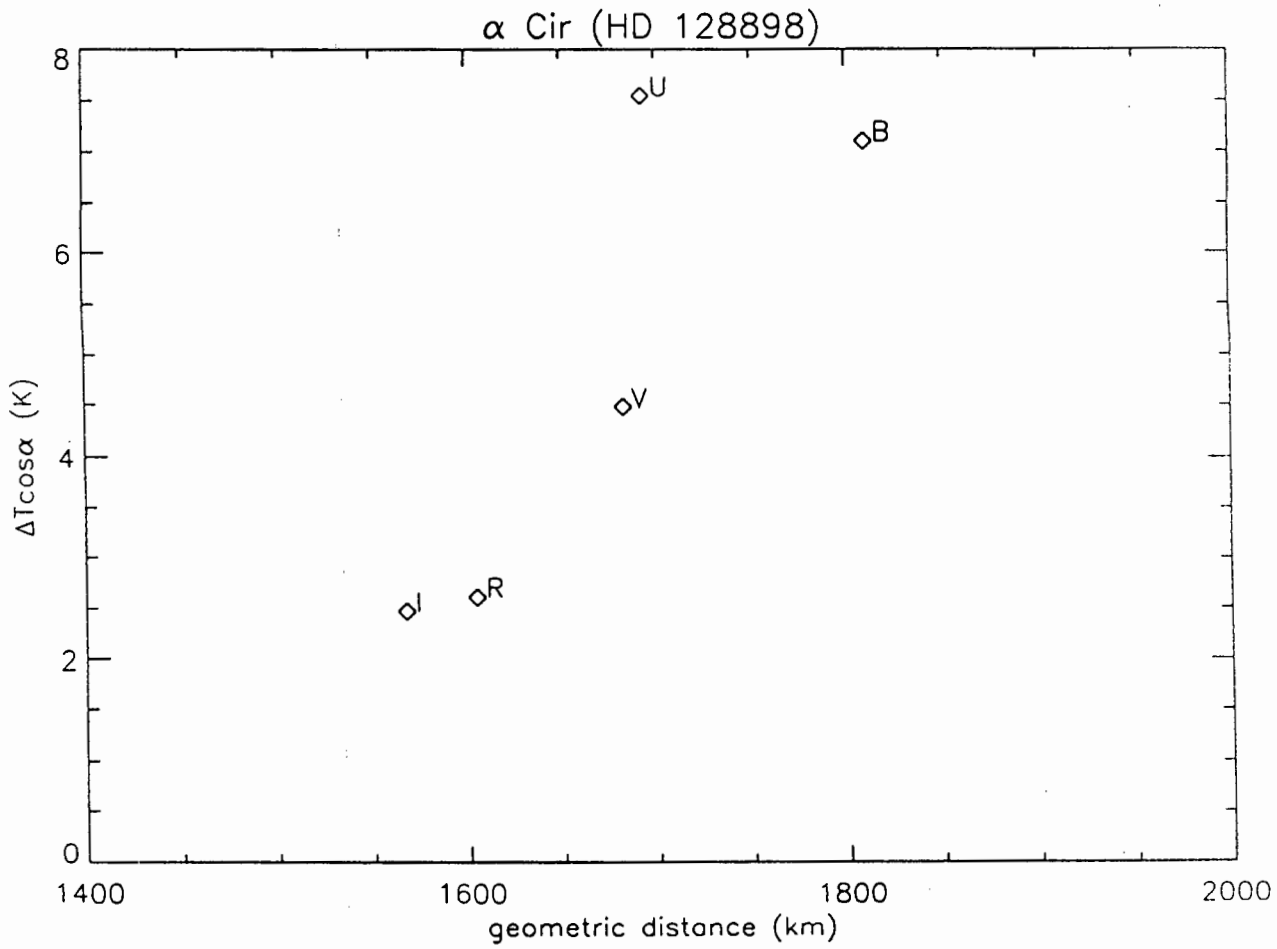

Figure 3.18: The $\Delta T \cos\alpha$ *vs* geometrical distance relation for α Cir. The amplitudes are calculated from equation 3.28. Notice that the U and the V values are at the same geometric depth yet they show different results.

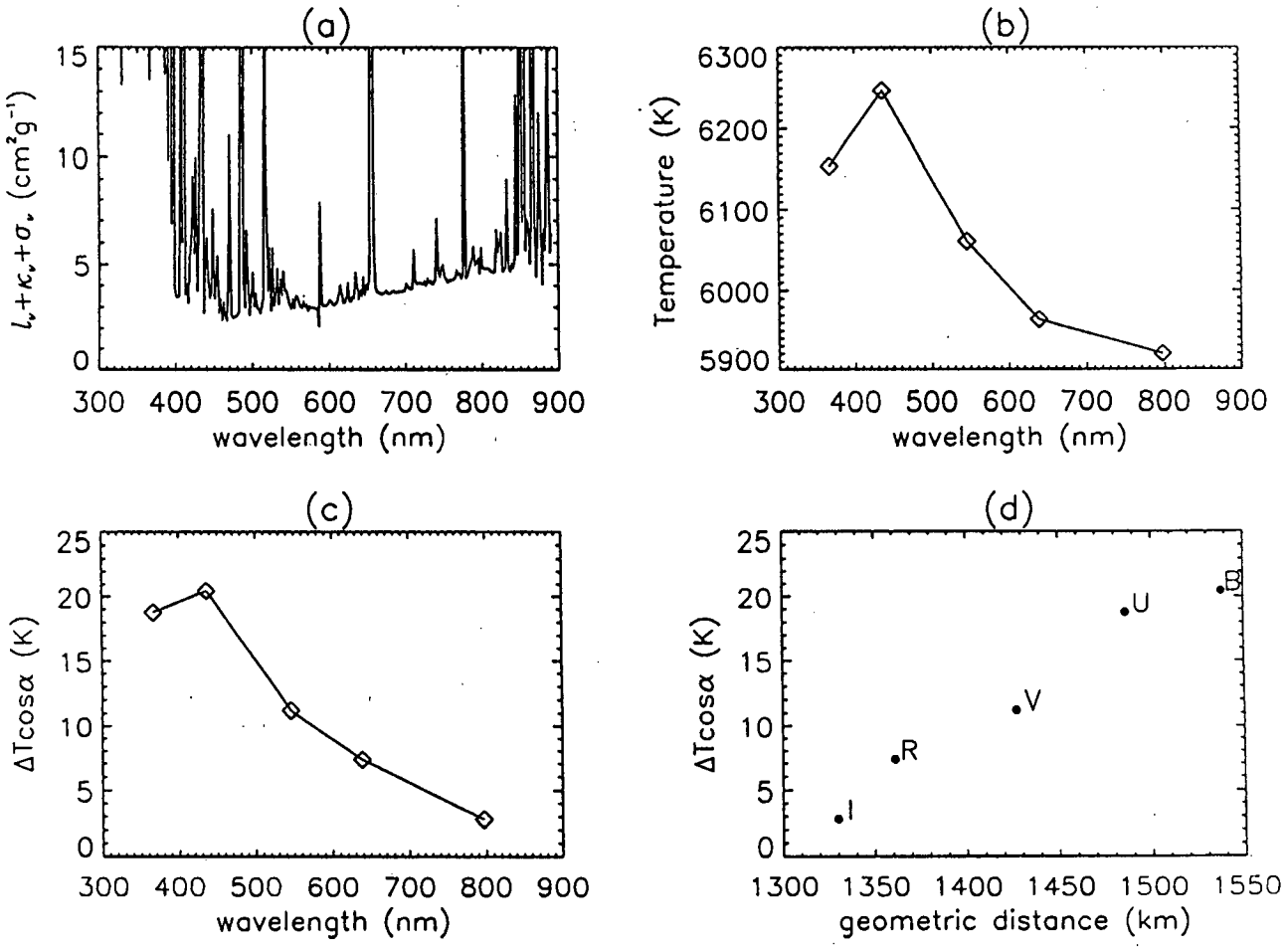

Figure 3.19: The variation of the total opacity with wavelength for the model atmosphere that I used to represent HD 101065 is shown in (a); (b) shows the derived temperature *vs* wavelength plot. The $\Delta T \cos\alpha$ as a function wavelength is shown in (c). Table 3.2 is used to convert plot (c) into a $\Delta T \cos\alpha$ *vs* atmospheric depth shown in (d). Here the U and the B values behave as expected (the U should be higher than B in the atmosphere because of the larger opacity in the U).

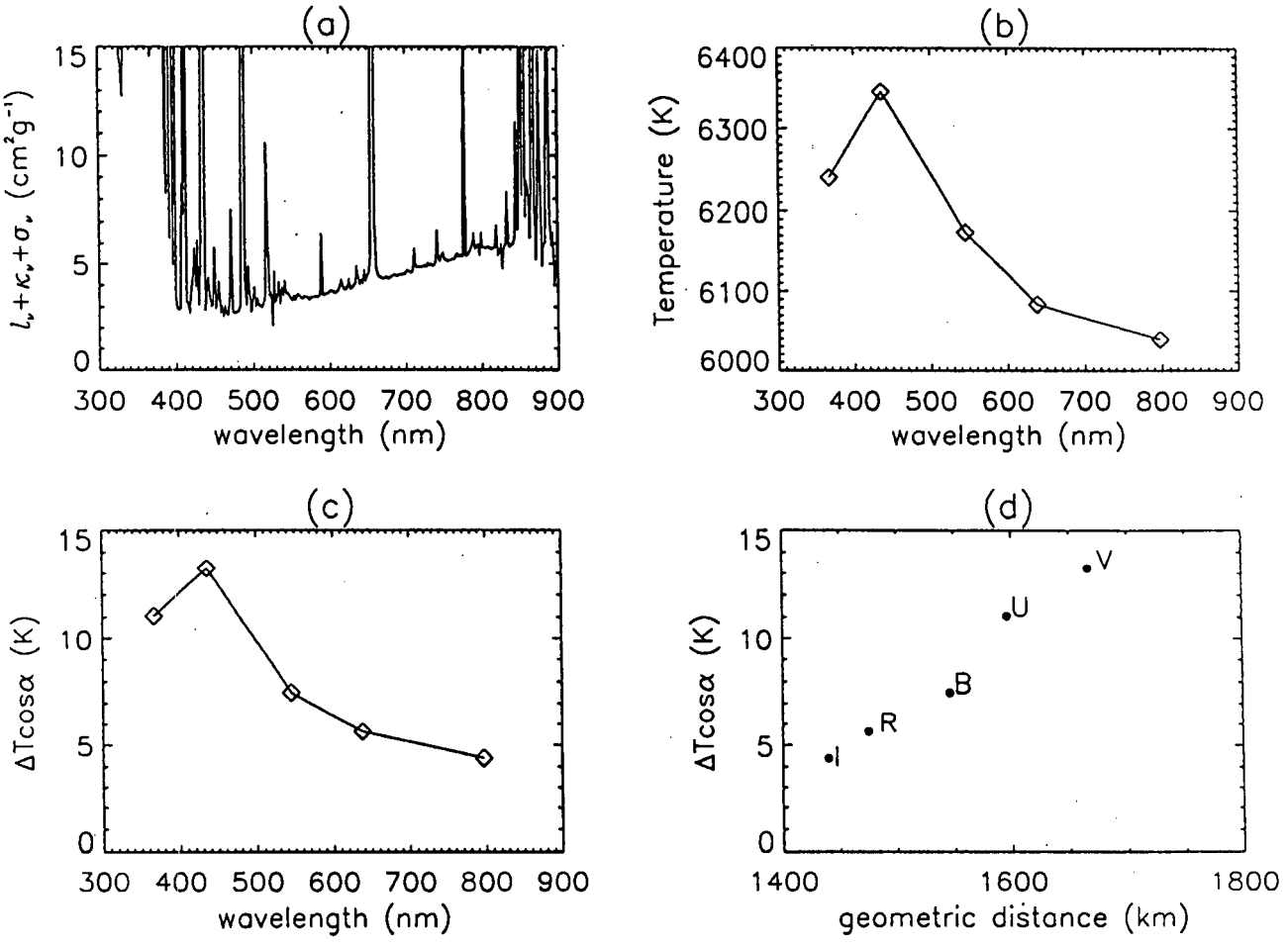

Figure 3.20: (a) The variation of κ_λ with wavelength. (b) The derived T(λ) relation. (c) The derived $\Delta T \cos\alpha$ *vs* wavelength. (d) The $\Delta T \cos\alpha$ *vs* geometrical distance relation. The behaviour of $\Delta T \cos\alpha$ is the same as that of HD 101065. These plots are for HD 134214.

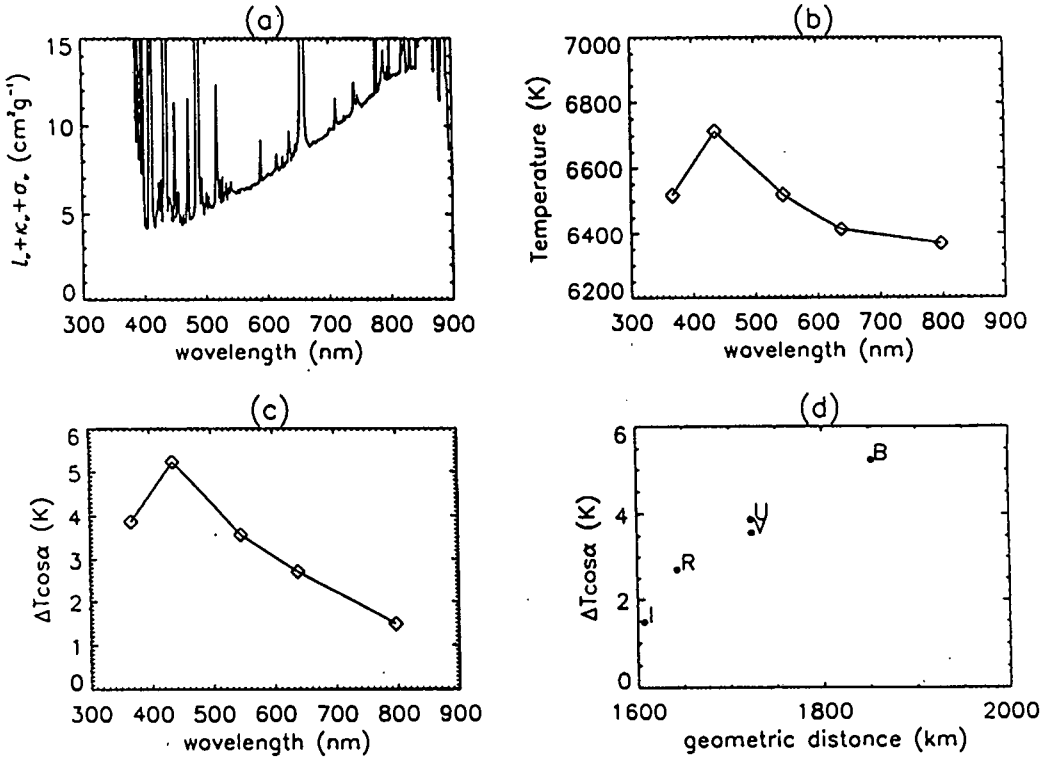

Figure 3.21: (a) The variation of κ_λ with wavelength. (b) The derived T(λ) relation. (c) The derived $\Delta T \cos\alpha$ *vs* wavelength. (d) The $\Delta T \cos\alpha$ *vs* geometrical distance relation. These plots are for HD 137949.

HR 3831

HR 3831 was monitored for 9 days to see how our results are affected by rotation. I need to mention that the results I present here are only preliminary, since the noise in the data is high; so the amplitudes derived for R and I are not very accurate. I assume that the temperature structure of this star does not change as it rotates and fit equation 3.28 to the data at various rotation phases shown in Table 2.3. The $\Delta T \cos\alpha$ *vs* wavelength for the Johnson UBVRI is shown in Figure 3.23. The *uvby*RI results are shown in Figure 3.24. The error bars indicate uncertainties due to the uncertainties in the observed pulsation amplitudes.

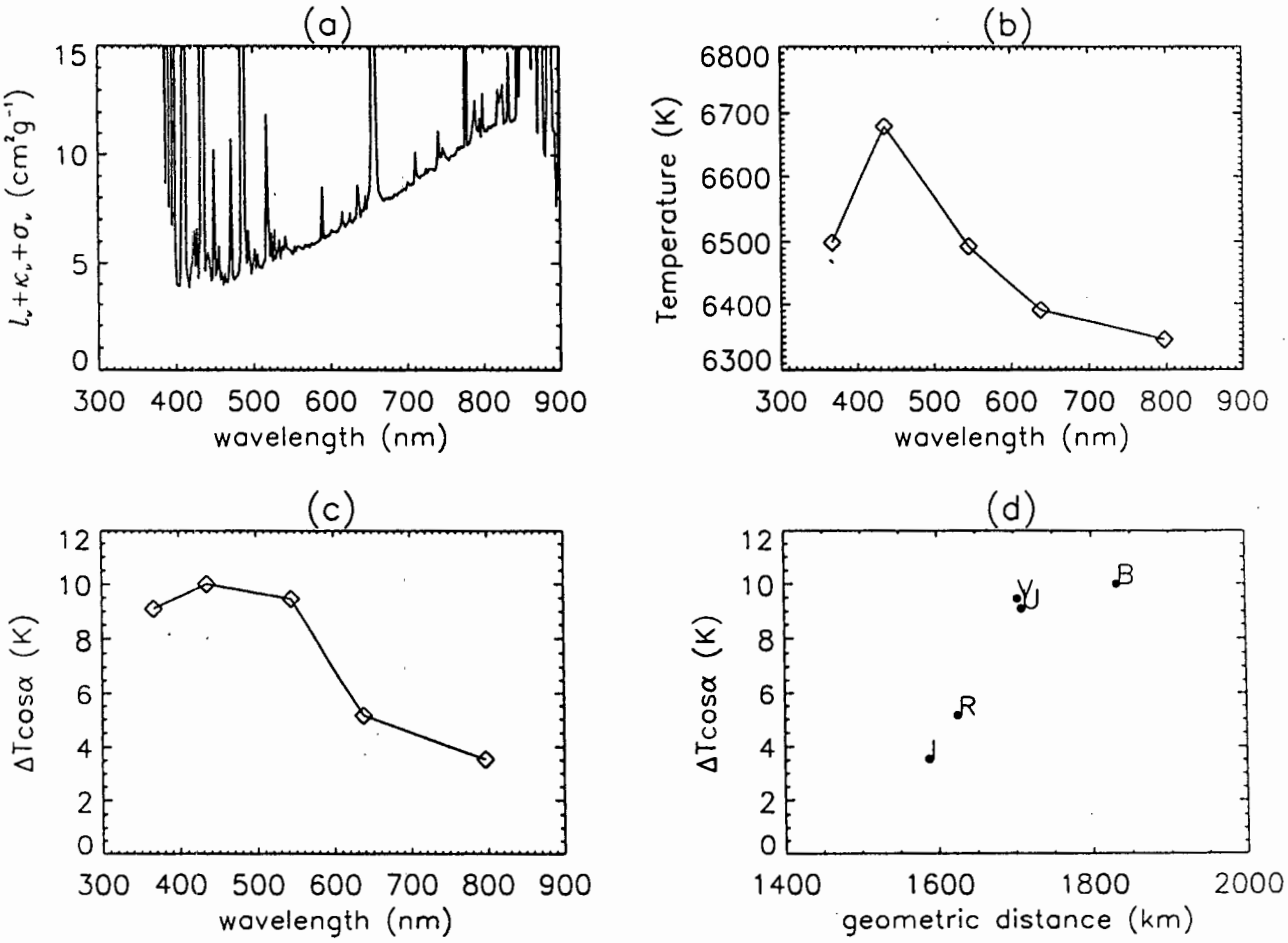

Figure 3.22: (a) The variation of κ_λ with wavelength. (b) The derived T(λ) relation. (c) The derived $\Delta T \cos\alpha$ *vs* wavelength. (d) The $\Delta T \cos\alpha$ *vs* geometrical distance relation. The U and the V are at the same depth, and the temperature semi-amplitude viewed through the two filters are similar to the α Cir case. These plots are for HR 3831 at rotation phase 0.57.

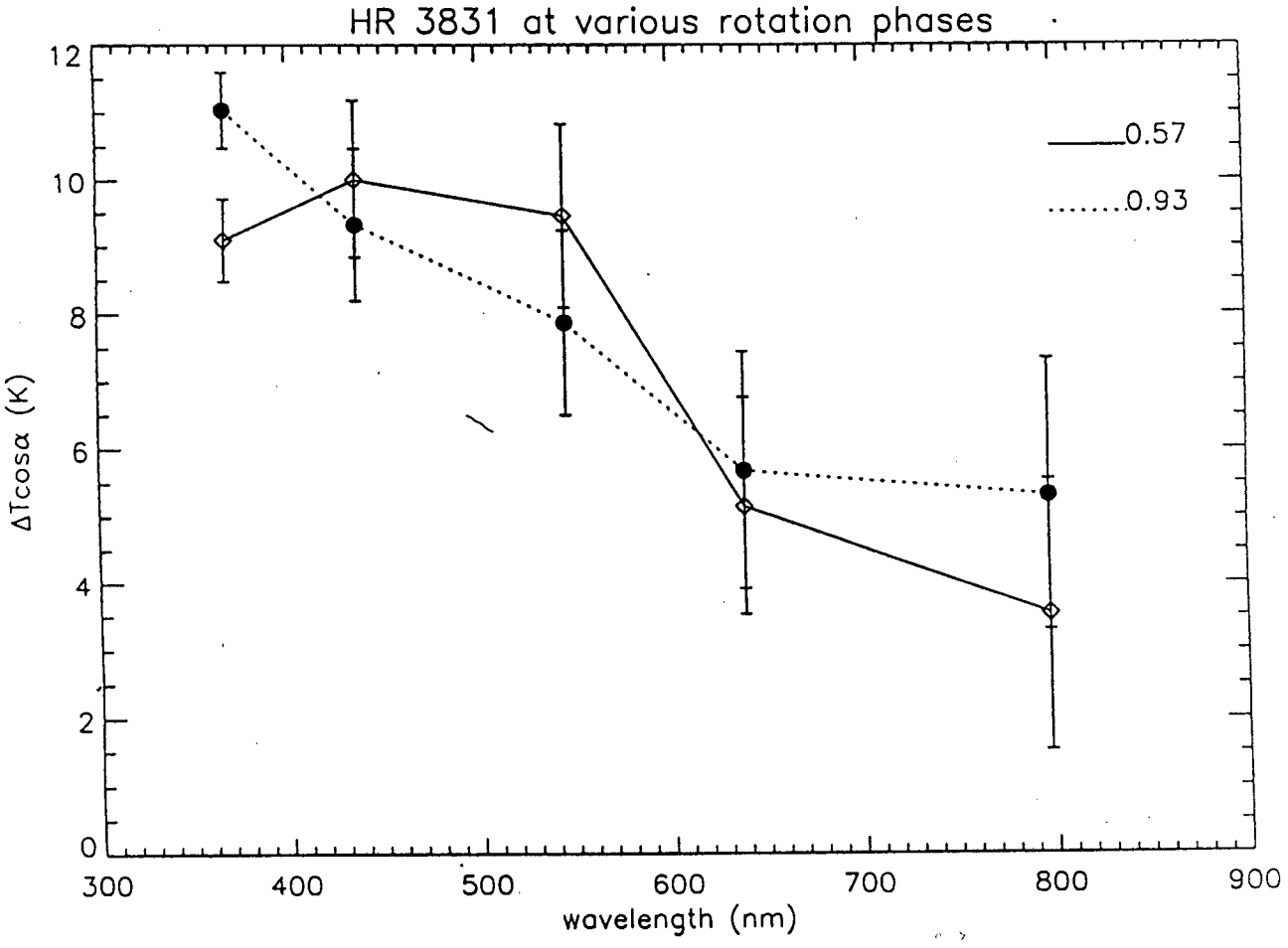

Figure 3.23: The $\Delta T \cos\alpha$ *vs* wavelength for phases 0.57 and 0.93 for HR 3831 (in the UBVRI). It is assumed that the temperature structure is maintained as the star rotates. The errors at each point are entirely due to the uncertainties in the measured pulsation amplitudes.

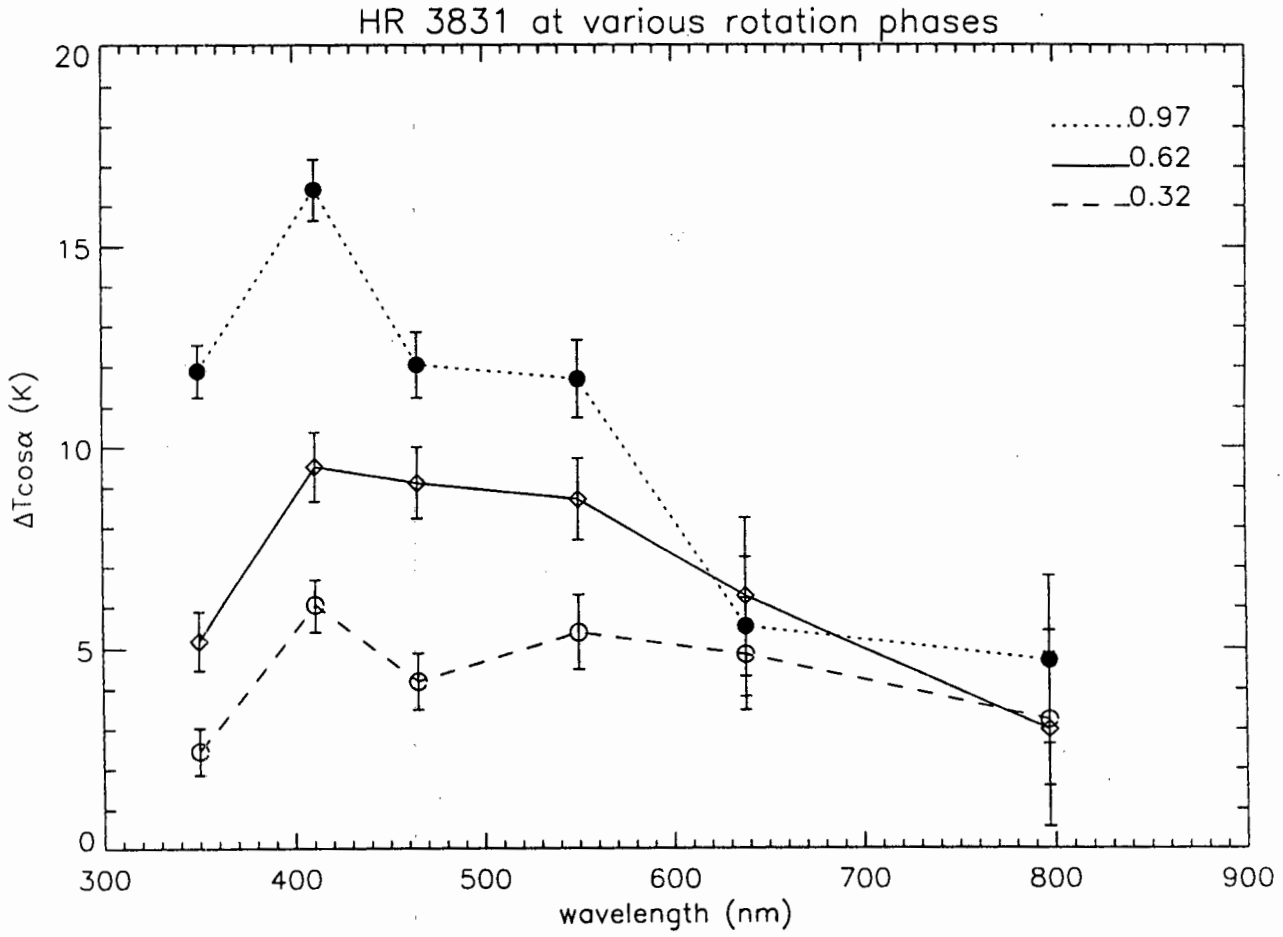

Figure 3.24: The $\Delta T \cos\alpha$ *vs* wavelength for various phases shown, for HR 3831 (in the uvyRI).

Chapter 4

Discussions and Conclusions

In this thesis an attempt has been made to show how several pulsation frequency analysis techniques can reveal vital information about the interior of the rapidly oscillating stars (and Ap stars in general). This is for the following reasons:

- The roAp stars are currently the only stars known unequivocally to pulsate in p modes similar to the sun. This means that some of the techniques applicable to the sun can also be used (albeit in a limited way) on them. There are major differences though. The pulsations of roAp stars are dominated by the strong magnetic field, and although the pulsation periods of the sun and the roAp stars are similar, the amplitudes of the roAp stars are a factor of 10^3 greater than those of the solar "five minutes" oscillations. Searches for p mode eigenfrequency patterns in the power spectra of velocity time series in solar–like stars have not yet produced definite results. Belmonte *et al.* (1990) could only find upper limits on the amplitudes of the p modes on HD 155543. An attempt to find oscillations on α Cen A was unsuccessful (Brown & Gilliland 1990). Gelly *et al.* (1986, 1988) reported detection of velocity oscillations on Procyon, the results which are now doubtful. Kjeldsen *et al.* (1995) reported detection of p mode oscillations in η Boo, their results are still to be confirmed by other independent measurements.

- The rich frequency spectrum of roAp stars have necessitated new techniques (discussed in sections 1.3.2 and 1.3.3) that have revealed information such as their rotation periods, rotational inclinations, evolutionary status, magnetic geometries, internal magnetic field strengths, radii, masses and luminosities. This thesis shows that roAp stars that pulsate in a single mode can also allow us to observe level effects in their atmospheres. Level effects have been observed in solar oscillations, but this is the first time they have been noted in stars other than the sun (Deubner 1996).

The linearised expression for the variation of the pulsation amplitude with wavelength for a dipole pulsator is given by equation 3.28. The most noticeable thing about this relation is the weak dependence of amplitude on limb–darkening. This result is obtained independently by numerical models which have realistic treatment of the variation intensity with wavelength in Figure 3.13. This means that the rapid decline of the pulsation amplitude with increasing wavelength does not give much information about limb–darkening. Therefore we are back to where we were, that is, the sun is still the only star for which T(τ) has been measured.

Parameters that can affect the variation of pulsation amplitude with wavelength are the temperature T and ΔT. The temperature decreases with increasing wavelength in the atmosphere of the Ap stars. But we have no idea *a priori* how the ΔT varies. There has not been any theoretical investigation of the variation of pulsation amplitude with atmospheric depth. Therefore, by having some knowledge of T(τ) from model atmospheres and feeding this, together with limb–darkening, to the pulsation models, I derived the variation of ΔT with depth in the stellar atmosphere (in the continuum). The $\Delta T(\tau)$ behaves as predicted by equation 3.28 for the BVRI but is unpredictable for the U. I attribute this to the large line plus continuum opacity in the U. A clearer picture will appear if more studies at short wavelengths are made. I caution that these results still need more improvements:

- The input model atmospheres need more improvements. Scaled solar models do not represent Ap atmospheres adequately. Individual abundances need to be used. Kupka & Piskunov (1996) are already producing reasonable model atmospheres, as I have shown with the α Cir model. It is for this reason that I believe that the $\Delta T(\tau)$ relation for α Cir is more realistic. More such models will be welcome. Another development that is welcome is the ATLAS12 model atmosphere program (Kurucz 1993a) that should allow better modelling of Ap atmospheres.

- The surface variation of temperature has not been taken into consideration.

- The effects of opacity changes due to pulsation have not been included in our pulsation models. I do not think this is a serious short–coming as the pulsation amplitudes are small.

- The effects of magnetic fields and rotation have not been included in the models. The data of HR 3831 observed at various rotation phases requires proper detailed interpretation, what I have shown is just a first order interpretation. I expect the presence of spots at various rotation phases to affect the $T(\tau)$ relation, and hence the $\Delta T \cos\alpha$ *vs* depth relation.

Our analysis is not accurate enough to locate the position of a pulsation node in the atmosphere. It would be interesting to calculate a theoretical eigenfrequency spectrum for α Cir to see where a node would be seen. An interesting development as far as the evidence of a node in the atmosphere of α Cir is concerned is that Viskum *et al.* (in preparation) find, from medium dispersion spectroscopic data covering 7 nights, significant variations in radial velocity amplitudes and phases for some metal lines (possibly divided into areas π radians out of phase with each other) in the spectrum of α Cir. This could be interpreted as an indication of a high overtone standing wave with a node in the atmosphere. Another interpretation, by Jaymie Matthews is that one is observing elements (in spots) on the opposite sides of the magnetic (pulsation) equator. The former interpretation, if true, is in agreement with our results.

Hideyuki Saio (private communication) suggests that high in the atmosphere the non–adiabatic effects may become important so that they might dominate the depth dependence of ΔT rather than the vertical wavelength doing so. Should this be the case then our models will have to be modified and we do not have any idea yet how the $\Delta T(\tau)$ varies with depth.

Appendix A

The convolutions

Brian Warner has pointed out that the simple convolution of equation 3.38 by the response function is not completely correct. When such a convolution is made one must take into consideration how the flux varies with wavelength, because it is the flux that is observed.

As an example, consider the wavelength dependence of κ_λ shown in Figure A.1. Regions with high κ_λ values have low flux values, so that for the above variation of κ_λ, the resulting flux will vary in a way shown in Figure A.2.

A simple weighting scheme of the form of equation 3.39 will give zero weight to the interval $[\lambda_1, \lambda_2]$ and non–zero weight to interval $[\lambda_2, \lambda_3]$. But most of the flux is observed in the interval $[\lambda_1, \lambda_2]$, so clearly the convolution I used (equation 3.39) requires some revision.

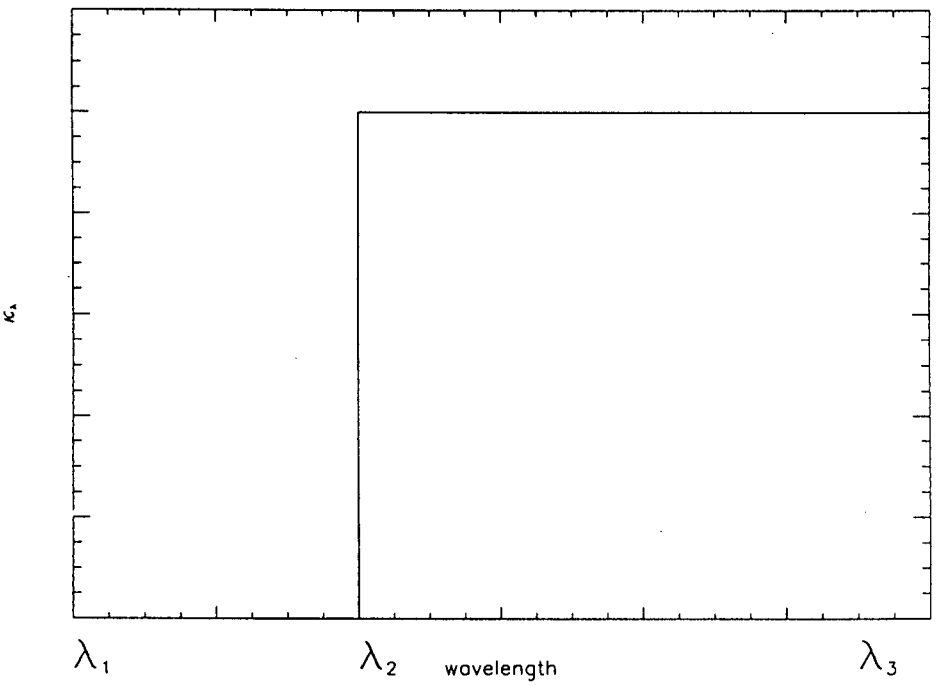

Figure A.1: The hypothetical variation of κ with wavelength to demonstrate the importance of looking at the variation of flux with wavelength in order to select a proper way of convoluting κ with the response function. κ is zero from λ_1 to λ_2, it is non–zero in the interval $[\lambda_2, \lambda_3]$.

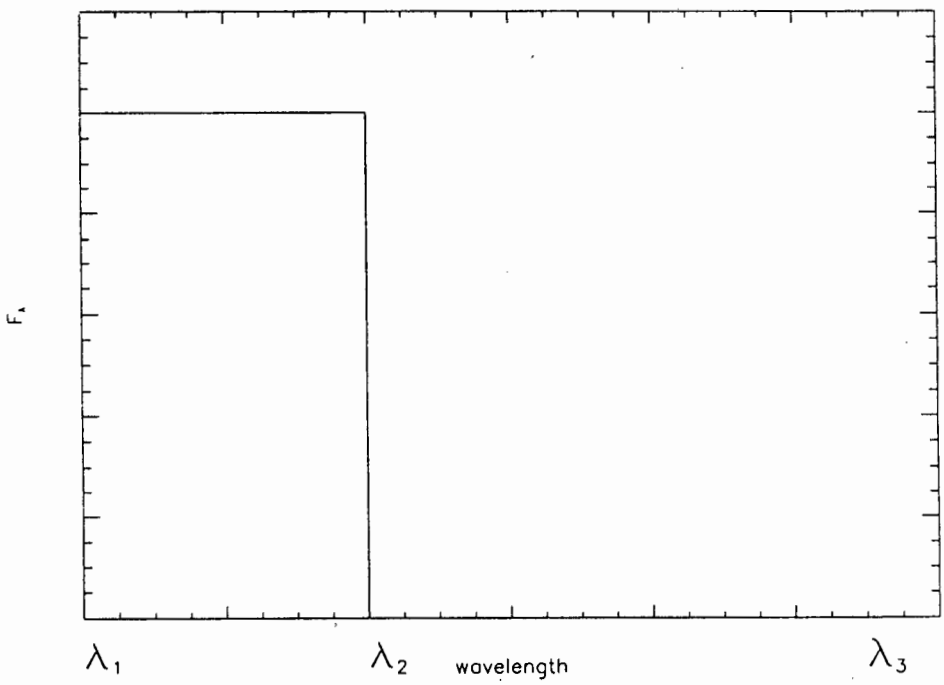

Figure A.2: The variation of flux with wavelength that will result from the κ_λ shown in Figure A.1. The flux is non–zero on the interval $[\lambda_1, \lambda_2]$, and zero on the interval $[\lambda_2, \lambda_3]$.

Bibliography

[1] Alecian, G., 1986, In *Upper Main Sequence Stars with Anomalous Abundances.* Proc. IAU Colloq. No. 90, p. 381, Dordrecht: Reidl, eds. C.R. Cowley, M.M. Dworetsky, C. Megessier

[2] Allen, C.W., 1963, Astrophysical Quantities, 2nd edition, The Athlone Press, University of London, 2 Gower Street, London, W.C.1.

[3] Babcock, H.W., 1958, ApJS, **3**, 141

[4] Bachmann, K.T., Brown, T.M., 1993, ApJ, **411**, L45

[5] Balona, L.A., 1988, LUCY user's manual, SAAO

[6] Balona, L.A., Stobie, R.S., 1979a, MNRAS, **187**, 187

[7] Balona, L.A., Stobie, R.S., 1979b, MNRAS, **189**, 649

[8] Belmonte, J.A., Pérez Hernández, F., Roca Cortés, T., 1990, In *Lecture Notes in Physics, Progress in Seismology of the Sun and Stars*, eds. T. Osaki, H. Shibahashi (Berlin, Springer–Verlag), 417

[9] Belmonte, J.A., Pérez, F., Roca, T., 1991, *Investigacion y Ciencia*, 178, 76

[10] Borra, E.F., Landstreet, J.D., 1975, PASP, **87**, 961

[11] Borra, E.F., Landstreet, J.D., 1980, ApJS, **42**, 421

[12] Borra, E.F., Landstreet, J.D., Mestel, L., 1982, ARA&A, **20**, 191

[13] Breger, M., 1979, PASP, **91**, 539

[14] Brown, T.M., Gilliland, R.L., 1990, ApJ, **350**, 839

[15] Carney, B.W., Peterson, R.C., 1985, MNRAS, **212**, 33

[16] Cowley, C.R., Cowley, A.P., Aikman, G.C.L., Crosswhite, H.M., 1977, ApJ, **216**, 37

[17] Deeming, T.J., 1975, Ap&SS, **36**, 137

[18] Deubner, F.-L., Waldschik, Th., Steffens, S., 1996, A&A, **307**, 936

[19] Deutsch, A.J., 1947, ApJ, **105**, 283

[20] Dolez, N., Gough, D.O., Vauclair, S., 1988, *Advances in Helio- and Asteroseismology. Proc. IAU Symp.* No. 123, 291, ed. J. Christensen-Dalsgaard, S. Frandsen (Dordrech: Reidel)

[21] Dziembowski, W., Goode, P.R., 1985, ApJ, **296**, L27

[22] Dziembowski, W., Goode, P.R., 1986, In *Seismology of the Sun and Distant Stars*, ed. D.O. Gough, p 441. Dordrecht: Reidel.

[23] Edmonds, A.R., 1957, *Angular Momentum in Quantum Mechanics.*, Princeton, NJ: Princeton University Press.

[24] Elsworth, Y., Howe, R., Isaak, G.R., McLeod, C.P., New, R., 1990, Nature, **345**, 322

[25] Gelly, B., Grec, G., Fossat, E., 1986, A&A, **164**, 383

[26] Gelly, B., Grec, G., Fossat, E., 1988, In *Advances in Helio- and Asteroseismology. Proc. IAU Symp.* No. 123, 249, eds. J. Christensen-Dalsgaard, S. Frandsen (Dordrech: Reidel)

[27] Hartoog, M.R., Cowley, C.R., Cowley, A.P., 1973, ApJ, **182**, 847

[28] Heck, A., Manfroid, J., Renson, P., 1976, A&AS, **25**, 143

[29] Heck, A., Mathys, G., Manfroid, J., 1987, A&AS, **70**, 33

[30] Heller, C.H., Kawaler, S.D., 1988, ApJ., **329**, L43

[31] Henden, A.A., Kaitchuk, R.H., 1982, Astronomical Photometry, Van Nostrand Reinhold Company Inc., 135 West 50^{th} Street, New York ,N.Y. 10020

[32] Houk, N., 1978, Michigan Spectral Catalogue, vol. 2., Department of Astronomy, University of Michigan, Ann Arbor

[33] Hurly, P.R., Warner, B., 1983, MNRAS, **202**, 761

[34] Jones, T.J., Wolff, S.C., Bonsack, W.K., 1974, Ap.J., **190**, 579

[35] Kilkenny, D., Balona, L.A., Carter, D.B., Ellis, D.T., Woodhouse, G.F.W., 1988, MNASSA, **47**, 69

[36] Kjeldsen, H., Bedding, T.R., Viskum, M., Frandsen, S., 1995, Astron. J., **109**, 1313

[37] Kreidl, T.J., 1985, IBVS, No. 2739

[38] Kreidl, T.J., Kurtz, D.W., Schneider, H., van Wyk, F., Roberts, G., Marang, F., Birch, P.V., 1994, MNRAS, **270**, 115

[39] Kupka, F., Gelbmann, U., Heiter, R., Kuschnig, R., Weiss, W.W., 1995, In *Astrophysical Applications of Stellar Pulsation*, ASPC, **83**, eds. R.S. Stobie, P.A. Whitelock.

[40] Kupka, F., Piskunov, N.E., in preparation

[41] Kupka, F., Ryabchikova, T.A., Weiss, W.W., Kuschnig, R., Rogl, J., Mathys, G., 1996, A&A, **308**, 886

[42] Kurtz, D.W., 1978, IBVS, No. 1436

[43] Kurtz, D.W., 1980, MNRAS, **191**, 115

[44] Kurtz, D.W., 1981, MNRAS, **196**, 61

[45] Kurtz, D.W., 1982, MNRAS, **200**, 807

[46] Kurtz, D.W., 1984, In *Proceedings of the Workshop on improvements to Photometry*, p. 56, ed. W.J. Borucki, A. Young, NASA Conference Publication 2350

[47] Kurtz, D.W., 1985, MNRAS, **213**, 773

[48] Kurtz, D.W., 1990, ARA&A, **28**, 607

[49] Kurtz, D.W., 1991, MNRAS, **249**, 468

[50] Kurtz, D.W., Balona, L.A., 1984, MNRAS, **210**, 779

[51] Kurtz, D.W., Cropper, M.S., 1981, IBVS, No. 1987

[52] Kurtz, D.W., Kanaan, A., Martinez, P., Tripe, P., 1992, MNRAS, **255**, 289

[53] Kurtz, D.W., Kanaan, A., Martinez, P., 1993b, MNRAS, **260**, 343

[54] Kurtz, D.W., Kreidl, T.J., 1985, MNRAS, **216**, 987

[55] Kurtz, D.W., Kreidl, T.J., O'Donoghue, D., Osip, D.J., Tripe, P., 1991, MNRAS, **251**, 152

[56] Kurtz, D.W., Martinez, P., Ashley, R.P., 1993a, MNRAS, **264**, 529

[57] Kurtz, D.W., Martinez, P., van Wyk, F., Marang, F., Roberts, G., 1994a, MNRAS, **268**, 641

[58] Kurtz, D.W., Matthews, J.M., Martinez, P., Seeman, J., Cropper, M., Clemens, J.C., Kreidl, T.J., Sterken, C., Schneider, H., Weiss, H., Kawaler, S.D., Kepler, S.O., van der Peet, A., Sullivan, D.J., Wood, H.J., 1989, MNRAS, **240**, 881

[59] Kurtz, D.W., Medupe, R., 1996, BAS. India, **24**, in press.

[60] Kurtz, D.W., Shibahashi, H., 1986, MNRAS, **223**, 557

[61] Kurtz, D.W., Sullivan, D.J., Martinez, P., Tripe, P., 1994b, MNRAS, **270**, 674

[62] Kurtz, D.W., van Wyk, F., Roberts, G., Marang, F., Medupe, R., Handler, G., in preparation.

[63] Kurtz, D.W., Wegner, G., 1979, ApJ, **232**, 510

[64] Kurucz, R.L., 1970, Smithsonian Ap. Obs. Spec. Rept., No. **309**

[65] Kurucz, R.L., 1979, ApJS, **40**, 1

[66] Kurucz, R.L., 1993a, In *Peculiar Versus Normal Phenomena in A-Type and Related Stars*, ASPC, **44**, p. 87, eds. M.M. Dworetsky, F. Castelli, R. Faraggiana

[67] Kurucz, R.L., 1993b, Smithsonian Ap. Obs, CDROM 13.

[68] Kurucz, R.L., Peytremann, E., Avrett, E.H., 1974, *Blanketed Model Atmospheres for Early–Type Stars*, Washington, DC: Smithsonian Institution Press.

[69] Lavagnino, C.J., 1960, Bol.Assoc.Argent.Astron., **2**, 40

[70] Libbrecht, K.G., Woodard, M.F., 1990, Nature, **345**, 779

[71] Ledoux, P., 1951, ApJ, **114**, 373

[72] Leibacher, J.W., Stein, R.F., 1971, Astrophys.Lett., **7**, 191

[73] Leighton, R.B., Noyes, R.W., Simon, G.W., 1962, ApJ, **135**, 474

[74] Loumos, G.L., Deeming, T.J., 1978, Ap&SS, **56**, 285

[75] Maitzen, H.M., 1984, A & A, **138**, 493

[76] Martinez, P., 1993, PhD thesis, University of Cape Town.

[77] Martinez, P., 1996, BAS. India, **24**, in press

[78] Martinez, P., Kurtz, D.W., 1990, MNRAS, **242**, 636

[79] Matthews, J.M., 1991, PASP, **103**, 5.

[80] Matthews, J.M., Wehlau, W.H., Walker, G.A., Yang, S., 1988, ApJ, **324**, 1099

[81] Matthews, J.M., Wehlau, W.H., Walker, G.A.H., 1990, ApJ, **365**, L81.

[82] Matthews, J.M., Wehlau, W.H., Rice, J., Walker, G.A.H., 1996, ApJ, **459**, 278

[83] Mathys, G., 1985, A&A **151**, 315

[84] Mathys G., 1991, A&AS, **89**, 121

[85] Michaud, G., 1970, ApJ, **160**, 641

[86] Mihalas, D., 1978, *Stellar Atmospheres*, W.H. Freeman and Company, San Francisco.

[87] Pierce, A.K., Waddell, J., 1961, Mem. RAS, **68**, 89

[88] Press, W.H., Teukolsky, S.A., Vetterling, W.T., Flannery, B.P., 1992, *Numerical Recipes in Fortran*, Cambridge University Press, Cambridge, p

[89] Preston, G.W., 1974, ARA&, **12**, 257

[90] Przybylski, A., 1963, Acta Astr., **13**, 217

[91] Przybylski, A., 1966, Nature, **210**, 20

[92] Przybylski, A., 1977a, MNRAS, **178**, 71

[93] Przybylski, A., 1977b, MNRAS, **178**, 735

[94] Przybylski, A., 1977c, Proc.astr.Soc., **3**, 143

[95] Renson, P., Manfroid, J., Heck, A., 1976, A&AS, **23**, 413

[96] Shibahashi, H., Saio, H , 1985, PASJ, **37**, 245

[97] Sinachopoulos, D., 1989, A&AS, **81**, 103

[98] Smart, W.M., 1977, Textbook on Spherical Astronomy (6^{th} edition), University Press, Cambridge.

[99] Stepien, K., 1968, ApJ., **154**, 945

[100] Stibbs, D.W.N., 1950, MNRAS, **110**, 395

[101] Tassoul, J., 1978, Theory Of Rotating Stars, Princeton University Press, Princeton, New Jersey.

[102] Tassoul, M., 1980, ApJS, **43**, 469

[103] Tassoul, M., 1990, ApJ., **358**, 313

[104] Ulrich, R.K., 1970, ApJ, **162**, 993

[105] Unno, W., Osaki,Y., Ando, H., Saio, H., Shibahashi, H., 1979, Nonradial Oscillations Of Stars (1st edition), University of Tokyo Press, Tokyo.

[106] Van den Heuvel, E.P., 1971, A&A, **11**, 461

[107] Viskum, M., Baldry, I.K., Kjeldsen, H., Frandsen, S., Bedding, T.R., in preparation

[108] Warner, B., 1966, Nature, **211**, 55

[109] Watson, R.D., 1988, Ap&SS, **140**, 255

[110] Wegner, G., Petford, A.D., 1974, MNRAS, **168**, 557

[111] Weiss, W.W., Schneider, H., 1984, A&A, **135**, 148

[112] Weiss, W.W., 1986, In: *Upper Main Sequence Stars With Anomalous Abundances.* Proc. IAU Colloq. No 90, p. 219, Dordrecht: Reidl, ed. C.R. Cowley, M.M. Dworetsky, C. Megessier

[113] Wolff, S.C., 1975, ApJ, **202**, 127

[114] Wolff, S.C., 1983, *The A-type Stars: Problems and Perspective.* NASA SP-463. Washington, DC: NASA

[115] Wolff, S.C., Hagen, W., 1976, PASP, **88**, 119

[116] Wood, F.B., 1963, In *Basic Astronomical data*, ed. KAA., Strand, The University of Chicago Press, 375

[117] Wood, H.J., Campusano, L.B., 1975, A&A, **45**, 30